THE UNIVERSITY OF CHICAGO

FUNCTIONAL CONNECTIVITY SIGNATURES OF INTERHEMISPHERIC COORDINATION AND VOCAL LEARNING IN THE ZEBRA FINCH BRAIN

A DISSERTATION SUBMITTED TO
THE FACULTY OF THE DIVISION OF THE SOCIAL SCIENCES
IN CANDIDACY FOR THE DEGREE OF
DOCTOR OF PHILOSOPHY

DEPARTMENT OF PSYCHOLOGY

BY
ELLIOT ANDREW LAYDEN

CHICAGO, ILLINOIS
JUNE 2019

TABLE OF CONTENTS

LIST OF TABLES

LIST OF FIGURES

LIST OF ABBREVIATIONS

AC	Anterior Commissure
ACME	Average Causal Mediation Effect
ADE	Average Direct Effect
AFP	Anterior Forebrain Pathway
ANTs	Advanced Normalization Tools
BOLD	Blood-Oxygen-Level-Dependent
CC	Corpus Callosum
CDT	Cluster-Defining Threshold
CM	Caudal Mesopallium
CNR	Contrast-to-Noise Ratio
CP	Critical Period
CSF	Cerebrospinal Fluid
DM	Dorsomedial Nucleus of the Intercollicular Complex
FC	Functional Connectivity
FDR	False Discovery Rate
FWE	Family-Wise Error
GE	Gradient Echo
GUI	Graphical User Interface
ICC	Intrinsic Connectivity Contrast
IEG	Immediate Early Gene
LFP	Local Field Potential
LMAN	Lateral Magnocellular Nucleus of the Anterior Nidopallium

LME	Linear Mixed-Effects
NCM	Caudomedial Nidopallium
OLS	Ordinary Least Squares
PMP	Posterior Motor Pathway
PNG	Portable Network Graphics
QA	Quality Assurance
RA	Robust Nucleus of the Arcopallium
RARE	Rapid Acquisition with Refocusing Echoes
RF	Radio Frequency
ROI	Region of Interest
rs-fMRI	Resting-state Functional Magnetic Resonance Imaging
S2V	Seed-to-Voxel
SC	Structural Connectivity
SD	Standard Deviation
SE	Spin Echo
SFNR	Signal-to-Fluctuation-Noise Ratio
SNR	Signal-to-Noise Ratio
SyGN	Symmetric Group-wise Normalization
SyN	Symmetric Image Normalization
T	Tesla

ACKNOWLEDGEMENTS

First, I would like to thank my advisor, Dr. Marc Berman, for all of his kindness and helpful feedback through the years. I feel very fortunate to have been welcomed into the congenial and supportive atmosphere of the Environmental Neuroscience Lab. I am also grateful to Marc for having not only permitted but also encouraged me to explore my intellectual interests that sometimes fell outside of the traditional bounds of academic research, including software development. In this way and many others, I appreciate Marc's emphasis on cultivating graduate students, not just as scholars, but also holistically as people.

I would also like to thank the rest of my committee, Dr.'s Sarah London, Edward Awh, and Monica Rosenberg, for all of their helpful feedback that has helped to shape this dissertation. I am especially grateful to Sarah for consistently providing me with timely and thorough feedback on manuscript drafts, and for her patience with my fledgling understanding of songbird epigenetics. I am also very grateful to Ed for providing me with a thoroughly engaging and enjoyable teaching experience in Mind.

I would also like to thank Dr. Olaf Sporns, who, when I was just an undergraduate student, provided me with fascinating datasets, gave me the tools and resources needed to analyze them, and introduced me to the study of complex brain networks. Olaf's mentorship was certainly an important factor that inspired me to pursue a PhD, and I'm very glad that we've been able to stay in touch over the years.

I would also like to thank Dr.'s John and Stephanie Cacioppo, in addition to the rest of the Social Neuroscience Lab. My critical thinking, writing ability, and rigor all benefited greatly from the time I spent with the lab.

I cannot forget to acknowledge the MRIS facility staff, who helped us tremendously with animal care and fMRI scanning. In particular, I would like to thank Xiaobing Fan, for his patience and invaluable advice regarding the optimization of our scanning procedure. Additionally, I would like to thank Kathryn Schertz and Frank Ibarra, who helped to collect a substantial portion of the data presented in this dissertation. Also, I would like to thank Elisa Gores, who helped with animal care, and Huibo Li, who helped with the curation and analysis of song recordings.

I also cherish the many friends and colleagues from my cohort and lab that I have had the privilege to know during my time at UChicago, and I hope that we will continue to stay in touch as we part ways on the next phase of our journeys.

I am also grateful to my parents, Ron and Jennifer, and brother, Patrick, who have never hesitated to lend an ear during the many trials and tribulations of graduate school. Similarly, I am very appreciative of my aunt Cathy, uncles Brian and Steve, and grandparents Carol and Gerry, who have cheered me on throughout my PhD. Last, but not at all the least, I would like to thank my wife, Mingjie, who has been here with me every step of the way, since our first weeks in Hyde Park in the antique Blackstone Villas. I am not sure that I would have made it this far without you; we have reassured and encouraged each other in the face of so many tough challenges. These last five years have certainly not always been easy, but having you in my life has made them inexpressibly more joyful.

ABSTRACT

The zebra finch (*Taeniopygia guttata*) songbird learns a "tutor" song during a single developmental critical period (CP), offering a window through which to study the neural mechanisms that enable the learning of complex behaviors. Zebra finch song relies on interactions among distributed multimodal brain regions, and maintaining a balance between hemispheric specialization and interhemispheric coordination may be essential. Accordingly, the zebra finch may also be a suitable model organism in which to study comparative mechanisms of interhemispheric integration. In this dissertation, I describe the use of longitudinal resting-state fMRI (rs-fMRI) functional connectivity (FC) analyses to offer insights into these topics. In Chapter 1, I detail the extensive methodological innovations that were required to develop our novel zebra finch rs-fMRI pipeline. These included the creation of (1) a custom zebra finch brain template; (2) the *NeuroViz* toolbox, used to digitally extract the zebra finch brain and delineate regions of interest; and (3) the *MRIqual* toolbox, used for rs-fMRI quality assurance. In Chapter 2, I show that the zebra finch brain exhibits brain-wide bilaterally symmetric intrinsic brain activity (i.e., homotopic FC), consistent with interhemispheric coordination for complex behaviors. Homotopic FC is identified across Eutherian (placental) mammals, and the corpus callosum (CC), unique to this clade, is thought to structurally mediate this functional architecture. Chapter 2 provides the first indication that homotopic FC extends further across vertebrate phylogeny, suggesting that the CC is not a requirement for homotopic FC in normal ontogeny. In Chapter 3, I use the methodological and analytic techniques developed in previous chapters to identify FC signatures of tutor experience during the CP for song learning. It is known that tutor experience regulates neural plasticity within the caudomedial nidopallium (NCM), a higher-order auditory region integral for tutor song memorization. Chapter 3 extends

these findings by showing that tutor experience also influences the centrality of left NCM within large-scale functional brain networks. Collectively, these chapters constitute the first reports of whole-brain rs-fMRI analyses in the zebra finch. The methodological advances and empirical findings presented here could help to pave the way for future investigations using rs-fMRI to answer comparative neuroscience questions.

GENERAL INTRODUCTION

The Zebra Finch as a Model Organism

This dissertation describes the first reports of whole-brain resting-state functional magnetic resonance imaging (rs-fMRI) analyses in the zebra finch (*Taeniopygia guttata*) songbird. For decades, the zebra finch has served as a preeminent animal model of vocal learning (Immelmann, 1969; Nottebohm, 1969). Much as humans acquire speech in early childhood, zebra finches learn to sing from an adult tutor during the first three months of life (London, 2017; Tchernichovski, Mitra, Lints, & Nottebohm, 2001). Moreover, the zebra finch vocal learning process exhibits deep genomic (Heston & White, 2015; Teramitsu, Kudo, London, Geschwind, & White, 2004), neural (Doupe, Perkel, Reiner, & Stern, 2005; Graybiel, 2005), and social parallels (Bolhuis, Okanoya, & Scharff, 2010; Doupe & Kuhl, 1999) with human speech acquisition (Doupe & Kuhl, 1999). These numerous parallels suggest that insights made into the zebra finch vocal learning process may also help to shed light on various aspects of human language learning (Jarvis, 2004) and developmental disorders of language (White, Fisher, Geschwind, Scharff, & Holy, 2006).

Through a series of electrophysiology (e.g., Mooney, 2000; Stripling, Kruse, & Clayton, 2001; Yanagihara & Yazaki-Sugiyama, 2016), lesion (e.g., Bottjer, Miesner, & Arnold, 1984; Scharff & Nottebohm, 1991; Sohrabji, Nordeen, & Nordeen, 1990), and molecular signaling studies (e.g., Ahmadiantehrani & London, 2017; London & Clayton, 2008) studies, the network of brain regions that supports learned song has become relatively well-characterized (for review, see Mooney, 2009). Distinct song nuclei scale to form network modules, which in turn underlie important song functions, including the premotor control of song (posterior motor pathway (PMP); Nottebohm, Stokes, & Leonard, 1976; Simpson & Vicario, 1990), sensorimotor error

correction (anterior forebrain pathway (AFP); Bottjer et al., 1984; Charlesworth, Warren, & Brainard, 2012; Ölveczky, Andalman, & Fee, 2005; Scharff & Nottebohm, 1991), and sensory learning (auditory forebrain; Ahmadiantehrani & London, 2017; Bolhuis & Gahr, 2006; Bolhuis & Moorman, 2015; Chew, Vicario, & Nottebohm, 1996; London & Clayton, 2008; Olson, Maeda, & Gobes, 2016; Phan, Pytte, & Vicario, 2006; Yanagihara & Yazaki-Sugiyama, 2016).

The Advantages of Neuroimaging Methods

Given this voluminous prior zebra finch vocal learning literature, what novel insights can neuroimaging methods contribute to our understanding of learned complex behaviors like zebra finch song? Neuroimaging methods offer at least two critical advantages for studying developmental processes: (1) they are non-invasive, allowing for repeated measures to be obtained from the same intact animals at multiple developmental time points, and (2) they enable researchers to easily conduct *in vivo* whole-brain analyses, rather than focus on a finite set of specific brain regions. Moreover, this latter advantage also allows researchers to conduct exploratory analyses in search of regions that might be involved in song outside of the traditionally studied song nuclei. Additionally, because aspects of human speech and language are actively researched using neuroimaging methods (e.g., Meltzer, Postman-Caucheteux, McArdle, & Braun, 2009; Tzourio-Mazoyer, Joliot, Marie, & Mazoyer, 2016), and these phenomena generally cannot be ethically researched using invasive techniques, neuroimaging of songbirds may enable more direct cross-species comparisons regarding the neural mechanisms supporting learned vocalizations. Finally, it is important to note that neuroimaging methods can play a complementary role within the research pipeline: insights made using *in vivo* whole-brain imaging can be submitted for further inspection using invasive cellular and molecular techniques.

Already, a growing body of research has begun to demonstrate the utility and efficacy of neuroimaging in songbirds. For example, several studies have successfully measured task-based blood-oxygen-level-dependent (BOLD) fMRI activations in response to song playback in lightly anesthetized songbirds (Boumans et al., 2008a; Boumans, Theunissen, Poirier, & Van Der Linden, 2007; Boumans et al., 2008b; Poirier, Boumans, Verhoye, Balthazart, & Van der Linden, 2009; Van Meir et al., 2005; Van Ruijssevelt et al., 2013; Van Ruijssevelt, Hamaide, Gurp, Verhoye, & Linden, 2017a; Van Ruijssevelt et al., 2017b; Voss, Salgado-Commissariat, & Helekar, 2010; Voss et al., 2007). These auditory fMRI studies have offered invaluable insights regarding the spatial extent and temporal properties of song-evoked activations in components of the auditory forebrain (Boumans et al., 2007; Van Meir et al., 2005; Van Ruijssevelt et al., 2017a), and they have provided evidence of functional lateralization for aspects of auditory processing (Van Ruijssevelt et al., 2017b; Voss et al., 2007). However, task-based fMRI methods are limited in their ability to elucidate the complex functional interactions that occur between brain regions, and these interactions are known to play significant roles in learning (e.g., Bassett et al., 2011) and cognition (e.g., Shirer, Ryali, Rykhlevskaia, Menon, & Greicius, 2012; Waites, Stanislavsky, Abbott, & Jackson, 2005) in humans.

Resting-state Functional MRI (rs-fMRI)

rs-fMRI offers researchers the ability to examine functional networks embedded within the brain's intrinsic activity, enabling analyses rooted in a network neuroscience perspective (Bullmore & Sporns, 2009). Specifically, rather than record BOLD responses evoked by tasks or stimuli, rs-fMRI records ongoing spontaneous, infra-slow (< 0.1 Hz) brain activity (Biswal et al., 2010; Biswal, Yetkin, Haughton, & Hyde, 1995; Mitra et al., 2018), in the absence of external stimuli. Functional connectivity (FC) can then be computed as the temporal dependency between

the intrinsic activations recorded from remote brain regions (for review, see van den Heuvel & Hulshoff Pol, 2010). Over the past two decades, rs-fMRI FC analyses have provided fundamental insights into the functional topography of the human brain (e.g., De Luca, Beckmann, De Stefano, Matthews, & Smith, 2006; Fox et al., 2005; Power et al., 2011), identified patterns of FC linked to neuropsychiatric disorders (e.g., Greicius et al., 2007; Zeng et al., 2012), and shown promise for predicting aspects of human cognitive function (e.g., Beaty et al., 2018; Rosenberg et al., 2016).

Human rs-fMRI protocols typically instruct participants to lie quietly within the scanner and to think of nothing in particular, while avoiding falling asleep (van den Heuvel & Hulshoff Pol, 2010). However, rs-fMRI has also been conducted during altered states of consciousness, including during sleep and under anesthesia. In general, the large-scale structure of major functional networks, such as the default mode network, appears to be largely preserved in these cases (Greicius et al., 2008; Horovitz et al., 2008; Larson-Prior et al., 2009; Martuzzi, Ramani, Qiu, Rajeevan, & Constable, 2010; Vincent et al., 2007), whereas the magnitude of FC between components of major functional networks may be somewhat reduced (Boveroux et al., 2010; Deshpande, Kerssens, Sebel, & Hu, 2010; Horovitz et al., 2009). Consequently, it has been proposed that large-scale resting-state networks do not necessarily reflect ongoing mentation, but rather they may reflect intrinsic processes fundamental to brain function that persist across levels of arousal (Larson-Prior et al., 2009).

A growing small animal rs-fMRI FC literature has recently emerged, particularly in anesthetized rodents (e.g., Grandjean, Schroeter, Batata, & Rudin, 2014; Hutchison, Mirsattari, Jones, Gati, & Leung, 2010; Jonckers, Audekerke, Visscher, Linden, & Verhoye, 2011; Mechling et al., 2014; Pawela et al., 2008; Sforazzini, Schwarz, Galbusera, Bifone, & Gozzi,

2014). However, we are unaware of any reports in the extant literature of whole-brain rs-fMRI in songbirds such as the zebra finch. In this dissertation, I describe the novel implementation of rs-fMRI FC analyses in zebra finches under a light dose of isoflurane anesthesia. First, I discuss the many methodological hurdles that needed to be overcome, in terms of data collection and preprocessing, to enable valid analyses. Then, I describe a series of FC analyses designed to (1) offer novel insights into interhemispheric coordination across phylogeny, and (2) identify FC signatures of tutor experience during the CP for song learning.

The Present Work

Chapter 1 covers the numerous methodological challenges that needed to be addressed before valid rs-fMRI analyses could be successfully implemented in the zebra finch. First, I review the literature that informed our decision to use a spin echo (SE), rather than gradient echo (GE), fMRI pulse sequence. Next, I discuss the implications of appropriate echo time (TE) and repetition time (TR) selection for an optimal tradeoff between BOLD signal sensitivity, temporal signal-to-noise ratio (*tSNR*), and temporal resolution. Then, I discuss the construction of a custom zebra finch brain template. Finally, I describe the design and development of two custom Matlab toolboxes, *NeuroViz* and *MRIqual*. NeuroViz allowed us to digitally extract the zebra finch brain template from surrounding tissues, delineate a set of twenty regions of interest (ROIs), and create state-of-the-art 3D visualizations of the zebra finch brain. MRIqual allowed us to conduct *tSNR* validation analyses and perform power spectral analyses, helping to assure the quality of our rs-fMRI data. Several of the methodological strategies outlined in Chapter 1 may potentially prove useful for future investigations utilizing MRI methodologies in small animals. The toolboxes NeuroViz and MRIqual are components of a manuscript in preparation.

Chapter 2 concerns a pattern of brain-wide bilaterally symmetric intrinsic activity (i.e., homotopic FC) within the zebra finch brain. Homotopic FC appears to be fundamental feature of the mammalian brain's functional architecture (Matsui, Murakami, & Ohki, 2016; Pan et al., 2011; Shen et al., 2015; Stark et al., 2008; Vincent et al., 2007; Zhang, Kendrick, Lu, & Feng, 2014; Zuo et al., 2010), and there are indications that it is largely mediated by the CC (Hermesdorf et al., 2016; Jarbo, Verstynen, & Schneider, 2012; Johnston et al., 2008; Roland et al., 2017; Shen et al., 2015), a large interhemispheric white matter tract unique to Eutherian (placental) mammals (Aboitiz & Montiel, 2003; Luo, Yuan, Meng, & Ji, 2011). Importantly, the CC is believed to help balance the bilateral coordination and hemispheric specialization critical for many complex multimodal brain functions, including human language (Gazzaniga, 2000; van der Knaap & van der Ham, 2011). However, the CC first emerged with the Eutherian (placental) mammals some 160 MYA and is not found among other vertebrates, including avians (Aboitiz & Montiel, 2003; Luo et al., 2011). Despite this, other vertebrates also exhibit complex brain functions that may rely on a balance of hemispheric specialization and coordination. Indeed, the zebra finch learns to sing from an adult tutor much as humans acquire speech (Doupe & Kuhl, 1999), and a balance of hemispheric specialization and coordination may be important for song (Avey, Phillmore, & MacDougall-Shackleton, 2005; Cynx, Williams, & Nottebohm, 1992; Moorman, Gobes, van de Kamp, Zandbergen, & Bolhuis, 2015; Moorman et al., 2012). We therefore asked whether the zebra finch also exhibits homotopic FC, despite lacking the CC. Chapter 2 has been published in Layden, E. A., Schertz, K. E., London, S. E., & Berman, M. G. (2019). Interhemispheric functional connectivity in the zebra finch brain, absent the corpus callosum in normal ontogeny. *NeuroImage*, *195*, 113-127.

In Chapter 3, we asked whether FC signatures of tutor experience are detectable at the systems level, by conducting longitudinal rs-fMRI scanning across the CP for song learning. Juvenile male zebra finches typically memorize their father's (or another adult male's) song during a CP from approximately day 30 post-hatch (P30) to P65 (Eales, 1985, 1987; Roper & Zann, 2006). The onset of this CP may be primarily initiated by neural maturational events, which enable the learning process to begin (London, 2017). In contrast, the close of the CP relies upon tutor song experience-dependent plasticity (i.e., on having successfully memorized a tutor song) (London, 2017). Birds who are isolated from tutor experience during the CP (*Isolates*) still have the potential to memorize a tutor song after P65 (Eales, 1985, 1987; Jones, ten Cate, & Slater, 1996, 1992; Morrison & Nottebohm, 1993), at which point the CP has typically closed in birds reared with normal tutor experience (*Normals*). Here, we examined the developmental trajectory of the intrinsic connectivity contrast (ICC; Martuzzi et al., 2011), a measure of voxel-wise FC strength, before (P25), in the middle of (P45), and at the end of (P65) the CP, as well as at the young adult stage (P90) in Isolate and Normal male zebra finches. Isolates were raised with two adult females, who make innate calls but do not sing. Normals were aviary-raised with access to multiple potential adult male tutors. An additional *Tutored* group was reared with one adult male tutor and one adult female, thus forming a direct comparison to the Isolates in terms of number of conspecifics, differing only in terms of tutor experience. We hypothesized that Isolates would show an altered developmental trajectory of ICC within higher-order processing regions of the auditory forebrain (the caudomedial nidopallium (NCM) and caudal mesopallium (CM)), given that a number of studies (for review, see Bolhuis & Moorman, 2015) have indicated that these regions are critical for tutor song memorization. Chapter 3 is currently a manuscript in preparation for publication.

CHAPTER 1 - COLLECTION, VALIDATION, AND PREPARATION OF ZEBRA FINCH RESTING-STATE FUNCTIONAL MRI DATA

Introduction

Prior to the study described in Chapter 2 of this dissertation, the published literature did not contain any whole-brain rs-fMRI studies in zebra finches, to the best of our knowledge. For this reason, and due to incompatibilities encountered with fMRI processing tools designed primarily for use with human data, the studies that follow required substantial original methods development and the use of alternative strategies to complete certain data processing steps. This chapter provides an overview of several of these issues, including (1) the selection of an appropriate fMRI pulse sequence, (2) the selection of various scanning parameters, (3) difficulties in brain normalization without a standard brain template or tissue probability maps, (4) brain extraction and ROI delineation, and (5) fMRI data quality assurance (QA). Additionally, it describes the creation of two custom Matlab® toolboxes which proved invaluable for solving several of these challenges. The first, NeuroViz, allowed us to (1) manually trace a brain mask for digital extraction of the zebra finch brain template from surrounding tissues, (2) manually delineate ROIs, and (3) visualize 2D brain slices and create 3D-rendered brain images. Many of the figures depicted within this dissertation were generated using NeuroViz and custom Matlab scripts, except where otherwise noted. The second toolbox, MRIqual, allowed us to (1) gauge fMRI data quality based on the *tSNR* and (2) conduct power spectral analyses. Both toolboxes have several additional features and capabilities that are described in greater detail below, in case they may prove useful for future research.

Spin Echo (SE) versus Gradient Echo (GE) Pulse Sequences

One of the first major methodological choices to be made in an fMRI study is the choice of an appropriate pulse sequence. Two of the major pulse sequences used for measuring BOLD signals in fMRI are the GE and SE sequences, of which several additional sequences are derivative. The GE pulse sequence consists of (1) a single radio frequency (RF) excitation pulse, (2) the application of a dephasing gradient field that modifies spin phase in a spatially varying manner, and (3) the application of a rephasing gradient of opposite polarity, which then forms a GE (Bernstein, King, & Zhou, 2004; Plewes & Kucharczyk, 2012). The SE pulse sequence consists of (1) a 90 degree RF pulse, (2) a short dephasing period *t*, (3) a 180 degree inversion RF pulse, and (4) an echo occurring at time 2*t* with strength proportional to e^{-2t/T_2}, where T_2 is the spin-spin relaxation time constant that varies between tissues (Bernstein et al., 2004; Plewes & Kucharczyk, 2012).

Many human fMRI studies default to using a T_2^*-weighted GE pulse sequence, due to its ease of implementation and the prospect of a short repetition time (TR) for rapid imaging (Yacoub et al., 2003). However, we also considered the potential advantages and disadvantages of utilizing a T_2-weighted SE pulse sequence. Although GE fMRI generally obtains higher contrast-to-noise ratio (CNR) than SE fMRI (Yacoub et al., 2003), SE fMRI tends to achieve higher spatial specificity for BOLD signals. This is demonstrable at a magnetic field strength of 3 Tesla (T) (Thulborn, Chang, Shen, & Voyvodic, 1997), but the difference becomes even more pronounced at higher magnetic field strengths (Poser & Norris, 2007), such as the 9.4 T used in the current studies. The gains in spatial specificity from SE result from the fact that SE fMRI measures BOLD signals with substantially reduced intravascular contributions from draining blood vessels distant from the site of brain activity (Budde, Shajan, Zaitsev, Scheffler, &

Pohmann, 2014; Uludağ, Müller-Bierl, & Uğurbil, 2009). This increased spatial specificity is perhaps particularly important for imaging small brains such as that of the zebra finch.

Perhaps more importantly are the substantial artifacts encountered when using GE fMRI to scan zebra finch brains at high magnetic field strength. Large susceptibility artifacts are known to occur in much of the brain due to the numerous air cavities present in the skulls of avian species, which are optimized for flight (Poirier & Van der Linden, 2011; Poirier, Verhoye, Boumans, & Linden, 2010). Thus, artifact-free whole-brain fMRI in zebra finches may only be achieved using SE sequences (Poirier et al., 2009, 2010). Together, these considerations led us to utilize SE, rather than GE, fMRI.

Selection of Echo Time (TE) and repetition time (TR)

Echo time (TE) and repetition time (TR) are two of the most important pulse sequence parameters to optimize for an fMRI experiment. TE refers to the amount of time between the application of an RF excitation pulse and the peak of the echo recorded. TR refers to the amount of time between consecutive pulses (Plewes & Kucharczyk, 2012). Thus, for rs-fMRI, TR directly determines the temporal resolution attainable. However, the TR attainable can also be limited by the TE in some cases (Preibisch et al., 2003). In general, BOLD sensitivity in GE fMRI peaks at TE ~ T_2^* of grey matter (van der Zwaag et al., 2009), and BOLD sensitivity in SE fMRI peaks at TE ~ T_2 of grey matter (Lee, Silva, Ugurbil, & Kim, 1999).

To our knowledge, the precise T_2 of grey matter in the zebra finch had not been explicitly measured, and we relied upon past measurements in rodents at high magnetic field strengths to select an appropriate TE. Importantly, the T_2 of grey matter shortens supralinearly with higher magnetic field strengths (Duong et al., 2003; Thulborn et al., 1997; Yacoub et al., 2003), meaning that an appropriate TE at 3 T will likely be too long at 9.4 T. We found that the T_2 of

mammalian brain tissue varied between approximately 30-41 ms at high magnetic field strength: 38.6 ms in rats at 9.4 T (Lee et al., 1999), 36-41 ms in mice at 7 T (Guilfoyle, Dyakin, O'Shea, Pell, & Helpern, 2003), and 40 ms in humans at 9.4 T (Uludağ et al., 2009). Notably, T_2 can also vary substantially between different brain regions. For example, bands of tissue running along the bank of the precentral gyrus exhibited a T_2 as short as 30 ms at 7.0 T (Harmer, Sanchez-Panchuelo, Bowtell, & Francis, 2012). Thus, it is unlikely that a single TE can be optimal throughout the entire brain (Smith et al., 2013).

Regardless of precise T_2 measurements, prior literature indicates that robust SE BOLD activations can be consistently obtained at 9.4 T using a TE as short as 27-30 ms: e.g., 1. Human motor cortex during finger tapping (TE = 28 ms, Budde et al. 2014), 2. Rat somatosensory cortex during forepaw stimulation (Lee et al., 1999), and 3. Cat visual cortex during visual stimulation (TE = 30 ms, Jin et al. 2006). In studies where direct comparisons are made between a longer and shorter TE (e.g., 28 ms vs 40 ms, Budde et al. 2014), differences in the distribution of activated voxels are generally minimal. In addition to these mammalian studies, SE fMRI data have also been successfully acquired in an avian species using a TE shorter than 27 ms (De Groof et al., 2013). In sum, although using a TE slightly below the T_2 of grey matter may provide suboptimal CNR, this generally should not interfere with obtaining robust BOLD signals, so long as TE remains relatively close to tissue T_2 (Budde et al., 2014; Jin et al., 2006; Lee et al., 1999).

Another potential concern with using a TE shorter than tissue T_2 is the possibility of including increased intravascular contributions to the BOLD signal from draining veins, as these can reduce the spatial specificity of the BOLD signal. However, intravascular contributions are thought to remain minimal at a TE of 27 ms for higher magnetic field strengths (Duong et al.,

2003). This is explained by the fact that the T_2 of blood shortens quadratically with increasing magnetic field strength, whereas the T_2 of grey matter only shortens supralinearly (Duong et al., 2003; Thulborn et al., 1997; Yacoub et al., 2003). More precisely, the T_2 of blood is around 5–7 ms at 9.4 T (Zhao, Wang, & Kim, 2004). Importantly, BOLD signals obtained from SE fMRI at 9.4 T with a TE of 27 ms are thought to still contain a superior ratio of microvasculature to macrovasculature (i.e., tissue to intravascular) contribution than BOLD signals obtained from GE fMRI using any parameter set or magnetic field strength tested (Budde et al., 2014; Uludağ et al., 2009). In sum, a TE slightly below the tissue T_2 at high magnetic field strength appears capable of capturing adequate BOLD signal without substantial intravascular contribution to the signal.

In a series of pilot scans, we found that, with a TE approximating the likely tissue T_2 at 9.4 T (35-40 ms), we were unable to achieve whole-brain coverage with an effective TR (i.e., sampling rate) below 4 seconds, due to hardware limitations. We considered that this TR was substantially higher than is standard for rs-fMRI studies (e.g., 2 seconds; Layden et al., 2017), and this also limited the number of volumes we could acquire within a limited time period, while the birds were under anesthesia. We therefore opted to use a shorter TE of approximately 27 ms, which still provides adequate BOLD signal based on the prior literature (Budde et al., 2014; Jin et al., 2006; Lee et al., 1999), and this allowed us to acquire whole-brain data with a faster effective TR of 3.20 seconds.

Brain Normalization without a Template or Tissue Probability Maps

Following the selection of an appropriate fMRI pulse sequence and scan parameters, we next faced the challenge of normalizing the individual brains into a common space for analysis. We were aware of only one published three-dimensional MRI atlas of the zebra finch brain (Poirier et al., 2008). This atlas was based on a single perfused adult male zebra finch brain, and

upon further inspection, we found that the brain morphology did not well-align with our data. This was possibly due to structural changes resulting from the fixative used in perfusion. The large differences in morphology made normalizing our data to this template problematic. Further complicating matters, we did not have access to standard tissue probability maps, which are commonly used for normalization (e.g., SPM; Ashburner & Friston, 2005; Friston et al., 1995) and tissue segmentation in a number of software packages (Tsang et al., 2008).

Brain Extraction and Region of Interest (ROI) Delineation

We faced similar difficulties when it came to brain extraction, brain mask creation, and ROI delineation. First, we attempted to use several standard pipelines for brain extraction, including FSL's brain extraction tool (Smith, 2002) and AFNI's 3dSkullStrip (Cox, 1996). Although the latter program provides specialized functionality for monkey, marmoset, and rat brains, we found that neither tool was suitable for extracting the zebra finch brain from surrounding tissues. In particular, the tissue intensity distributions of the zebra finch eyes and brain appeared to overlap substantially, and the eyes were consistently extracted along with the brain.

Ultimately, we concluded that manual brain extraction was the only viable option. Given that we were unable to normalize our data to the only available 3D MRI atlas of the zebra finch brain (Poirier et al., 2008), this meant that we would also need to manually trace a set of ROIs for subsequent analyses. I surveyed software packages capable of accomplishing these tasks: I found that MRIcroGL (Rorden, 2012) was capable of 2D slice and 3D rendered displays of the zebra finch brain, and also allowed for ROI drawing. However, the ROI drawing feature did not appear to allow for flexible scanning through slices while concurrently drawing ROIs, which was necessary for our purposes. Additionally, I found that 3D slicer (Pieper, Halle, & Kikinis, 2004)

could accomplish these tasks but appeared to require a steep learning curve, and also incorporated a number of features that were not relevant for our purposes.

NeuroViz. To help overcome these issues and to enable manual brain extraction and ROI delineation, I created NeuroViz, a custom Matlab toolbox enabling state-of-the-art 2D and 3D visualization of brain images, as well as flexible editing of brain images and ROI drawings. Given that most of the analyses presented in this dissertation were conducted in Matlab, NeuroViz was designed to be easily accessible from the Matlab command line, enabling fast and efficient interactive data visualization during analyses, and avoiding the need to repeatedly export data to external software for visualization. A modular design was used to allow the user to call separate command-line functions to create mosaic slice displays, 3D renderings, or 2D displays of individual brain slices. The generated graphics can also easily be embedded within pre-made Matlab figures or axes, enabling a user to create multi-panel figures from scratch using only the Matlab command line or scripts. The creation and basic features of this toolbox are described in Methods below, and most of the figures included in this dissertation were created using NeuroViz, except where otherwise noted.

fMRI Quality Assessment

The quantification of image quality metrics such as the *tSNR* may be particularly important for novel scanning paradigms and/or for use with model organisms, for which scanning parameters are often less well-established (Kalthoff, Seehafer, Po, Wiedermann, & Hoehn, 2011). Additionally, descriptions of fMRI signal properties, such as the frequency distribution from power spectral analyses, can provide a useful point of comparison to data from prior literature (Grandjean et al., 2014; Kalthoff et al., 2011).

Temporal signal-to-noise ratio (*tSNR*). The fraction of the fMRI BOLD signal that arises from brain activity generally comprises only a small proportion of the total variance of the fMRI signal (de Zwart, van Gelderen, Fukunaga, & Duyn, 2008). In contrast, contributions from thermal noise inherent to MRI, instrumental instability, head motion, and physiological fluctuations constitute relatively larger fractions (de Zwart et al., 2008). Although best efforts are made to filter out the effects of head motion and physiological fluctuations, substantial noise of non-neural origin likely remains in the BOLD signal in most cases. For this reason, the *tSNR*, measured simply as the temporal mean signal divided by the temporal standard deviation (SD) (Murphy, Bodurka, & Bandettini, 2007; Triantafyllou et al., 2005), represents one of the most widely used metrics to gauge whether an experiment is sufficiently sensitive to detect small BOLD signals in the presence of substantial background noise. *tSNR* remains the rs-fMRI data quality index of choice for many large-scale multi-institutional rs-fMRI efforts, including the Human Connectome Project (Marcus et al., 2013; Smith et al., 2013). Importantly, higher *tSNR* is associated with increased sensitivity for detecting resting-state networks (Marcus et al., 2013; Van Dijk, Sabuncu, & Buckner, 2012), and the regional distribution of test-retest reliability for rs-fMRI FC is strongly associated with the spatial distribution of *tSNR* ($r = 0.61$; Mueller et al. 2015, p. 4669).

Power spectral analyses. The human rs-fMRI literature (Duff et al., 2008; Kim, Van Dijk, Libby, & Napadow, 2014) and the murine literature, which routinely utilizes isoflurane anesthesia (Grandjean et al., 2014; Kannurpatti, Biswal, Kim, & Rosen, 2008), both consistently identify $1/f$ power spectrums for rs-fMRI data. Resting-state power generally peaks in low frequency bands (< 0.1 Hz). In particular, resting-state time series obtained from isoflurane

anesthetized mice (Grandjean et al., 2014) and rats (Kannurpatti et al., 2008) have demonstrated peaks in the power spectrum at very low frequencies (~0.01 Hz).

MRIqual. We sought to quantify *tSNR* and conduct power spectral analyses in order to gauge the quality of our rs-fMRI data, and also to provide a reference point to past literature regarding rs-fMRI signal characteristics. I created the MRIqual Matlab toolbox to accomplish these tasks. MRIqual allows for the quantification of *tSNR*, the signal-to-fluctuation-noise ratio (SFNR; Hu & Glover, 2007; Lai & Glover, 1998), functional SNR, and mean power within a specified frequency range, such as the resting-state (~0.008-0.10 Hz; Whitfield-Gabrieli & Nieto-Castanon, 2012). Additionally, it allows the user to visualize rs-fMRI quality metric spatial maps, rs-fMRI signals before and after various preprocessing steps (e.g., detrending and bandpass filtering), and power spectrums. The creation and features of the MRIqual toolbox are described further below in Methods, and results from *tSNR* and power spectral analyses are reported.

Method

Selection of the Repetition Time (TR) and Echo Time (TE)

Prior to collecting the data used for the subsequent chapters, we first conducted a small set of experimental pilot scans to determine the optimal scan parameters for maximizing whole-brain *tSNR*, power within the resting-state frequency range [0.01-0.10 Hz], and spatial resolution, while simultaneously minimizing TR and maximizing temporal resolution. For example, we compared the following three sets of scan parameters in this pilot sample, while holding constant the animal preparation procedures, isoflurane dose, and other factors.

1. Image Size = 140 x 42 x 15 voxels; TE = 25.8 ms; TR = 1.25 s; Sampling Rate = 3.75 s
2. Image Size = 128 x 36 x 15 voxels; TE = 30.7 ms; TR = 1.08 s; Sampling Rate = 3.25 s
3. Image Size = 150 x 48 x 15 voxels; TE = 41.8 ms; TR = 1.42 s; Sampling Rate = 5.68 s

Brain Normalization without a Template or Tissue Probability Maps

We identified Advanced Normalization Tools (ANTs; Avants, Tustison, & Song, 2009) as an ideal toolkit with which to normalize our zebra finch brain data and create a custom brain template, without the need for tissue probability maps. The ANTs symmetric image normalization (SyN; Avants, Epstein, Grossman, & Gee, 2008) method compares favorably among other commonly used nonlinear deformation algorithms (Avants et al., 2011; Klein et al., 2009). ANTs also provides a state-of-the-art template creation technique, called symmetric group-wise normalization (SyGN; Avants et al., 2010). SyGN outputs both an unbiased group-averaged brain template, as well as the normalized individual anatomical scans. We used an average of the bias-corrected anatomical scans from our sample as an initialization for SyGN. Template creation then proceeded by iteratively registering each anatomical scan to a custom brain template using affine and nonlinear transformations. As image registration improved, the custom template was updated in each iteration. Cross-correlation was implemented as the similarity metric for image comparison, and four template construction iterations were completed. We then evaluated the accuracy of registration by computing voxel-wise spatial correlations between the individual normalized anatomical scans and the group-wise brain template.

NeuroViz

Design of NeuroViz. NeuroViz can be called from the Matlab command line, specifying the images to load as name-value pairs, or NeuroViz can be called as a command without inputs, in which case the user will be prompted to select an image to load via graphical user interface (GUI). To load and save images, NeuroViz relies upon "Tools for NIfTI and ANALYZE image" (Shen, 2014). After loading an image, the main GUI will display (Figure 1.1). By default, a

middle axial slice of the loaded image is shown, along with a color-bar (denoting the mapping between voxel intensity values and colors), and a menu bar with various options.

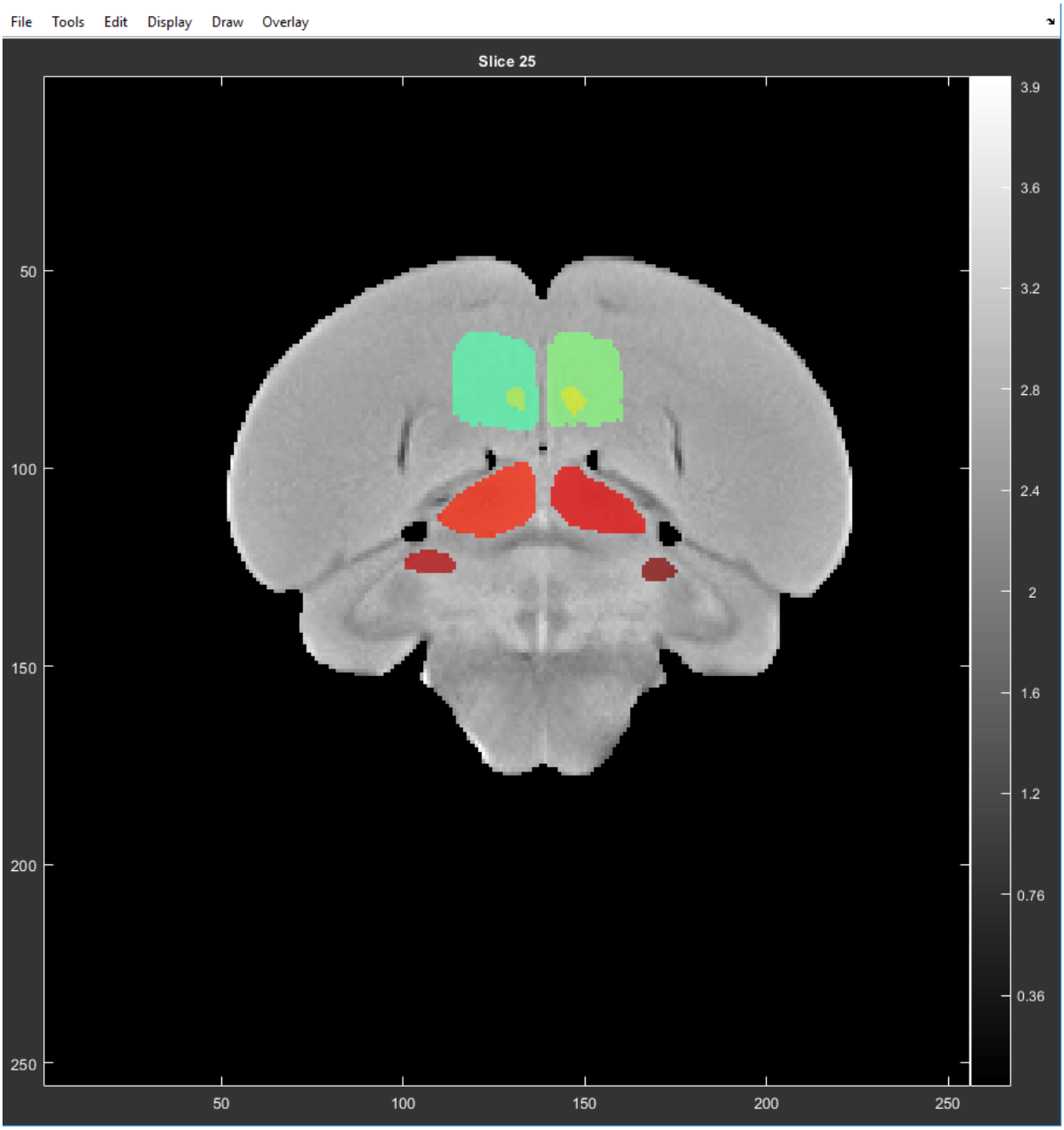

Figure 1.1. The NeuroViz graphical user interface. A coronal view of the group-wise zebra finch brain template with ROIs overlaid is displayed.

The menu bar contains a number of sub-menus, including File, Tools, Edit, Display, Draw, and Overlay. The File menu allows a user to (1) open a new image, (2) save the current

image, along with any edits made to the underlying data, (3) save the current ROI drawing, or (4) print the current display as a portable network graphics (PNG) file. The Tools menu allows the user to switch between (1) a crosshair tool that permits the user to click on the image to retrieve voxel coordinates, image intensity values, and overlay/drawing values at a given voxel, (2) a drawing tool, or (3) a panning tool. The Edit menu allows the user to (1) undo the last drawing action, (2) redo the last drawing action, or (3) navigate directly to a different slice. The Display menu allows the user to (1) change orientation (axial, coronal, sagittal, or 3D rendering), (2) change the color-map or color scale, and (3) customize various display settings. The Draw menu contains a number of options for drawing ROIs and editing overlays, allowing the user to switch between editing the main image or editing an overlay image, change drawing colors and opacity, draw various shapes, and propagate drawings through multiple slices. Finally, the Overlay menu allows the user to load statistical overlay images and to adjust overlay display settings.

NeuroViz: 3D rendering. NeuroViz includes a separate 3D rendering module (Figure 1.2) which is accessible from the Display menu of the main GUI, or, alternatively, this module can be accessed directly from the command line. Similar to options provided for plotting 2D brain slices, the command-line utility for 3D rendering allows 3D rendered graphics to be embedded within preexisting axes and figures, enabling the easy creation of multi-panel figures. The GUI contains four main submenus: File, Tools, View, and Display. The File menu allows the user to save the current GUI state as a Matlab figure file (.fig), print the current view as a static PNG image, or write the rendered 3D surface as an STL file for 3D printing. The Tools menu allows the user to switch between the rotate, zoom, and pan tools. The View menu allows a user to change between a set of standard views (Left, Right, Anterior, Posterior, Superior, and Inferior). Finally, the Display menu allows the user to adjust rendering Effects (Normal,

Emphasis, Sketch, Shiny, Metal, Flat), change the background color, adjust various axes properties, change between physical or voxel axes units, and to adjust a number of other display properties (e.g., brightness, smoothness, opacity, and lighting).

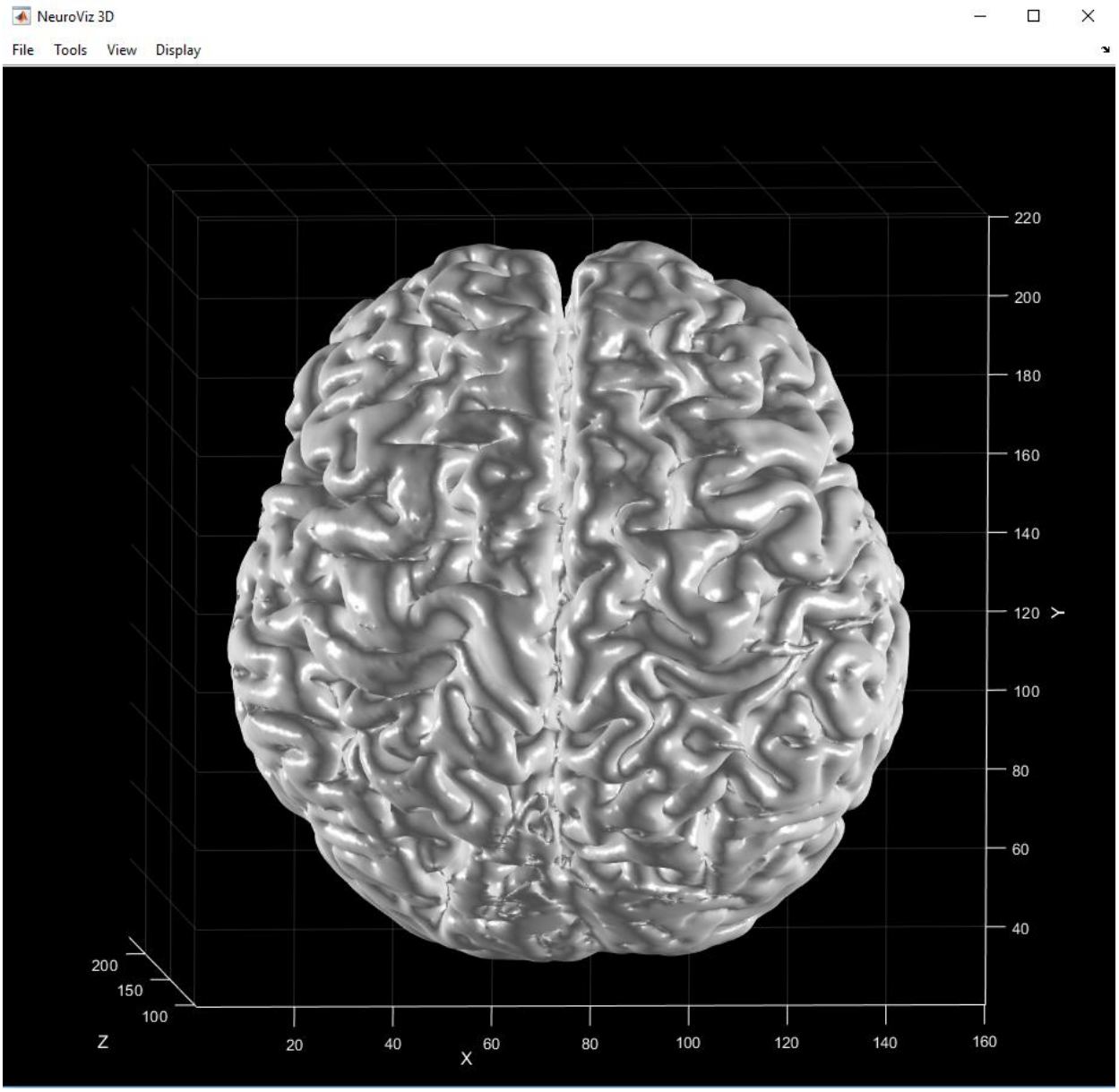

Figure 1.2. The NeuroViz 3D module. A 3D rendered human brain is depicted in a superior/horizontal view, with anterior toward the top of the image.

Brain extraction using NeuroViz. Using NeuroViz, I manually extracted the zebra finch group-wise brain template from surrounding tissues, including skull, cerebrospinal fluid, and

sinuses. This process involved tracing the outline of the brain slice-by-slice to create a brain mask. This brain mask was then applied to the template image, setting voxels outside of the mask equal to zero. The brain mask was subsequently used to confine voxel-wise statistical analyses to the boundaries of the brain.

Region of interest (ROI) delineation using NeuroViz. Using NeuroViz, committee member S. E. L. manually delineated a set of ten pairs of bilateral ROIs (i.e., twenty in total), including regions important for sensory, sensorimotor, and premotor processing. To facilitate this process, NeuroViz allowed for visual comparisons to be made between anatomical references found within our custom group-wise brain template and a previously published zebra finch brain atlas (Poirier et al., 2008). A mouse scroll-wheel zooming functionality allowed for fine-grained inspection of brain images and more accurate ROI tracing. Additionally, the ability to flexibly scan through brain slices using the arrow keys while concurrently drawing ROIs, and the ability to propagate an ROI drawing from a given slice through multiple other slices, significantly expedited ROI delineation. The specific functional roles of the ROIs, and their relevance to the zebra finch song network, are described in greater depth in Chapter 2.

MRIqual

MRIqual: design. I designed MRIqual primarily as an easy-to-use GUI for MRI QA. However, I also provided a command-line utility, quality_report_func.m, which enables similar functionality to the GUI. The GUI can be started by simply running the command ‘MRIqual’ in Matlab. The main MRIqual interface, as shown in Figure 1.3 below, then becomes visible.

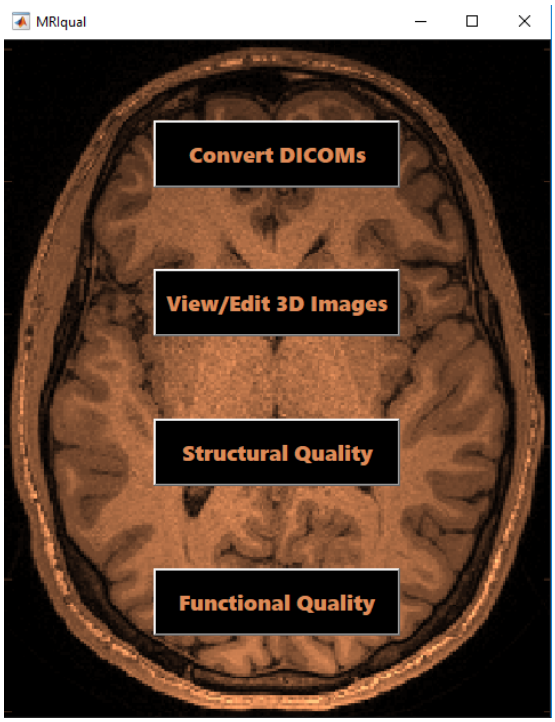

Figure 1.3. The MRIqual main interface.

From the main interface, a user can navigate to one of four modules: (1) Convert DICOMs, (2) View/Edit 3D Images, (3) Structural Quality, and (4) Functional Quality. The first module enables the user to convert DICOM files to NIfTI or .img/.hdr format. The user is prompted to select a folder containing a series of DICOM files, select an output folder, and to specify a new file name. The DICOM module interface is shown in Figure 1.4 below.

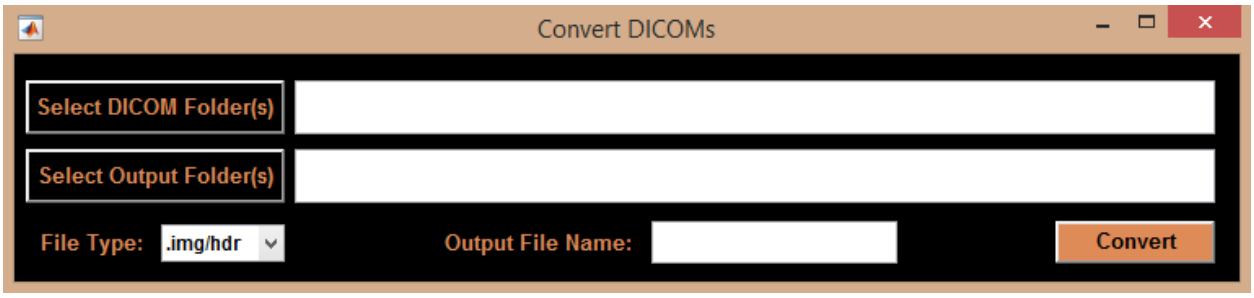

Figure 1.4. The MRIqual DICOM conversion module.

The second module, View/Edit 3D Images, enables NeuroViz to be used within MRIqual.

MRIqual: structural quality. The structural quality module (Figure 1.5) allows users to

measure, display, and save data concerning the signal-to-noise ratio (SNR) of 3D anatomical images. SNR can be calculated as the "SNR (Noise SD)," or the mean voxel intensity within a "signal" ROI (often a central region of an image known to contain adequate signal) divided by the SD of voxel intensities within a "noise" or background ROI (generally near the outer edges of an image where only background is present). This quotient is then multiplied by a correction factor accounting for the Rician distribution of the noise (Gudbjartsson & Patz, 1995). Alternatively, SNR can be calculated as the "SNR (Noise Mean)," or the mean voxel intensity of a signal ROI divided by the mean voxel intensity within a background/noise ROI, again multiplied by a correction factor (Dietrich, Raya, Reeder, Reiser, & Schoenberg, 2007). Either of these SNR definitions can be used within MRIqual.

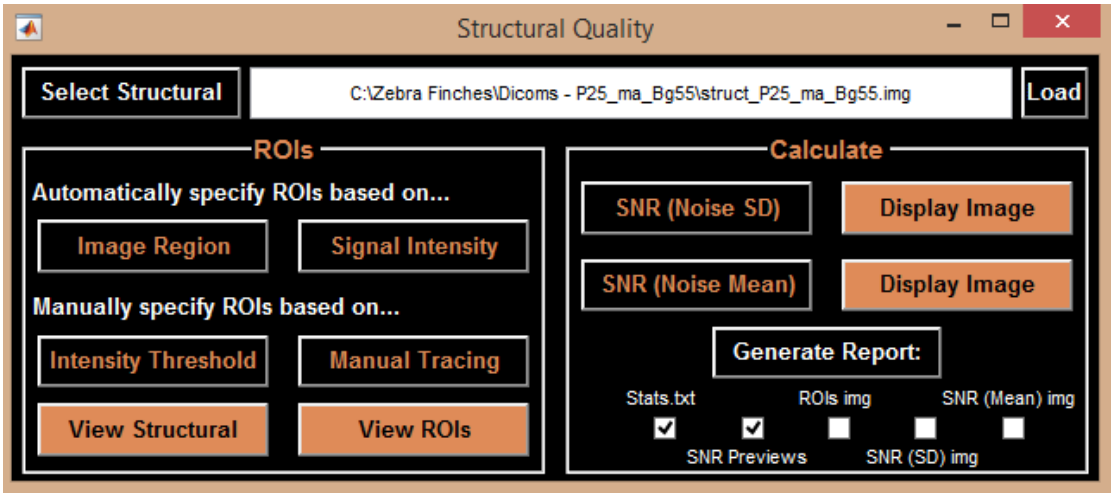

Figure 1.5. The MRIqual structural quality module.

However, prior calculating SNR, a user must first specify the "signal" and "noise" ROIs to be used for the calculation. This can be accomplished in a variety of ways. First, the "Image Region" option automatically draws a central rectangular signal ROI, along with two long, thin rectangular noise ROIs on each side of the image. These ROIs are approximate, and the user should check whether they correspond appropriately to the specific image and background by

clicking “View ROIs” (this opens the ROI image as an overlay in NeuroViz). A second option, “Signal Intensity,” thresholds the image in such a way as to approximately segment the brain from the background. Thresholds are automatically calculated so as to avoid the inclusion of hyperintensities and artifacts in either the signal or noise ROI. Note, however, that if skull is included as part of the anatomical image, it will likely be considered to be part of the signal ROI, along with the brain. Third, the “Intensity Threshold” option, allows users to specify their own custom signal intensity cutoffs for the signal and background ROIs. Finally, the “Manual Tracing” option allows users to manually trace custom ROIs using NeuroViz.

The structural quality module can generate a report detailing statistical findings. Selecting “Generate Report” will allow the user to select the output directory for this report. Beforehand, users can select which outputs are desired, including 1. a Stats.txt file that records the structural file name, the type of signal and noise ROIs used, the number of voxels within the signal and noise ROIs, and the SNR values as calculated using each method; 2. “SNR Previews,” or 2D images showing the local SNR of the middle slice of the 3D image; 3. “ROIs Image,” or a NIfTI file storing the signal and noise ROIs; 4. “SNR (SD) img,” or a NIfTI file storing the local SNR image calculated using the Noise SD method; and 5. “SNR (Mean) img,” a NIfTI file storing the local SNR image calculated using the Mean Noise method.

MRIqual: functional quality. The fourth module, functional quality (Figure 1.6), allows users to easily measure, display, and save QA measures for fMRI and rs-fMRI data. First, *tSNR* is calculated as the temporal mean signal divided by the temporal SD (Murphy et al., 2007; Triantafyllou et al., 2005). A summary measure for *tSNR* can be computed by averaging voxel-wise *tSNR* values across a specified signal ROI, or across the whole brain. The SFNR is essentially a refinement of the *tSNR*, calculated as the temporal mean signal divided the temporal

SD of the residual signal following linear and quadratic detrending (Friedman, Glover, & The FBIRN Consortium, 2006). “SNR-Funct” is the functional equivalent of anatomical SNR, calculated identically to the latter, but after first taking the temporal average of a functional image. Finally, “Mean Power” allows for the calculation of average power within a specified frequency range, such as the resting-state range.

The functional quality module implements the same ROI specification options as the structural quality module. Similarly, it also offers the ability to generate a report summarizing the statistical findings. An additional option in this module is the ability to run basic preprocessing prior to the calculation of the functional QA measures. The user can choose to implement linear or quadratic detrending, and the results of this operation can be visualized by comparing signals before and afterwards. Similarly, the user can bandpass filter the data and visualize the power spectrums before and after this operation using the “Power Spectrum” option. Power spectrums can be calculated using either Welch’s method (Welch, 1967) or the multitaper method (for review, see Babadi & Brown, 2014).

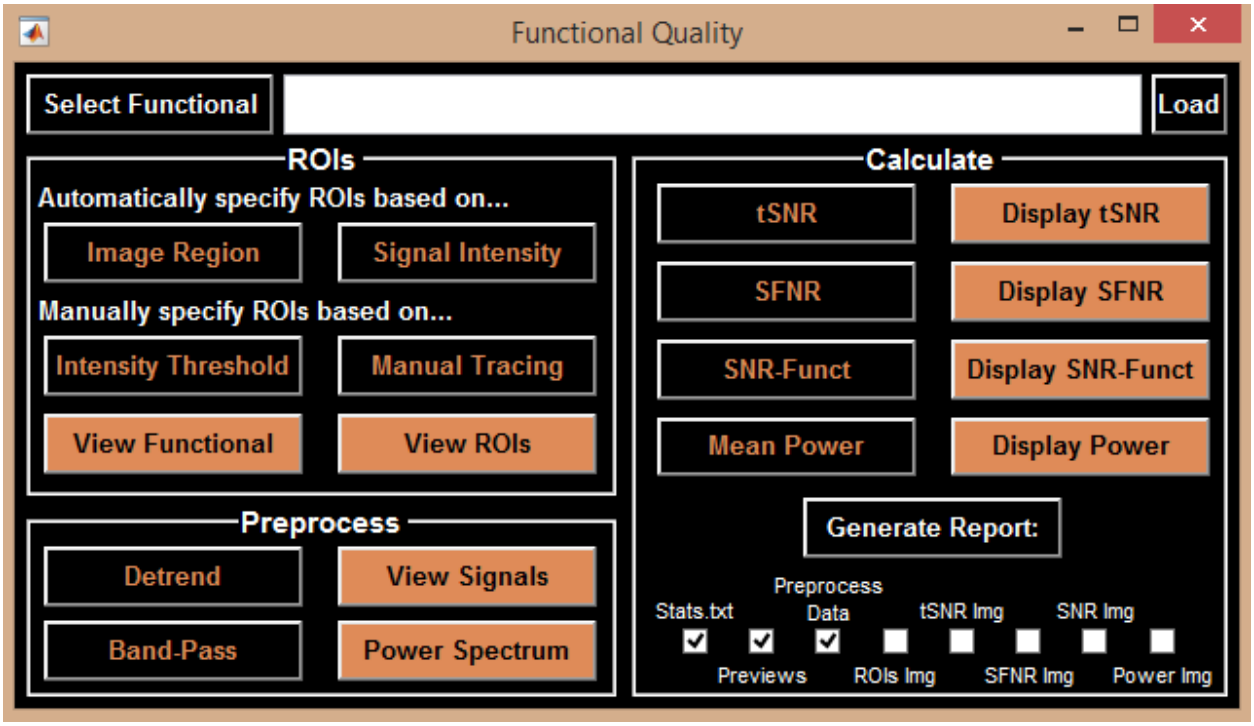

Figure 1.6. The MRIqual functional quality module.

MRIqual: rs-fMRI validation analyses.

Temporal signal-to-noise ratio (tSNR). With MRIqual, we calculated voxel-wise *tSNR* values, and these were averaged across all voxels within the brain mask to summarize whole-brain *tSNR*. Spatial smoothing is known to markedly enhance *tSNR* (Molloy, Meyerand, & Birn, 2014), and many studies only report *tSNR* for either smoothed or unsmoothed data (e.g., Harmer et al. 2012; Chang et al. 2018). This factor (and heterogeneous smoothing protocols) may help to account for the wide variability observed for *tSNR* values reported in prior literature (range: [4.42, 280], Welvaert and Rosseel 2013). Therefore, to enable easier comparison to prior studies, we calculated whole-brain *tSNR* for both unsmoothed and smoothed (0.422 x 1.000 x 1.125 mm FWHM, corresponding to 3 x 2 x 1.5 voxels, respectively) rs-fMRI scans. We then compared *tSNR* values from this study to those obtained in prior studies utilizing sub-millimeter voxel resolutions at high magnetic field strengths (Barth & Norris, 2007; Chang et al., 2018; Desai et al., 2010; Huber et al., 2018; Kemper et al., 2015; Liska, Galbusera, Schwarz, & Gozzi, 2015;

Rua et al., 2017; Yoshida et al., 2016). Given the small volume of our functional voxels (0.141 x 0.500 x 0.750 mm), *tSNR* was expected to be lower than in human resting-state scans collected at lower spatial resolution, because *tSNR* is known to be strongly positively associated with voxel volume (i.e., larger voxel volume yields higher *tSNR*; Triantafyllou et al. 2005; Murphy et al. 2007; Hutton et al. 2011; Zwaag et al. 2012).

Power spectral analyses. The power spectrum for each resting-state functional series was calculated within the infra-slow frequency range (~0.008-0.1 Hz; Cordes et al. 2001). Average power was calculated via Welch's power spectral density estimate, implemented using the Matlab function pwelch.m integrated within MRIqual. The power spectrums obtained were compared to those reported in the human resting state literature (Duff et al., 2008; Kim et al., 2014) and to those reported in the murine literature, which routinely utilizes isoflurane anesthesia (Grandjean et al., 2014; Kannurpatti et al., 2008). Both literatures have consistently identified 1/*f* power spectrums, with resting-state power highest in low frequency bands (< 0.1 Hz). In particular, resting-state time series obtained from isoflurane anesthetized mice (Grandjean et al., 2014) and rats (Kannurpatti et al., 2008) have demonstrated peaks in the power spectrum at very low frequencies (~0.01 Hz).

Results

Selection of the Repetition Time (TR) and Echo Time (TE)

We compared the following three sets of scan parameters in our pilot sample, while holding constant the animal preparation procedures, isoflurane dose, and other factors:

1. Image Size = 140 x 42 x 15 voxels; TE = 25.8 ms; TR = 1.25 s; Sampling Rate = 3.75 s;
Outcome: mean unsmoothed *tSNR* = 7.36, mean power [0.01-0.10 Hz] = 125.5

2. Image Size = 128 x 36 x 15 voxels; TE = 30.7 ms; TR = 1.08 s; Sampling Rate = 3.25 s;
Outcome: mean unsmoothed *tSNR* = 7.49, mean power [0.01-0.10 Hz] = 128.7

3. Image Size = 150 x 48 x 15 voxels; TE = 41.8 ms; TR = 1.42 s; Sampling Rate = 5.68 s; Outcome: mean unsmoothed *tSNR* = 5.48, mean power [0.01-0.10 Hz] = 120.7

We found that *tSNR* and mean power within the resting-state were lower for a TE of 41.8 ms compared to either TE = 25.8 ms or 30.7 ms. Additionally, we encountered a concomitant increase in TR when using longer TE's, due to scanner hardware limitations (e.g., TE = 41.8 ms resulted in a sampling rate of 5.68 s per functional volume). This was a lower temporal resolution than we deemed acceptable. Although our voxel resolution also varied in these pilot scans, the findings regarding *tSNR* (Duong et al., 2003; Harmer et al., 2012; Lee et al., 1999; Li & Mirowitz, 2003; Poirier et al., 2010; Uludağ et al., 2009; Yacoub et al., 2003) and acquisition time (Budde et al., 2014; Li & Mirowitz, 2003) are both consistent with prior literature. Thus, we chose a slightly lower TE than optimal for BOLD sensitivity (based on mammalian T_2) to maximize temporal resolution, power within the resting-state, and *tSNR*.

Brain Normalization without a Template or Tissue Probability Maps

With ANTs SyGN, we successfully created a group-wise zebra finch brain template, and as part of this process, we normalized each individual anatomical scan to this template. To assess the quality and consistency of spatial normalization, we computed voxel-wise Pearson correlations between the group-wise template and all 68 of the individual normalized anatomical scans across voxels (r_{mean} = 0.94, *SD* = 0.01). We also performed this assessment for the normalized functional scans, averaged across time (r_{mean} = 0.86, *SD* = 0.03). Both assessments indicated a robust and consistent spatial normalization across scans, comparable to prior literature (e.g., Layden et al., 2017).

Brain Extraction and ROI Delineation Using NeuroViz

Using NeuroViz, we successfully extracted the group-wise brain template from surrounding tissues, and we were also able to delineate a set of twenty ROIs, ten within each

hemisphere. The ROIs overlaid on the group-wise brain template are displayed below in Figure 1.7, and Table 1.1 lists the number of voxels, physical volume, and distance from origin for each ROI. The functional importance of each ROI is described further in Chapters 2 and 3.

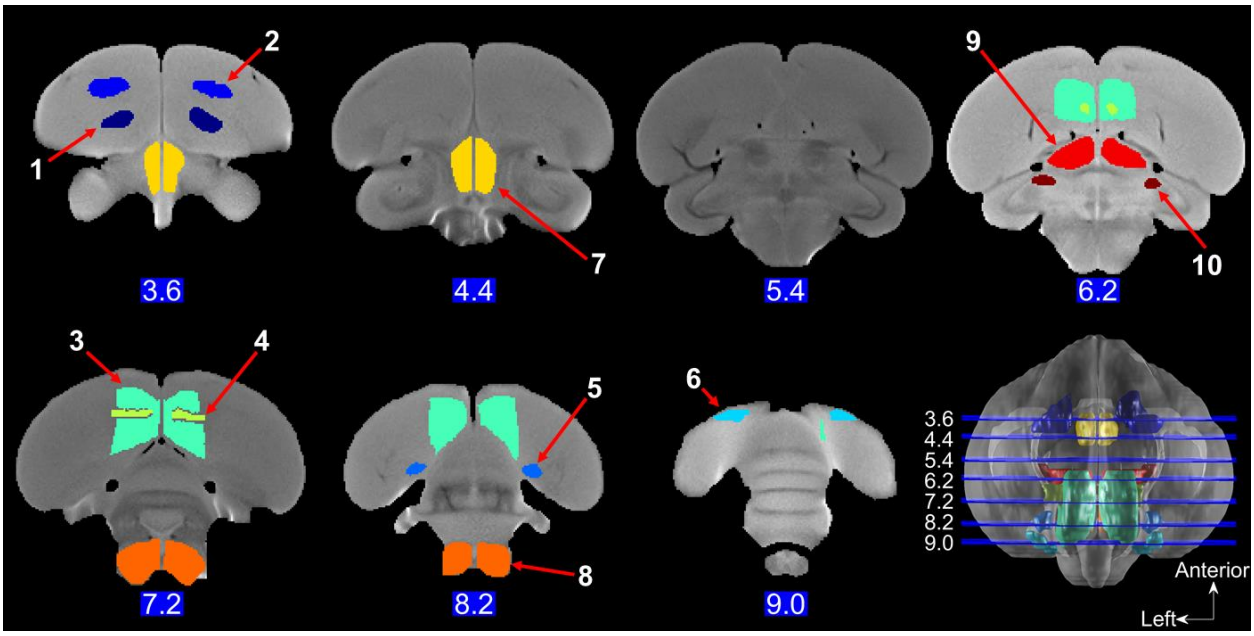

Figure 1.7. Group-wise brain template and regions of interest. **Song Network:** 1. Area X (*Midnight Blue*); 2. Lateral magnocellular nucleus of the anterior nidopallium (LMAN) (*Royal Blue*); 3. Auditory Forebrain (*Light Green*); 4. Field L (*Light Yellow*); 5. Robust nucleus of the arcopallium (RA) (*Blue*); 6. HVC (*Teal*); **Homotopic-SC ROIs: 7.** Medial Diencephalon (*Yellow*); 8. Medulla (*Orange*); 9. thalamic nucleus uvaeformis (Uva) (*Red*); 10. dorsomedial nucleus of the intercollicular complex (DM) (*Maroon*). The brain slices shown are 3.6, 4.4, 5.4, 6.2, 7.2, 8.2, and 9.0 millimeters from the anterior tip of the telencephalon.

Table 1.1. Zebra finch regions of interest

Song System	# Voxels	Volume (mm^3)	mm from Origin [x,y,z]
R Area X	1096	1.1	[-1.5, 0.24, -3.2]
L Area X	876	0.87	[1.7, 0.22, -3.4]
R LMAN	651	0.64	[-2.1, 1.5, -3.7]
L LMAN	566	0.56	[2.1, 1.4, -3.8]
R RA	273	0.27	[-2.4, -1.3, -7.9]
L RA	267	0.26	[2.4, -1.3, -7.9]
R HVC	293	0.29	[-2.3, 1, -8.9]
L HVC	259	0.26	[2.6, 1, -8.8]
R Aud. Forebrain	7947	7.9	[-1, 0.82, -7.3]
L Aud. Forebrain	7397	7.3	[1, 0.74, -7.3]
R Field L	609	0.6	[-1.1, 0.78, -6.8]
L Field L	743	0.73	[1.3, 0.78, -6.8]
R Diencephalon	1762	1.7	[-0.36, -1.7, -4]
L Diencephalon	1911	1.9	[0.47, -1.7, -4]
R Medulla	4536	4.5	[-0.81, -5, -7.3]
L Medulla	4452	4.4	[0.87, -5, -7.3]
R Uva	1118	1.1	[-0.96, -1.2, -6.1]
L Uva	1048	1.0	[1.1, -1.3, -6.1]
R DM	199	0.2	[-2.2, -2.2, -5.9]
L DM	171	0.17	[2.4, -2.3, -5.9]

Note. The origin was defined as a medial voxel at the anterior most portion of the brain in template slice 56.

MRIqual: rs-fMRI Validation Analyses

Temporal signal-to-noise ratio (*tSNR*). We noted robust *tSNR* across all 68 rs-fMRI scans (smoothed: $M = 56.36$, $SD = 13.10$; unsmoothed: $M = 26.44$, $SD = 3.24$). *tSNR* was comparable to other recent fMRI studies utilizing sub-millimeter voxel sizes and high magnetic field strengths. For example, three mouse studies reported similar *tSNR* values for smoothed data (e.g., *tSNR* = 27.7 ± 5.8, Chang et al. 2018; *tSNR* = 23-40, Liska et al. 2015; *tSNR* = 53 ± 4, Yoshida et al. 2016). Also, one mouse study (*tSNR* = 15-17, Desai et al. 2010) and four human studies (*tSNR* = 15-20, Barth and Norris 2007; *tSNR* = 18 ± 4, Huber et al. 2018; *tSNR* ≈ 5-15, Kemper et al., 2015; *tSNR* ≈ 10, Rua et al. 2017) reported similar *tSNR* values for

unsmoothed data. Table 1.2 below shows representative *tSNR* values from individual scans for the first five birds in our sample, which were all aviary-reared.

Table 1.2. Temporal signal-to-noise ratio

Bird	Unsmoothed	Smoothed
P25 Male 1	15.59	49.59
P45 Male 1	12.96	38.80
P65 Male 1	14.04	51.46
P90 Male 1	13.74	53.46
P25 Male 2	14.74	51.82
P45 Male 2	12.22	52.20
P65 Male 2	14.83	59.65
P90 Male 2	14.23	59.16
P25 Male 3	24.55	103.37
P45 Male 3	15.37	68.15
P65 Male 3	12.86	41.80
P90 Male 3	15.17	61.09
P25 Male 4	20.56	55.92
P45 Male 4	14.83	59.01
P65 Male 4	14.59	53.34
P90 Male 4	14.48	66.34
P25 Male 5	14.73	62.69
P45 Male 5	15.07	59.67
P65 Male 5	14.64	61.53

Note. the reported temporal signal-to-noise ratio (tSNR) values represent the average tSNR of all voxels within the brain mask for each individual resting-state scan.

Power spectral analyses. Consistent with prior rs-fMRI data, the zebra finch rs-fMRI signals exhibited power spectrums with a $1/f$ (frequency) distribution, with the highest power at low frequencies (Kannurpatti et al. 2008; Grandjean et al. 2014). Specifically, this observation concerns the relative distribution of power within the resting-state frequency range and not necessarily between the resting-state and non-resting-state frequency ranges. Figure 1.8 shows the power spectrums for individual scans from the first five birds from our sample, which were aviary-reared.

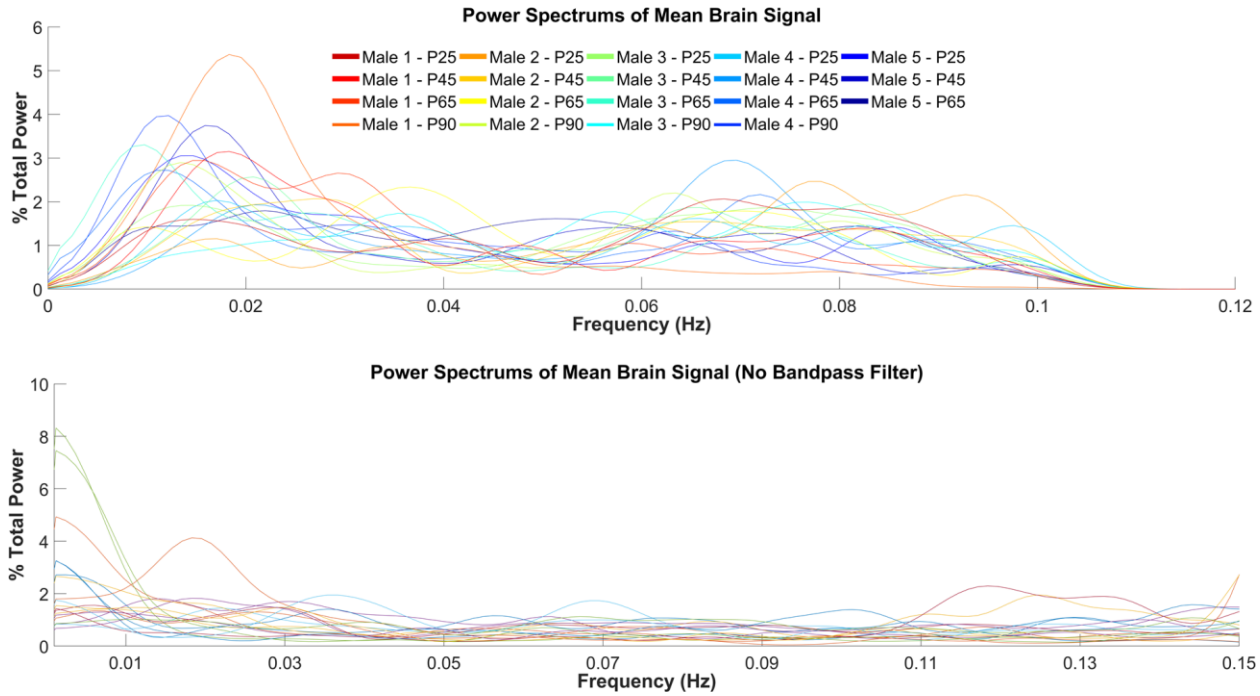

Figure 1.8. Power spectrums of global brain signal. **Top:** power spectrums after bandpass filtering [0.008, 0.1 Hz]. **Bottom:** power spectrums before bandpass filtering (but with linear and quadratic detrending).

Discussion

In sum, careful consideration of the prior literature, pilot scanning to optimize scan parameters, and custom software development allowed us to obtain valid longitudinal rs-fMRI measurements in the zebra finch songbird. The careful consideration of prior literature led us to select an SE, as opposed to GE, pulse sequence, so as to avoid susceptibility artifacts and to improve the spatial specificity of BOLD signals. A combination of pilot scanning and consideration of prior validations in the fMRI literature allowed us to select a TE and TR that provided an optimal tradeoff between BOLD sensitivity, *tSNR*, and temporal resolution. State-of-the-art normalization techniques provided by ANTs allowed us to build a custom brain template and to register our brain images into a common space for analysis. Finally, the custom NeuroViz and MRIqual toolboxes allowed us to (1) digitally extract the group-wise brain template from surrounding tissue, (2) manually trace a set of twenty ROIs, (3) create state-of-the-art

visualizations of 2D and 3D data, (4) conduct *tSNR* validation analyses, and (5) conduct power spectral analyses. Collectively, these methodological innovations allowed us to collect, validate, and prepare our rs-fMRI data for the subsequent theoretically-driven studies detailed in Chapters 2 and 3 of this dissertation.

CHAPTER 2 - INTERHEMISPHERIC FUNCTIONAL CONNECTIVITY IN THE ZEBRA FINCH BRAIN, ABSENT THE CORPUS CALLOSUM IN NORMAL ONTOGENY

A version of this chapter was published in NeuroImage, *195, 113-127* (2019).

Co-authors: **Schertz, K.E., London, S.E., & Berman, M.G.**

Introduction

Bilaterally symmetric neural activity is among the most striking characteristics of the Eutherian (i.e., placental) mammalian brain's intrinsic functional architecture. This pattern is consistently observed both in humans (Shen et al., 2015; Stark et al., 2008; Zhang et al., 2014; Zuo et al., 2010) and in other mammalian species such as macaques (Shen et al., 2015; Vincent et al., 2007) and rodents (Matsui et al., 2016; Pan et al., 2011). Symmetric brain activity is typically studied by examining temporal correlations (i.e., FC) embedded within intrinsic (i.e., spontaneous) infra-slow (< 0.1 Hz) brain activity, conveniently recorded as BOLD signals from rs-fMRI (Biswal et al. 1995, 2010; Mitra et al. 2018). However, consistent results are also obtained using other methods, such as wide-field calcium imaging (Matsui et al., 2016) and local field potentials (LFP; Pan et al., 2011). FC between geometrically corresponding, bilateral brain regions is termed homotopic FC (Shen et al., 2015; Stark et al., 2008; Zhang et al., 2014; Zuo et al., 2010). Homotopic FC is: 1) generally much stronger than either ipsilateral or asymmetric interhemispheric (i.e., heterotopic) FC (Shen et al., 2015; Stark et al., 2008; Zhang et al., 2014), 2) more stable across various task and non-task settings than ipsilateral or heterotopic FC (Mišić et al., 2014; Shen et al., 2015), and 3) important for shaping whole-brain network dynamics (Zhang et al., 2014). Homotopic FC also appears to be clinically relevant, with reductions in

homotopic FC implicated in diverse human neuropsychiatric (Kelly et al., 2011; Zhang et al., 2014) and neurodegenerative (Zhou et al., 2013) disorders.

FC is only moderately linked to structural connectivity (SC), such as white matter projections ($r \approx 0.50$; Honey et al. 2009), and FC is also capable of arising from functional interactions traversing indirect polysynaptic SC pathways (Honey et al., 2009; Lu et al., 2011; Vincent et al., 2007). Nonetheless, substantial evidence indicates that the direct homotopic SC of the CC (Jarbo et al. 2012) largely mediates homotopic FC in Eutherian mammals. Strong causal evidence supporting the importance of the CC for mediating homotopic FC comes from cases of intractable epilepsy in which the CC was therapeutically severed (i.e., callosotomy). Pre- vs. post-operative rs-fMRI scans revealed that homotopic FC was almost completely abolished following complete callosotomy (Johnston et al., 2008) and markedly reduced following partial callosotomy (Roland et al., 2017). Long-term follow-up (2-7 years postoperative) in a subset of cases revealed no recovery of homotopic FC (Roland et al. 2017; but also see Uddin et al. (2008), a single case report of partially recovered homotopic FC 45 years postoperative, and Casimo et al. (2018), a single case report of preserved FC after incomplete anterior callosotomy). The importance of the CC as a structural mediator of homotopic FC has also been evidenced in healthy humans and macaques; specifically, the signal conduction efficacy of intact CC fibers is positively associated with homotopic FC magnitude (Hermesdorf et al., 2016; Shen et al., 2015).

Nevertheless, homotopic FC's reliance on the CC as a structural substrate appears to be somewhat region-specific, and alternative SC permits the maintenance of homotopic FC in some regions following CC damage. For example, homotopic FC between multimodal regions of frontal and parietal cortices is almost completely abolished following callosotomy, whereas homotopic FC between sensorimotor and primary visual areas is generally reduced, yet

somewhat spared (O'Reilly et al., 2013; Roland et al., 2017). Parallel behavioral evidence from macaques suggests that callosotomy spares the interhemispheric transfer of simple visual information (e.g., color) but impairs interhemispheric transfer of more complex visual stimuli (e.g., visual discrimination learning tasks; Glickstein and Sperry 1960; Glickstein et al. 1998; van der Knaap and van der Ham 2011). It is likely that the anterior commissure (AC; Glickstein et al. 1998; Glickstein 2009; van der Knaap and van der Ham 2011), thalamocortical connections (Toulmin et al., 2015), and/or visuomotor transfer via the cerebellum (Glickstein, 2009; Glickstein et al., 1998; van der Knaap & van der Ham, 2011) mediates this residual interhemispheric transfer. Consistent with a potentially important role of the AC in functional adaptations following callosotomy, O'Reilly et al. (2013) noted that for a single macaque in which the CC was lesioned but the AC was spared, homotopic FC was moderately reduced, but to a lesser extent than for monkeys in which both the CC and AC were lesioned.

In examining the primacy of the CC for homotopic FC, and whether it plays a causal role, a critical distinction must be drawn between evidence obtained from callosotomy patients versus evidence obtained from individuals born without a CC (i.e., callosal dysgenesis/agenesis). Dysgenesis patients often do not exhibit the classic disconnection syndrome characteristic of callosotomy patients, a well-known purported discrepancy sometimes referred to as the Sperry paradox (Paul et al., 2007; Sperry, 1968; Tovar-Moll et al., 2014). Some dysgenesis patients exhibit reduced but not abolished homotopic FC (Paul et al., 2007; Quigley et al., 2003), and some also exhibit analogous functional deficits to callosotomy patients (Paul et al., 2007). Yet, others exhibit near normal homotopic FC and fewer behavioral deficits (Khanna et al., 2012; Tyszka, Kennedy, Adolphs, & Paul, 2011). These mixed findings have been clarified by the discovery of aberrant long-range homotopic structural plasticity, which likely develops during a

CP for axonal targeting *in utero* (Tovar-Moll et al., 2014, p.). In other cases, preserved homotopic FC in dysgenesis, as opposed to complete agenesis, may be attributable to partially preserved CC projections (Khanna et al., 2012; Roland et al., 2017). In sum, evidence supports a causal role for the CC in supporting homotopic FC, but also suggests that aberrant long-range structural plasticity can preserve homotopic FC in cases of CC dysgenesis, and that alternative structural pathways may be capable of at least partially compensating for loss of the CC occurring later in development.

Despite a wealth of evidence gleaned from Eutherian mammals, much less is known regarding the interhemispheric FC of either non-Eutherian mammals (e.g., opossums, platypus, etc.) or non-mammalian vertebrates (e.g., avians and amphibians), all of which lack the evolutionarily novel CC in normal ontogeny (Aboitiz & Montiel, 2003; Luo et al., 2011). Notwithstanding this, many non-mammalian vertebrates demonstrate similarly complex multimodal behaviors as Eutherian mammals, requiring a well-calibrated balance between interhemispheric coordination and hemispheric specialization, functions thought to normally be mediated by the CC (Gazzaniga, 2000; van der Knaap & van der Ham, 2011).

One such behavior is learned vocal communication. In humans, language learning is among the most complex of multimodal distributed brain processes (Geschwind, 1970), and the CC is thought to play a critical role by helping to integrate lateralized processing streams from each hemisphere (Gazzaniga, 2000). Analogously, songbirds such as the zebra finch (*Taeniopygia guttata*) exhibit vocal learning for song, a process with deep genomic, neural, behavioral, developmental, and social parallels with human speech acquisition (Doupe & Kuhl, 1999). Similar to humans, zebra finches exhibit lateralization of vocal learning and auditory processing (Avey et al., 2005; Cynx et al., 1992; Moorman et al., 2015, 2012), yet they also

require tight interhemispheric coordination of premotor activity to enable vocal production (Ashmore, Bourjaily, & Schmidt, 2008). Such functional parallels between Eutherian mammals and non-mammalian vertebrates, which implicate a simultaneous need for both hemispheric specialization and interhemispheric integration, are particularly notable in light of the obvious divergence in SC (i.e., CC vs. no CC). It remains an open question whether non-mammalian vertebrates such as avians exhibit a similar pattern of homotopic FC to Eutherian mammals, despite this clear structural divergence.

Although no CC is present, the avian brain is connected bilaterally by the evolutionarily ancient AC (its largest interhemispheric connection), which connects bilateral regions of the caudal telencephalon (Letzner, Simon, & Güntürkün, 2016). However, in contrast to the mammalian CC, its projections are primarily heterotopically organized and unidirectional (as opposed to reciprocal), with the exception of a relatively small arcopallial and amygdaloid cluster of homotopic SC (notably, these regions are not believed to directly support song learning) (Letzner et al., 2016). Thus, the avian AC provides a less obvious structural substrate for homotopic FC compared to the CC of Eutherian mammals, or even compared to the AC of non-Eutherian mammals, which is more well-developed than the AC of some non-mammalian vertebrates, such as avians or reptiles (Aboitiz & Montiel, 2003; Heath & Jones, 1971; Letzner et al., 2016).

In addition to the AC, some polysynaptic structural pathways have been identified in songbirds which link bilateral regions of the telencephalon via interhemispheric connections within the thalamus, midbrain, and brainstem (Ashmore et al., 2008; Schmidt, Ashmore, & Vu, 2006). However, these are only known to connect a small subset of premotor regions within the telencephalon (Ashmore et al., 2008; Schmidt et al., 2006). Therefore, these structural

connections do not provide an obvious structural substrate for mediating the brain-wide homotopic FC commonly observed in Eutherian mammals, nor for mediating homotopic FC between a more distributed set of song network regions. It thus remains an open question whether additional polysynaptic pathways, linked to either the AC or the sub-telencephalic pathways described, might enable a more widespread distribution of homotopic FC throughout the avian brain, including additional regions of the song network.

Based on evidence obtained from callosotomy and dysgenesis patients, and the observed parallels between species for complex vocal learning, we hypothesized that the zebra finch brain would exhibit a pattern of homotopic FC similar to that of Eutherian mammals, despite lacking the CC. We performed five sets of analyses to examine this hypothesis from multiple angles. First, we tested whether homotopic FC was present within a network of well-characterized brain regions specialized for learned song. Second, we examined whether a set of sub-telencephalic regions (parts of thalamus, midbrain, and hindbrain) that display direct interhemispheric SC show stronger homotopic FC than regions without homotopic SC, as is the case in Eutherian mammals (Shen et al., 2015). Third, we examined whether homotopic FC between particular structurally connected bilateral regions was related to homotopic FC within the song network. Fourth, we complimented ROI analyses by examining homotopic FC across the whole brain using a data-driven voxel-wise analysis, a technique for which *in vivo* neuroimaging is particularly well-suited. Fifth, given that homotopic FC in humans decreases globally from childhood to middle adulthood (Zuo et al., 2010), we used a longitudinal design to investigate whether the zebra finch brain exhibits a similar developmental trajectory across the sensitive period for song acquisition. Critically, non-invasive rs-fMRI allowed us to obtain repeated measures from intact animals across development. In combination, these analyses provide the

strongest test to date of the possibility that polysynaptic connections traversing interhemispheric pathways between sub-telencephalic nuclei, or relying on the largely heterotopic fibers of the avian AC, are sufficient to establish homotopic FC, absent the CC in normal ontogeny.

Methods

Animals

All animal procedures were approved by the Institutional Animal Care and Use Committee of the University of Chicago in accordance with the NIH Guide for the Care and Use of Laboratory Animals. Five male zebra finches (only males sing) were scanned longitudinally at four post-hatch (P) days to capture the approximate beginning, middle, and end of the song learning process (P25, P45, P65, and P90; N=5 each age). A P90 MRI scan was not successfully obtained for one bird, yielding a final sample of 19 functional series. Due to scanner availability limitations, not all birds could be scanned on the exact target days: P25 (range: P24-P26), P45 (range: P44-P46), P65 (range: P64-P67), and P90 (range: P88-P91). All birds were maintained under a 14/10 hour light/dark photoperiod throughout the experiment, with food provided *ad libidum*.

Scanning Procedure

MRI data were collected at the MRIS Facility of the University of Chicago. Zebra finches were anesthetized using an admixture of oxygen and isoflurane gas (anesthesia induction: 1.5-2.25%; maintenance: 1-2%), administered via a tube fitted to the zebra finch beak. This procedure has been widely validated in prior zebra finch fMRI research (Boumans et al. 2007; Poirier et al. 2009, 2010; Van Ruijssevelt et al. 2013; Van Ruijssevelt et al. 2017). For example, Van Ruijssevelt et al. (2017) found that auditory-evoked BOLD responses in zebra finches are similar between isoflurane-anesthetized and awake animals. The shape of hemodynamic

responses in anesthetized animals is known to be similar to that of awake animals (Shtoyerman et al. 2000; Fukuda et al. 2005; Zhao et al. 2007), and resting-state networks such as the default-mode network are well-preserved under a variety of anesthetics (Greicius et al. 2003; Vincent et al. 2007; Boveroux et al. 2010; Martuzzi et al. 2010).

Isoflurane doses varied slightly between birds within the specified range (1-2%), because we noted during pilot scans that doses <1.5% were insufficient to prevent some birds from awakening during scanning (particularly P90's), whereas doses as high as 2% posed a health hazard to some birds (particularly P25's). Thus, isoflurane doses were adjusted for each individual animal to the minimum required to maintain stable physiological readings during scanning. Notably, however, any dose adjustments nearly always occurred prior to functional acquisition, and isoflurane varied during functional acquisition for only a single bird at one time point (bird #4 at P90). We controlled for this variation in a nuisance regression described below (in "Data extraction and denoising").

Following anesthesia administration, birds were fitted with a temperature probe and respiration monitoring pad, allowing for vitals to be monitored throughout the scanning period. A previously validated feedback-controlled heating system within the scanner was used to maintain constant body temperature within the normal physiological range (~40 °C; Poirier et al. 2009, 2010; Van Ruijssevelt et al. 2013; Ruijssevelt et al. 2017).

Imaging Data Acquisition

Neuroimaging data were acquired using a 30 cm bore, 9.4 T Bruker small animal MRI scanner. A TurboRARE-T2 multi-slice anatomical scan was acquired first during each scanning session (TR = 3.5 s, TE = 20 ms, Matrix Size: 256 x 256, in-plane resolution = 70.3 μm x 70.3 μm, slice-thickness = 200 μm, 59 slices, 9 averages). Next, resting-state SE (Poirier & Van der

Linden, 2011) MR images were acquired (TR = 1.07 s, TE = 27 ms (Budde et al., 2014; Jin et al., 2006; Lee et al., 1999), rapid acquisition with refocusing echoes (RARE) Factor = 12 (3 repetitions per acquisition), Matrix Size: 128 x 36, in-plane resolution = 141 μm x 500 μm, slice-thickness = 750 μm, 15 slices). Slices were acquired in an interleaved, ascending order. 180 volumes were acquired consecutively with an effective sampling rate of one volume per 3.20 seconds and a total resting-state scan time of 9.60 minutes. To avoid T1-equilibration effects, the first five volumes of each functional series were discarded.

The sampling rate utilized represented a trade-off between image structural resolution, full brain coverage, and scanner limitations, versus temporal resolution. Although our sampling rate was slower than the two-second TR often used in human neuroimaging studies, it still easily met the Nyquist criterion for alias free signal sampling. Specifically, for a bandwidth of 0.092 Hz (0.008-0.10 Hz passband), which is commonly used to define rs-fMRI frequencies of interest, a Nyquist rate of 0.184 Hz (2 times the bandwidth, equivalent to one sample every 5.43 seconds) is needed to successfully resolve the underlying function without aliasing. It is also worth noting that the fastest of the slow hemodynamic fluctuations measured in the resting-state (0.1 Hz) complete one cycle every 10 seconds.

Preprocessing

Image preprocessing was completed using a combination of ANTs (Avants et al. 2009, 2011), Statistical Parametric Mapping (SPM12; Penny et al. 2011), and custom Matlab scripts. First, DICOM files were converted to NIfTI format using the MRIqual toolbox. Second, the "N4" bias field correction algorithm (Tustison et al., 2010) was used to correct images for magnetic field intensity inhomogeneity. Third, an average of the bias-corrected anatomical scans was selected as an unbiased starting point for SyGN (Avants et al. 2010) and template-building

using ANTs. This process involved iteratively registering each anatomical scan to a custom brain template using affine and nonlinear transformations. As image registration improved, the custom template was recursively updated in each iteration. Cross-correlation was implemented as the similarity metric for image comparison, and four template construction iterations were completed.

Fourth, functional scans were corrected for slice timing differences using SPM (Johnstone et al., 2006; Sladky et al., 2011). Fifth, each 3D functional volume was realigned to the first volume in its series using ANTs, and the six rigid-body motion parameters were retained for later nuisance regression. Sixth, the first functional volume of each series was co-registered to the corresponding bias-corrected anatomical volume via affine transformation in ANTs. To minimize the number of interpolations applied, all affine and nonlinear transformations obtained from functional realignment, coregistration, and structural normalization were combined into 3D volume-specific deformation fields using the ANTs routine "antsApplyTransforms." Seventh, deformation fields were applied in a single step to each slice timing corrected 3D functional volume. Lastly, we assessed the quality and consistency of spatial normalization by computing voxel-wise Pearson correlations between the custom template and normalized anatomical scans across voxels (r_{mean} = 0.94, SD = 0.01, r_{min} = 0.91), as well as between the normalized functional scans averaged across time and the custom template (r_{mean} = 0.87, SD = 0.02, r_{min} = 0.81). These analyses indicated a robust and consistent spatial normalization across scans.

Data Preparation

Regions of interest (ROIs). As described in Chapter 1, coauthor S. E. L. manually delineated six key components of the zebra finch song network within each hemisphere. These ROIs included two sensory processing areas (1. Field L and 2. auditory forebrain (here defined

as NCM and CM), three sensorimotor regions (1.
lateral magnocellular nucleus of the anterior nidopallium (LMAN), 2. Area X, and 3. HVC (used as a proper name)), and one premotor region (1. robust nucleus of the arcopallium (RA)). Tract tracing studies have indicated that these regions do not exhibit homotopic SC (Ashmore et al., 2008; Schmidt et al., 2006; Striedter & Vu, 1998; Wild, Li, & Eagleton, 1997), and therefore they will henceforth be referred to as "homotopic non-structurally connected" (*homotopic-nSC*) ROIs. We also delineated four additional bilateral ROIs that include brain areas known to receive bilateral inputs and/or direct homotopic SC: the medulla, medial diencephalon, thalamic nucleus uvaeformis (Uva), and the dorsomedial nucleus of the intercollicular complex (DM) (Ashmore et al., 2008; Striedter & Vu, 1998; J. M. Wild, Li, & Eagleton, 1997; J. Martin Wild, Williams, & Suthers, 2000). These latter ROIs will henceforth be referred to as "homotopic structurally connected" (*homotopic-SC*) ROIs. This procedure yielded twenty ROIs total, comprised of ten bilateral homotopic pairs. Finally, in addition to these ROIs, co-author S. E. L. manually traced a conservative cerebrospinal fluid (CSF) mask, comprised of voxels within brain ventricles.

Data Extraction and Denoising

Data extraction and denoising were accomplished using custom Matlab scripts and NIfTI Tools (Shen, 2014) for loading and saving NIfTI files. For each resting-state functional series, BOLD time series were extracted from the voxels comprising each ROI and averaged. We followed the default approach used in CONN Toolbox (Whitfield-Gabrieli & Nieto-Castanon, 2012) by extracting ROI signals from unsmoothed functional data, so as to avoid contamination of the ROI signals with signal from neighboring regions. However, our main results were robust to using either unsmoothed or smoothed functional data for ROI extraction. Next, a nuisance regression was performed in which the six rigid body motion parameters (Bright & Murphy,

2015), the first five principal components of CSF signals (Behzadi, Restom, Liau, & Liu, 2007; Layden et al., 2017; Whitfield-Gabrieli & Nieto-Castanon, 2012), linear and quadratic trends (Tanabe, Miller, Tregellas, Freedman, & Meyer, 2002), and body temperature were removed from each ROI time series. The residual ROI time series were then bandpass filtered (range: 0.008 to 0.1 Hz; Hallquist et al. 2013) using the bst_bandpass_filtfilt function from Brainstorm (Tadel, Baillet, Mosher, Pantazis, & Leahy, 2011). See Figure 2.1 for a visual depiction of this process.

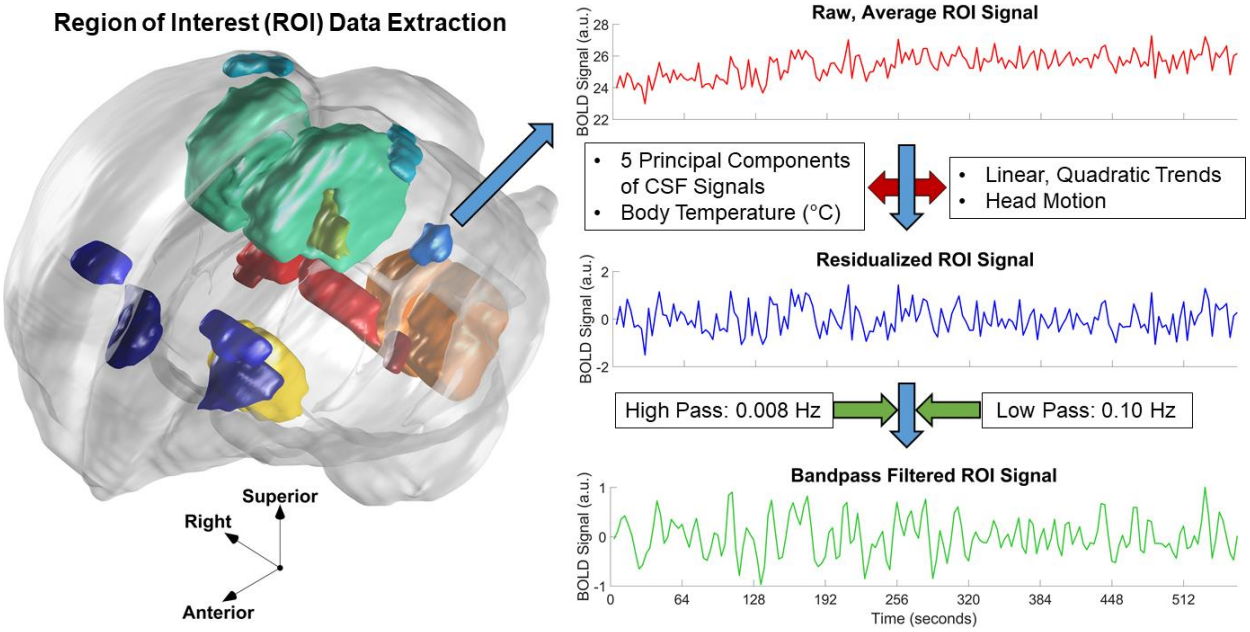

Figure 2.1. Data extraction and preprocessing. *Left:* ROIs displayed within a 3D rendering of the zebra finch brain template. 3D axes show brain orientation. *Right:* The basic data extraction and preprocessing steps are shown using data from left RA in bird 1 at P25. Signals extracted from all voxels of an ROI were averaged (top), nuisance regression was performed (middle), and ROI signals were bandpass filtered (bottom).

FC of Anatomical Connections

Anatomical connectivity is known to moderately predict FC at rest in humans (Honey et al., 2009). However, distinct brain networks are associated with the resting-state as compared to various task states (Greicius, Krasnow, Reiss, & Menon, 2003). Therefore, it is uncertain to what

extent we might expect to observe FC between previously delineated premotor and motor pathways during the resting-state. However, we proceeded to investigate whether there was consistency between the FC measured in the present study and SC known from prior research.

In particular, an ipsilateral projection from HVC to RA comprises an important component of the descending motor pathway for song production, and this anatomical connection has been observed previously using diffusion tensor imaging in starlings (De Groof et al., 2006). Notably, projections from HVC to RA do not project into RA until after ~P30, and they are thought to increase in density and conduction efficacy from P30 to adulthood (≥ P90; Mooney and Rao 1994). Therefore, we restricted our search for any analogous FC between HVC and RA to birds P45 or older, and we additionally investigated whether FC increased with age.

Another widely studied anatomical pathway is the projection from LMAN to RA, a connection crucial for song learning during development but less involved in stereotyped song production during adulthood (Aronov, Andalman, & Fee, 2008). This projection is known to be present as early as P15 (Mooney & Rao, 1994) but becomes functionally less important as song becomes crystalized (Aronov et al., 2008). We thus investigated whether FC between LMAN and RA was present across all ages. Finally, we also investigated FC between another prominent ipsilateral structural connection between Field L (primary auditory region) and auditory forebrain (association auditory region) (Vates, Broome, Mello, & Nottebohm, 1996).

We utilized one-sample *t*-tests to determine whether FC was positive and significant across birds for these known structural connections. Also, we used a linear mixed-effects (LME) model to examine the fixed-effect of age on HVC to RA FC, controlling for a random intercept for bird. Additional investigations of known ipsilateral projections are detailed in Table 2.1.

Homotopic FC Analyses

ROI-to-ROI FC was computed separately for each bird at each age. FC was defined as the Fisher's *Z*-transformed Pearson correlation between the preprocessed time series of a pair of ROIs. This FC measure reliably detects homotopic FC in Eutherian mammals (Shen et al., 2015; Stark et al., 2008; Zuo et al., 2010) and provides results consistent with alternative measures of brain connectivity (Matsui et al., 2016; Pan et al., 2011).

We first sought to determine whether homotopic FC is relatively stronger than ipsilateral or heterotopic FC across the ROIs of the zebra finch brain, as has been shown consistently in Eutherian mammals. To do so, we implemented an LME random-intercept model in which ROI-to-ROI FC across all ROIs served as the criterion variable. Connection type (homotopic, heterotopic, and ipsilateral) was entered as a three-level nominal fixed-effect, with ipsilateral coded as the reference category. We also controlled for the fixed-effect of age and included a random intercept for bird to account for repeated measures. This LME model was optimized for maximum likelihood using the Matlab function "fitlme." A contrast was performed for the effect of homotopic vs. ipsilateral FC. We then redefined heterotopic as the reference category for the connection type variable, so that an effect size for the homotopic vs. heterotopic FC contrast could also be estimated. Finally, we also report the main effect of connection type based on a likelihood-ratio drop-test.

Additional Controls

We sought to control for a variety of nuisance factors known to influence resting-state FC. For instance, the Euclidean distance between a pair of ROIs is known to be inversely associated with the FC strength of the pair (Honey et al., 2009; Mišić et al., 2014; Salvador, Suckling, Schwarzbauer, & Bullmore, 2005). Additionally, increased ROI volume is associated

with increased FC strength (Salvador et al., 2008; Wang et al., 2009). Therefore, we added these covariates to our previously described LME model. Additionally, we added isoflurane dose and average body temperature over the duration of functional acquisition as additional covariates for our LME model.

FC of Individual Homotopic Connections

To examine whether homotopic FC was specific to a subset of ROIs or presented as a more global feature of the zebra finch brain, we computed one-sample *t*-tests to determine whether the FC of each individual homotopic ROI pair significantly differed from zero across birds and ages. We corrected for multiple comparisons across homotopic connections using the false discovery rate (FDR). Next, we constructed a grand mean ROI-to-ROI FC network by averaging Fisher's *Z* values across birds and ages (Figure 2.2). This grand mean FC network was thresholded at $p < 0.05$ for display purposes.

Isoflurane and Homotopic FC

Our analyses above examined whether homotopic FC was stronger than ipsilateral or heterotopic FC, controlling for any effect of isoflurane dose. Interestingly, however, a recent study found that increasing isoflurane dose from 1.1 to 2% selectively and causally decreased homotopic FC in mice (Bukhari, Schroeter, & Rudin, 2018), consistent with prior correlational results in rats (Hutchison, Hutchison, Manning, Menon, & Everling, 2014). Thus, we added the interaction between connection type and isoflurane dose to our LME model to determine whether increasing isoflurane dose was associated with selectively reduced homotopic FC in the zebra finch.

Homotopic-SC vs. Homotopic-nSC

In humans and macaques, homotopic FC appears to depend on the direct SC of the CC (Johnston et al., 2008; Quigley et al., 2003; Roland et al., 2017; Shen et al., 2015). Thus, to gauge whether homotopic SC also serves to augment homotopic FC in the zebra finch brain, we examined whether FC was significantly stronger between homotopic-SC ROI pairs compared to homotopic-nSC ROI pairs. We implemented an LME model, here considering only the FC of homotopic connections. Connection type was added as a binary categorical variable (homotopic-SC vs. homotopic-nSC), and age and a random intercept for bird were included as covariates. In a follow-up regression, we also included the covariates described in "Additional controls."

Test for Mediation of Homotopic-nSC FC by Homotopic-SC FC

A minority of ipsilateral anatomical connections have been identified that connect homotopic-SC and homotopic-nSC ROIs (Ashmore et al., 2008; Schmidt et al., 2006). Therefore, a natural question is whether FC between homotopic-SC ROIs might indirectly mediate the homotopic FC observed between homotopic-nSC ROI pairs. In particular, the thalamic nucleus Uva is known to make direct ipsilateral projections to HVC while receiving direct bilateral inputs from DM (a midbrain nuclei) and PAm (a medullary nuclei; Schmidt et al. 2006; Ashmore et al. 2008). This circuit is thought to be critical for enabling the interhemispheric coordination of descending motor output for song production (Ashmore et al., 2008; Galvis, Wu, Hyson, Johnson, & Bertram, 2018; Hamaguchi, Tanaka, & Mooney, 2016; Schmidt et al., 2006), although little is known regarding its role in the interhemispheric coordination of intrinsic brain activity. Therefore, we sought to investigate whether Uva homotopic FC or Uva-HVC FC might mediate HVC homotopic FC, as this connection in particular appeared to be the most likely candidate for the mediation of homotopic-nSC FC by homotopic-SC FC. To investigate this

possibility, we first undertook a series of bivariate correlation analyses, examining whether the homotopic FC of bilateral HVC was correlated with 1. L Uva to L HVC ipsilateral FC, 2. R Uva to R HVC ipsilateral FC, 3. Uva homotopic FC, 4. the interaction between Uva homotopy and L Uva to L HVC FC, or 5. the interaction between Uva homotopy and R Uva to R HVC. If merited by the results of this analysis, we planned to subsequently undertake more extensive regression-based mediation analyses.

Homotopy as a Function of Development

In human subjects, global homotopic FC decreases from early childhood through middle adulthood, a trend which may reflect the development of increasing hemispheric specialization (Zuo et al., 2010). Thus, we investigated whether a similar trajectory of changes in homotopic FC might be observed in zebra finches across the developmental time-course of song learning. To do so, we added a term denoting the interaction between age and connection type (Homotopic, Ipsilateral, and Heterotopic) to the LME model described above in section 2.5. We then conducted a follow-up analysis in which we parsed the homotopic connection type into Homotopic-SC and Homotopic-nSC to investigate whether age effects were specific to either type.

Full Model Predicting ROI-to-ROI FC

Finally, to examine homotopic FC when comprehensively controlling for all effects and interactions investigated in previous sections, we implemented an LME model which included all of the following fixed-effects covariates: (1) connection type (homotopic-nSC, homotopic-SC, ipsilateral, heterotopic), (2) age, (3) body temperature, (4) isoflurane dose, (5) Euclidean distance, (6) ROI volume, (7) connection type by age interaction, and (8) connection type by

isoflurane dose interaction. Additionally, a random intercept was included for bird. We examined whether this model could be further reduced to minimize AIC.

Voxel-wise Homotopic FC

To further interrogate the distribution of homotopic FC agnostically, without pre-defined ROIs, we implemented the experimenter-blind voxel-mirrored homotopic connectivity (VMHC; Zuo et al. 2010) analysis, using a combination of custom Matlab scripts, SPM12, the Data Processing & Analysis for (Resting-State) Brain Imaging (DPABI) toolbox, and ANTs. VMHC analysis allowed us to characterize the voxel-wise distribution of homotopic FC across the entire brain. Specifically, VMHC quantifies FC between each voxel in one hemisphere with its mirror-symmetric counterpart in the contralateral hemisphere. The VMHC analysis proceeded as follows: first, a symmetric group-wise brain template was formed by mirroring the right hemisphere of our custom brain template across the midline. Each individual anatomical scan was then renormalized to this symmetric brain template. The transformation parameters obtained from normalization were then applied to each corresponding functional series, using ANTs. Subsequently, each functional scan was smoothed using a Gaussian kernel (0.422 x 1.000 x 1.125 mm FWHM, corresponding to 3 x 2 x 1.5 voxels in functional dimensions) in SPM12 to help account for any registration errors and/or individual-specific brain anatomy. Spatial smoothing may be especially critical for VMHC analysis, given that VMHC compares pairs of symmetric voxels, requiring great spatial precision (Zuo et al., 2010). Additionally, sufficient spatial smoothing is an important assumption of random-field theory-based methods (Eklund, Nichols, & Knutsson, 2016) and helps to overcome potential errors in registration and realignment (Mikl et al., 2008).

Next, Fisher's *Z*-transformed Pearson correlations were computed between each pair of homotopic brain voxels, and voxel-wise *t*-statistics were calculated to summarize the strength of homotopic FC across birds and time points. Finally, all voxels within a distance of 0.281 mm (i.e., four structural voxels, two functional voxels) from either side of the midline were set to zero to avoid obtaining artefactual homotopic FC as a result of spatial smoothing (for FWHM = 0.422 mm, $\sigma \cong 0.179$ mm, yielding an approximate cut-off for signal contamination at 3σ = 0.537 mm, corresponding to 7.64 structural voxels or 3.82 functional voxels).

Significant clusters of homotopic FC were detected using the cluster-extent based thresholding method, as implemented in the DPABI toolbox (primary/voxel-level threshold: *p-uncorrected* < 0.001, family-wise error (FWE)-corrected cluster-extent threshold: *pFWE* < 0.05; Yan et al. 2016). By illuminating regional clusters of homotopic FC, such an analysis has the potential to be informative for future studies investigating putative neural pathways underlying interhemispheric coordination in the avian brain. We next calculated the overlap between significant homotopic FC clusters and our previously delineated homotopic-nSC song ROIs as the number of intersecting voxels divided by the total number voxels included within homotopic-nSC ROIs. To compare this overlap to chance, we utilized a permutation test in which the voxel indices of homotopic FC clusters were randomly permuted 10,000 times, and the proportion of overlap with our homotopic-nSC ROIs was calculated in each case. The original observed overlap proportion was then compared to the null distribution of overlap proportion obtained via permutations to derive a non-parametric *p*-value.

Quantitative Comparison of Voxel-wise Homotopic vs. Ipsilateral and Heterotopic FC

In addition to examining the regional distribution of homotopic FC, we also sought to quantitatively compare the distribution of voxel-wise homotopic FC to the distributions of voxel-

wise ipsilateral and heterotopic FC, in a manner similar to what was done previously for ROI-based analyses. Therefore, we calculated the average voxel-wise FC for each connection type (homotopic, ipsilateral, heterotopic) for each bird, and at each time point. This allowed us to fit a mixed-effects random intercept model in which average FC served as the criterion variable, and fixed-effects predictors were connection type, age, isoflurane dose, and body temperature; a random intercept was included for bird. We examined the main effect of connection type using a likelihood-ratio drop-test, and then we examined the simple effect contrasts for homotopic vs. other connection types. For reference, we also computed the effect size (as Cohen's *d*) of the difference between all voxel-wise homotopic connections and ipsilateral or heterotopic connections across birds.

Full Model for Voxel-wise FC

Finally, we replicated the optimal model for predicting ROI FC (Table 2.3) using average voxel-wise FC. Euclidean distance and ROI volume were ROI-specific measures, and they could not be used in this case given that the criterion variable here was average voxel-wise FC across the whole brain. We therefore implemented an LME random intercept model which included all of the following fixed-effects: (1) connection type (homotopic, ipsilateral, reference: heterotopic), (2) age, (3) body temperature, (4) isoflurane dose, (5) a connection type by age interaction, and (6) a connection type by isoflurane dose interaction. Additionally, a random intercept was included for bird. We examined whether this model could be further reduced to minimize AIC.

Figure Creation

Figures 2.1-2.5 were created using NeuroViz and custom Matlab scripts.

Data and Code Availability

Key fMRI data, analysis code, ROI masks, and the custom group-wise brain template are all openly available from our G-Node Open Data repository (https://doi.org/10.12751/g-node.6b6170).

Results

FC of Anatomical Connections

First, we examined the FC between brain regions known to be connected by ipsilateral SC from invasive tract tracing studies. We noted a trend toward positive FC for L HVC – L RA, an important component of the descending motor pathway for song production, for birds aged P45-90 ($t(13) = 1.82$, $p = 0.091$). Interestingly, the FC of this connection increased significantly with age, from P25 through P90 ($B = 0.47$, $t(17) = 2.33$, $p = 0.032$), consistent with its previously characterized structural developmental trajectory (Mooney & Rao, 1994). However, FC was not significant for the right hemispheric homologue of this connection ($t(13) = 0.23$, $p > 0.80$), nor was there a significant trend with age ($B = 0.03$, $t(17) = 0.13$, $p > 0.80$). We also found that Field L and Auditory Forebrain exhibited robust ipsilateral FC in both hemispheres across birds (R Field L – R Aud. Forebrain: $t(18) = 12.30$, $p < 0.001$; L Field L – L Aud. Forebrain: $t(18) = 6.85$, $p < 0.001$). Notably, despite their close spatial proximity, these ipsilateral connections remained significant after regressing out the effects of Euclidean distance across connections (R Field L – R Aud. Forebrain: $t(18) = 12.80$, $p < 0.001$; L Field L – L Aud. Forebrain: $t(18) = 7.17$, $p < 0.001$). Finally, we failed to find significant FC for LMAN to RA in either hemisphere (both $p > 0.45$). Additional analyses investigating the FC of known structural connections are detailed in Table 2.1.

Table 2.1. Structural and functional connectivity associations

Connection & Test	*t*(*df*)	*p*
L Field L - L Aud. Forebrain	6.85 (18)	< 0.001
R Field L - R Aud. Forebrain	12.30 (18)	< 0.001
L HVC - L RA FC	1.82 (13)	0.092
L HVC - L RA ~ Age	2.33 (17)	0.032
R HVC - R RA FC	0.23 (13)	> 0.80
R HVC - R RA ~ Age	0.13 (17)	> 0.80
L HVC - L Area X FC	0.97 (18)	0.347
R HVC - R Area X FC	1.51 (18)	0.148
L LMAN - L RA FC	-0.64 (18)	> 0.50
R LMAN - R RA FC	-0.74 (18)	> 0.45
L RA - L Medulla FC	0.74 (18)	> 0.45
R RA - R Medulla FC	3.35 (18)	0.004
L Area X - L Medial Diencephalon FC	1.68 (18)	0.110
R Area X - R Medial Diencephalon FC	1.98 (18)	0.063

Homotopic Functional Connections Are Among the Strongest Within the Song Network

To test our first hypothesis, that homotopic FC would be observed among a set of distributed regions important for learned song, we analyzed homotopic FC across the homotopic-nSC regions of the song network. We fit an LME random intercept model predicting ROI-to-ROI FC via connection type (homotopic, ipsilateral, heterotopic), controlling for age and bird-specific effects. This revealed a strong main effect of connection type as evidenced by a likelihood-ratio drop-test ($\chi^2(2) = 91.33$, $p < 0.001$), such that homotopic connections were significantly stronger than either ipsilateral ($B = 0.15$, $t(1250) = 9.08$, $p < 0.001$) or heterotopic connections ($B = 0.16$, $t(1250) = 9.50$, $p < 0.001$). This effect was not explained by the Euclidean distance between ROIs, the average volume of ROI pairs, isoflurane dose, or body temperature. The FC strength of homotopic connections remained higher than that of the other connection types after controlling for these nuisance variables (homotopic vs. ipsilateral: $B = 0.17$, $t(1246) = 10.62$, $p < 0.001$;

homotopic vs. heterotopic: $B = 0.12$, $t(1246) = 7.45$, $p < 0.001$), and the main effect of connection type remained significant ($\chi^2(2) = 109.45$, $p < 0.001$).

We next analyzed the FC of individual homotopic ROI pairs. One-sample *t*-tests revealed significant positive FC among all homotopic ROI pairs after correction for multiple comparisons using FDR. Average homotopic FC values (mean Fisher *Z*-transformed correlations) and FDR-corrected *p*-values (*pFDR*) were as follows: Area X ($Z = 0.19$, $pFDR < 0.001$), LMAN ($Z = 0.17$, $pFDR = 0.001$), RA ($Z = 0.06$, $pFDR = 0.012$), HVC ($Z = 0.16$, $pFDR = 0.002$), Auditory Forebrain ($Z = 0.48$, $pFDR < 0.001$), and Field L ($Z = 0.15$, $pFDR = 0.001$). Figure 2.2 displays FC values for the entire song network thresholded at $p < 0.05$ for display purposes.

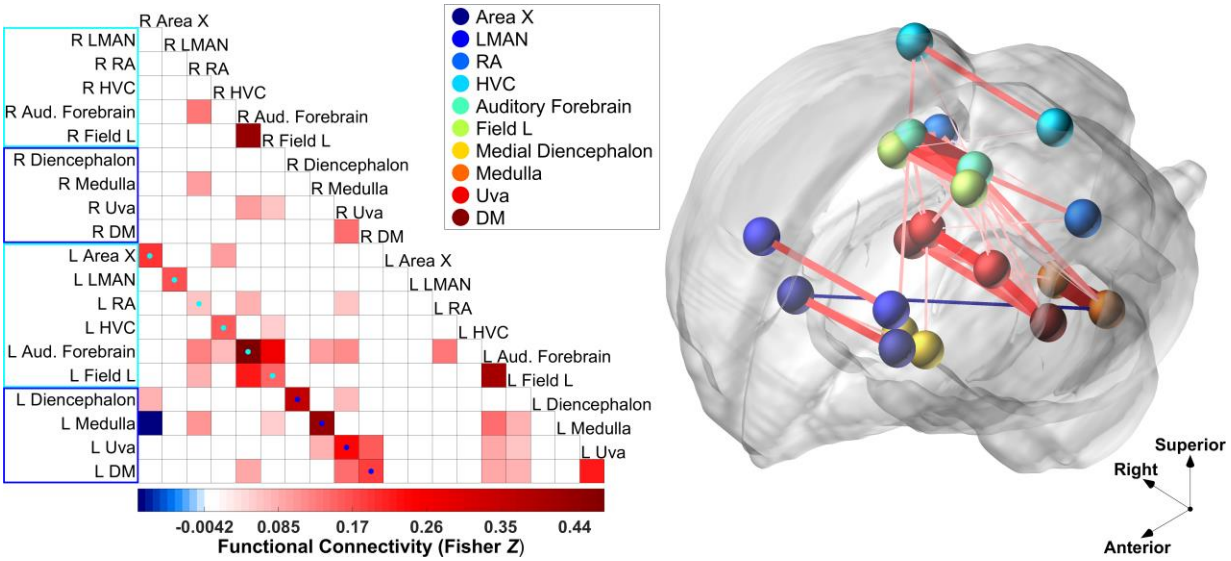

Figure 2.2. A prominent pattern of homotopic functional connectivity. *Left:* The grand mean FC matrix thresholded at *p-uncorrected* < 0.05. The blue-red color scale corresponds to average Fisher *Z*-transformed Pearson product-moment correlations across all birds and ages. Homotopic connections are displayed on the diagonal highlighted by teal and blue dots. Teal boxes and dots: the song network ROIs (no direct homotopic SC) and homotopic connections, respectively. Blue boxes and dots: homotopic-SC ROIs and homotopic connections, respectively. *Right:* The grand mean FC network overlaid on a 3D rendering of the group-average brain template. Spheres are located at the centroids of each corresponding ROI listed in the legend. Connections depict the Fisher *Z* values (left panel), with both line thickness and color proportional to the association strength. 3D axes show brain orientation.

Isoflurane and Homotopic FC

Although the main effect of isoflurane dose was not significant in the model described above (B = -0.02, $t(1246)$ = -1.29, $p > 0.19$), we next examined whether isoflurane dose interacted with connection type, as has been found in prior literature. We found that the overall interaction between isoflurane dose and connection type, as measured by a likelihood-ratio drop-test, was significant ($\chi^2(2) = 8.24$, $p = 0.016$). Higher isoflurane doses were associated with selectively lower homotopic FC, relative to either ipsilateral (B = -0.12, $t(1244)$ = -2.41, p = 0.016) or heterotopic FC (B = -0.14, $t(1244)$ = -2.87, p = 0.004). In contrast, isoflurane dose was not differentially associated with heterotopic versus ipsilateral FC (B = -0.02, $t(1244)$ = -0.80, $p > 0.40$). Notably, Homotopic FC remained stronger than ipsilateral (B = 0.42, $t(1244)$ = 4.64, $p < 0.001$) or heterotopic (B = 0.34, $t(1244)$ = 3.69, $p < 0.001$) FC after controlling for the interaction between isoflurane dose and connection type.

SC predicts stronger homotopic FC in zebra finches

As expected, all homotopic-SC ROIs exhibited significant homotopic FC (all $pFDR < 0.05$; Figure 2.2). More interestingly, homotopic-SC connections demonstrated significantly stronger FC than homotopic-nSC connections (B = 0.10, $t(187)$ = 2.97, p = 0.003; Figure 2.3) even after controlling for nuisance covariates (B = 0.07, $t(183)$ = 2.18, p = 0.030).

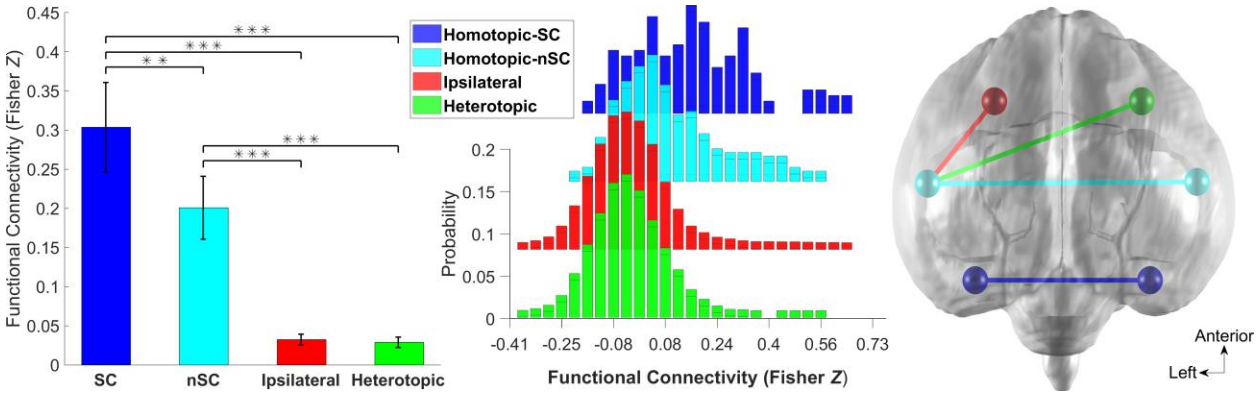

Figure 2.3. The relative functional connectivity of each connection type. *Left:* Bar plot showing mean FC values as Pearson product-moment correlations apportioned by connection type. Error-bars represent 95% confidence intervals. *** = $p < 0.001$, ** = $p < 0.01$. Effect sizes for the contrast between homotopic-SC and other connection types were as follows: $d = 0.44$ (homotopic-nSC), $d = 1.77$ (ipsilateral), $d = 1.89$ (heterotopic). Effect sizes for the contrast between homotopic-nSC and other connection types were as follows: $d = 1.10$ (ipsilateral), $d = 1.19$ (heterotopic). *Middle:* Histograms showing the distribution of FC values for each connection type. Histogram bins were normalized as the probability of FC of a given magnitude for each connection type. *Right:* A schematic illustrating each connection type overlaid on a superior view of the zebra finch brain template. Axes show brain orientation.

No Evidence that Homotopic-SC Connections Mediate Homotopic-nSC Connections

Across birds, HVC homotopic FC was uncorrelated with: 1. R Uva to R HVC ipsilateral FC ($r(17) = -0.01$, $p > 0.90$), 2. L Uva to L HVC ipsilateral FC ($r(17) = -0.16$, $p > 0.50$), 3. Uva homotopic FC ($r(17) = 0.18$, $p > 0.45$), 4. the interaction between Uva homotopy and R Uva to R HVC FC ($r(17) = 0.12$, $p > 0.60$), and 5. the interaction between Uva homotopy and L Uva to L HVC FC ($r(17) = -0.09$, $p > 0.70$). Thus, our results offered no indication that the FC of homotopic-SC ROIs, specifically involving Uva, mediated the homotopic FC of HVC. As such, we did not consider these results to merit more extensive regression-based mediation analyses.

Homotopy as a Function of Development

To investigate the developmental trajectory of homotopic FC, we added an age by connection type interaction to the random intercept model described previously, again controlling for effects of Euclidean distance between ROIs, the average volume of ROI pairs,

isoflurane dose, and body temperature. The interaction main effect was significant, as evidenced by a likelihood-ratio drop-test ($\chi^2(2) = 6.95$, $p = 0.031$). Consistent with human findings, zebra finch homotopic FC decreased significantly more with age than did ipsilateral ($B = -0.0012$, $t(3600) = -2.59$, $p = 0.010$) or heterotopic ($B = -0.0010$, $t(3600) = -2.10$, $p = 0.035$) FC. In contrast, heterotopic and ipsilateral FC did not developmentally differ ($B = -0.0002$, $t(3600) = -1.08$, $p > 0.25$).

A follow-up analysis, in which homotopic connections were parsed into homotopic-SC and homotopic-nSC sub-types, again revealed a significant age by connection type interaction ($\chi^2(3) = 16.09$, $p = 0.001$). Interestingly, analysis of simple effects revealed that homotopic-SC connections decreased significantly with age ($B = -0.0028$, $t(3598) = -3.98$, $p < 0.001$), whereas homotopic-nSC connections did not ($B = -0.0001$, $t(3598) = -0.20$, $p > 0.80$).

Full Model

Finally, to examine homotopic FC when comprehensively controlling for all fixed-effects and interactions investigated in previous sections, we implemented an LME model which included all of the following fixed-effects covariates: (1) connection type (homotopic-nSC, homotopic-SC, ipsilateral, heterotopic), (2) age, (3) body temperature, (4) isoflurane dose, (5) Euclidean distance, (6) ROI volume, (7) connection type by age interaction, and (8) connection type by isoflurane dose interaction. Additionally, a random intercept was included for bird. We found that this model was not further reducible based on AIC (i.e., AIC was increased by removing any predictor). Model parameters are displayed in Table 3 below.

Table 2.2. Full model including all fixed-effects covariates

Fixed Effects	Estimate	*SE*	*β*	*T*	*p*	95% CI
Intercept	0.4868	0.1069	-	4.55	<0.001	[0.277, 0.697]
Homotopic-nSC	0.3851	0.0829	0.93	4.65	<0.001	[0.223, 0.548]
Homotopic-SC	0.6248	0.1005	1.38	6.21	<0.001	[0.428, 0.822]
Ipsilateral	-0.0280	0.0294	-0.13	-0.95	0.340	[-0.086, 0.030]
Age	0.0003	0.0002	0.04	1.55	0.120	[-0.000, 0.001]
Body Temperature	-0.0086	0.0028	-0.06	-3.05	0.002	[-0.014, -0.003]
Isoflurane	-0.0265	0.0122	-0.05	-2.18	0.029	[-0.050, -0.003]
Euclidean Distance	-0.0220	0.0017	-0.21	-12.76	<0.001	[-0.025, -0.019]
ROI Volume	0.0165	0.0015	0.16	10.88	<0.001	[0.014, 0.019]
Homotopic-nSC:Age	0.0003	0.0006	0.04	0.43	0.670	[-0.001, 0.001]
Homotopic-SC:Age	-0.0024	0.0007	-0.36	-3.35	0.001	[-0.004, -0.001]
Ipsilateral:Age	-0.0003	0.0002	-0.04	-1.21	0.227	[-0.001, 0.000]
Homotopic-nSC:Isoflurane	-0.1410	0.0456	-0.28	-3.09	0.002	[-0.230, -0.052]
Homotopic-SC:Isoflurane	-0.1538	0.0552	-0.30	-2.78	0.005	[-0.262, -0.046]
Ipsilateral:Isoflurane	0.0116	0.0161	0.02	0.72	0.473	[-0.020, 0.043]

Random Effects

Groups	Name	Std. Dev.	95% CI
Bird	Intercept	0.005	[0.001, 0.023]
Error	Residual	0.142	[0.139, 0.146]

Note. *DFE* = 3595, R^2 = 0.179, *Adjusted* R^2 = 0.176

A Medially-biased, Brain-wide Pattern of Homotopic FC

VMHC analyses revealed a distributed pattern of homotopic FC, notably similar to the voxel-wise pattern observed in the human brain (Stark et al., 2008; Zuo et al., 2010). For example, homotopic FC appeared to be more pronounced within medial portions of the zebra finch brain (Zuo et al., 2010), spanning the medulla to the superior telencephalon, with lesser homotopic FC observable in more lateral regions (Figure 2.4). Similar to the findings of Zuo et al. (2010) in humans, a single, large significant cluster of homotopic FC was identified which encompassed 87.8% of the total brain volume (primary threshold: $p < 0.001$, cluster-extent threshold: $pFWE < 0.05$) (Figure 2.4). The proportion of voxels within this cluster that overlapped with song network ROIs (5.38%) exceeded that which would be expected by chance

(*Mdn* null overlap: 4.84%, 95% CI = [4.80%, 4.87%], $p < 0.0001$).

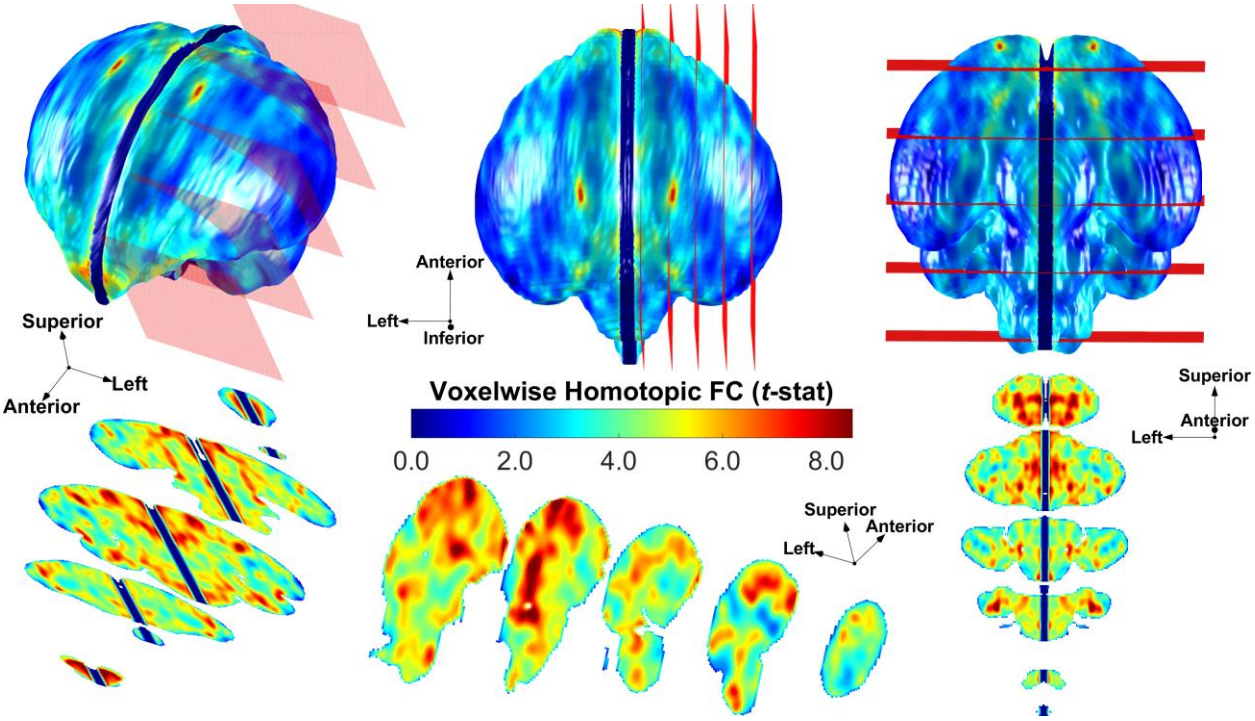

Figure 2.4. Zebra finch voxel-mirrored homotopic connectivity. *Top row:* three views (*left:* left lateral/anterior diagonal view, *middle:* dorsal view, *right:* posterior view) of a 3D rendering of the zebra finch brain template, with homotopic FC (as *t*-statistics from one-sample tests for homotopic FC across birds and ages) plotted on its surface. Red meshes indicate the location of slices used for the bottom row of plots. *Bottom row*: three slice orientations (*left:* coronal, *middle:* sagittal, *right:* axial) depicting homotopic FC. 3D axes display panel orientation. A single, large significant cluster of homotopic FC was identified, encompassing 87.8% of the total brain volume (primary threshold: $p < 0.001$, cluster-extent threshold: $pFWE < 0.05$). The color bar [range: 0-8.5] indicates the color-scaling of *t*-statistics.

Voxel-wise Homotopic FC is Stronger than Ipsilateral or Heterotopic FC

An LME random intercept model was fit in which average voxel-wise FC served as the criterion variable, and fixed-effects predictors included connection type, age, isoflurane dose, and body temperature; a random intercept was included for bird. The main effect of connection type was significant ($\chi^2(2) = 58.14$, $p < 0.001$). Simple effect contrasts revealed that homotopic FC was significantly stronger than either ipsilateral FC ($B = 1.51$, $t(51) = 8.43$, $p < 0.001$) or heterotopic FC ($B = 1.63$, $t(51) = 9.08$, $p < 0.001$), whereas heterotopic and ipsilateral FC were

not significantly different (B = -0.12, $t(51)$ = -0.65, p > 0.50). The voxel-wise distributions of FC for each connection type are displayed in Figure 2.5.

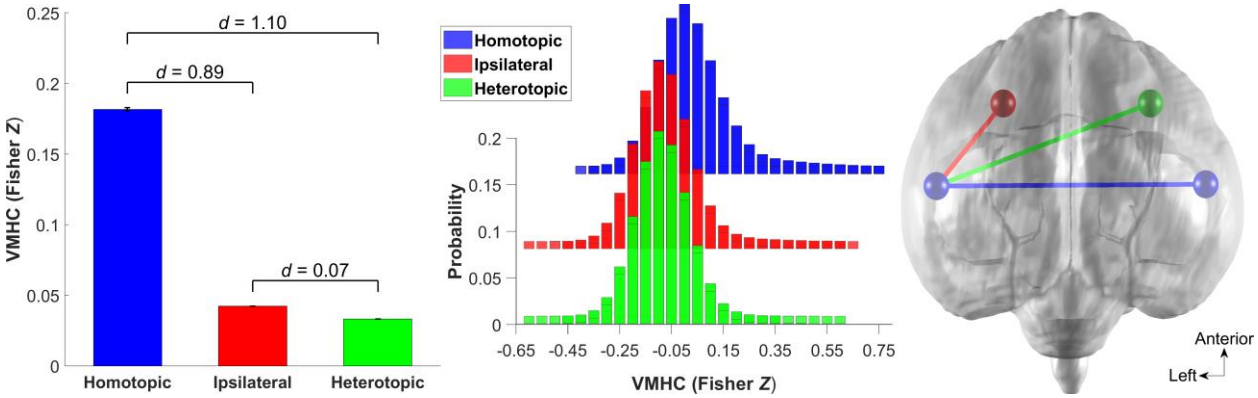

Figure 2.5. Voxel-mirrored homotopic connectivity strength by connection type. *Left:* Bar plot showing mean voxel-wise FC values as Fisher *Z*-transformed Pearson correlations apportioned by connection type. Error-bars represent 95% confidence intervals, and Cohen's *d* effect sizes are displayed above each connection type contrast. *Middle:* Histograms showing the distribution of FC values for each connection type. Histogram bins were normalized as the probability of FC of a given magnitude for each connection type. *Right:* A schematic illustrating each connection type overlaid on a superior view of the zebra finch brain template. Axes show brain orientation.

Full Model for Voxel-wise FC

Finally, we replicated the optimal model for predicting ROI FC (Table 2.3), here using average voxel-wise FC. Euclidean distance and ROI volume were ROI-specific measures, and they could not be controlled for in this case, given that the criterion variable here was average voxel-wise FC across the whole brain. We therefore implemented an LME random intercept model which included all of the following fixed-effects covariates: (1) connection type (homotopic, ipsilateral, heterotopic), (2) age, (3) body temperature, (4) isoflurane dose, (5) a connection type by age interaction, and (6) a connection type by isoflurane dose interaction. Additionally, a random intercept was included for bird. We then proceeded to reduce the model by minimizing AIC, assuring that nested models were significantly different based on likelihood-ratio drop-tests: (1) the age by connection type interaction was not significant ($\chi^2(2)$ = 1.00, p >

0.60) and was dropped (ΔAIC = 3.00; Burnham and Anderson 2004); (2) the main effect of age was not significant (B = 0.003, $t(49)$ = 0.88, $p > 0.35$) and was dropped (ΔAIC = 1.23). The model was not further reducible based on AIC (i.e., dropping additional predictors yielded higher AIC), thus yielding the final model displayed in Table 2.3 below.

Consistent with ROI-based analyses, homotopic FC was significantly stronger than heterotopic FC (B = 4.92, $t(50)$ = 5.34, $p < 0.001$), whereas ipsilateral and heterotopic FC were not significantly different (B = 0.15, $t(50)$ = 0.16, $p > 0.85$). Also consistent with ROI-based analyses, we noted a significant isoflurane dose by connection type interaction ($\chi^2(2) = 14.99$, $p < 0.001$), such that higher isoflurane dose was associated with selectively reduced homotopic FC, relative to heterotopic FC (B = -1.83, $t(50)$ = -3.63, $p < 0.001$). In contrast, ipsilateral and heterotopic FC did not significantly differ based on isoflurane dose (B = -0.017, $t(50)$ = -0.03, $p > 0.90$).

Table 2.3. Voxel-wise functional connectivity model

Fixed Effects	**Estimate**	***SE***	***β***	***T***	***P***	**95% CI**
Intercept	8.8938	2.5355	-	3.51	0.001	[3.801, 13.986]
Ipsilateral	0.1468	0.9205	0.12	0.16	0.874	[-1.702, 1.996]
Homotopic	4.9166	0.9205	1.63	5.34	<0.001	[3.068, 6.765]
Isoflurane	0.1373	0.3750	0.04	0.37	0.716	[-0.616, 0.890]
Body Temperature	-0.2401	0.0648	-0.27	-3.71	0.001	[-0.370, -0.110]
Ipsilateral:Isoflurane	-0.0168	0.5054	-0.01	-0.03	0.974	[-1.032, 0.998]
Homotopic:Isoflurane	-1.8330	0.5054	-0.57	-3.63	0.001	[-2.848, -0.818]

Random Effects			
Groups	**Name**	**Std. Dev.**	**95% CI**
Bird	Intercept	0.111	[0.021, 0.599]
Error	Residual	0.480	[0.369, 0.582]

Note. *DFE* = 50, R^2 = 0.769, *Adjusted* R^2 = 0.742

Discussion

To our knowledge, these results provide the first indication of widespread homotopic FC in a non-Eutherian brain at rest. Non-invasive rs-fMRI enabled us to obtain repeated measures

across development from the same intact male zebra finches, and allowed us to conduct voxel-wise analyses to examine the spatial distribution of homotopic FC across the entire zebra finch brain. We noted robust homotopic FC throughout a brain network necessary for learned song, and follow-up analyses revealed that, consistent with Eutherian brain connectivity (Honey et al., 2009; Shen et al., 2015), homotopic FC was stronger between regions that also shared homotopic SC. Also, consistent with the developmental increases in lateralization observed in humans from childhood through middle adulthood (Zuo et al., 2010), we found that homotopic FC decreased across development in the zebra finch brain, but this result appeared to be specific to homotopic-SC connections. Beyond extending the finding of homotopic FC across phylogeny, the present results also underline the efficacy of rs-fMRI paradigms for investigating both comparative neuroscience questions and vocal learning in songbirds. The ability to conduct longitudinal investigations during a short sensitive period for vocal development makes the zebra finch an ideal model organism for such investigations.

VMHC analyses revealed that homotopic FC is a brain-wide phenomenon in the zebra finch, apparent even when examined without *a priori* defined ROIs. Interestingly, the voxel-wise distribution of homotopic FC exhibited an apparent medial bias, notably similar to the voxel-wise pattern observed in the human brain (Stark et al., 2008; Zuo et al., 2010). Importantly, the midline homotopic FC observed here was not an artefact of spatial smoothing, as we discarded data within a four-voxel radius of the midline before proceeding to data analyses. Although homotopic FC appeared widely distributed, we also found that the song network exhibited greater spatial overlap with the significant voxel-wise homotopic FC cluster than expected by chance. This provides an initial suggestion that bilateral coordination may be of particular

functional importance for song, a complex and distributed multimodal brain process. Future studies will benefit from the incorporation of song data to further test this intriguing possibility.

Notably, we failed to find evidence to suggest that the FC of sub-telencephalic homotopic-SC connections mediated song network homotopic FC. We examined a well-characterized circuit that links bilateral HVC, relying critically on Uva of the thalamus (Ashmore et al., 2008; Schmidt et al., 2006). Although this circuit did not appear to mediate the homotopic FC observed between bilateral HVC, as measured in terms of intrinsic brain activity, evidence suggests that it likely *does* mediate interhemispheric premotor coordination during vocalization (Ashmore et al., 2008; Schmidt et al., 2006). Thus, it is possible that this pathway represents a task-specific structural mechanism for interhemispheric coordination, as opposed to a more domain-general SC pathway for mediating widespread intrinsic homotopic FC such as that observed here in the resting-state. It is also possible that interhemispheric coordination via Uva SC occurs on a timescale not detectable via rs-fMRI measurements of infra-slow brain activity. However, evidence does suggest that synchronization in the amplitude envelope fluctuations of much faster signals (e.g., Gamma) can be detected by rs-fMRI (Hacker, Snyder, Pahwa, Corbetta, & Leuthardt, 2017; He, Snyder, Zempel, Smyth, & Raichle, 2008; Ko, Darvas, Poliakov, Ojemann, & Sorensen, 2011; Mantini, Perrucci, Gratta, Romani, & Corbetta, 2007; Sadaghiani et al., 2010). In light of these results, an informative topic for future studies would be to investigate additional sub-telencephalic SC pathways that might underlie domain-general interhemispheric coordination of intrinsic, as opposed to task-related, brain activity. For instance, future studies might further explore the role played by the indirect SC of the AC, perhaps with the aid of diffusion imaging (Hamaide et al., 2017).

Interestingly, the reliance of homotopic FC on the CC in Eutherian mammals appears to be somewhat region specific (O'Reilly et al., 2013; Paul et al., 2007; Roland et al., 2017) and resilient to structural insults (Khanna et al., 2012; O'Reilly et al., 2013; Uddin et al., 2008), leading to the suggestion that dual structural mechanisms may underlie homotopic FC in these organisms: (1) a cortical mechanism relying on interhemispheric transfer via the CC, and (2) a subcortical mechanism relying on interhemispheric structural projections between sub-telencephalic regions such as the thalamus, midbrain, brainstem, and/or other subcortical nuclei (Uddin et al., 2008). It has been posited that the former mechanism predominates in normal ontogeny, but that the latter mechanism may compensate in cases of loss or damage of the CC by retaining the transfer of simpler, often unimodal information (Glickstein, 2009; Glickstein et al., 1998; Glickstein & Sperry, 1960; Paul et al., 2007; Uddin et al., 2008). The present results, in an organism that lacks the CC in normal ontogeny, suggest the possibility that the largely heterotopic and much less extensive avian AC (Letzner et al., 2016) may be sufficient for mediating widespread homotopic FC via indirect SC. It is notable that we not only observed robust homotopic FC in the zebra finch brain between primary sensory regions such as Field L, which might be predicted from studies of CC dysgenesis, but also between higher-level processing areas such as the auditory forebrain (here, NCM and CM), among others.

In addition to interhemispheric communication via SC, other potential mechanisms underlying homotopic FC have also been proposed, including 1. brain activity driven by symmetric sensory inputs (Shen et al., 2015; Van Essen, 2005) and 2. neuromodulation by bilaterally symmetric ascending arousal systems (e.g., acetylcholine; Ryan and Arnold 1981; Sakaguchi and Saito 1989; Everitt and Robbins 1997; Shen et al. 2015; Turchi et al. 2018). The first hypothetical mechanism appears unlikely to underlie homotopic FC in the present study,

given that homotopic FC was widespread throughout the brain and not limited to primary sensory regions. Additionally, while registration of sensory input does still occur in songbirds under anesthesia (Boumans et al., 2007; Van Meir et al., 2005), the zebra finches' eyes were closed during scanning, limiting visual input, and foam earplugs were provided to limit scanner noise and auditory input. Although these precautions likely did not eliminate the potential for symmetric sensory input driving brain activity, they at least helped to mitigate this potential.

Although the second hypothetical mechanism is an interesting possibility, a recent study in macaques found that inactivation of ascending arousal systems in one hemisphere leads to a drop in fMRI signal amplitude ipsilaterally, but it does not appear to abolish homotopic FC, nor does it significantly change the shape of well-known resting-state networks (Turchi et al., 2018). These results do not support the notion that ascending arousal systems are critical for homotopic FC in Eutherian mammals. Regardless of which specific mechanism (or combination of mechanisms) underlies homotopic FC in non-Eutherian vertebrates, the zebra finch, which lacks the CC in normal ontogeny, and which presumably also lacks any compensatory structural plasticity observed in callosal dysgenesis (Tovar-Moll et al., 2014), provides an ideal model organism for investigating the role of alternative mechanisms to direct SC that may also contribute to interhemispheric coordination.

Notably, we designed our scanning paradigm to utilize a light dose of isoflurane anesthesia based on prior work demonstrating the validity of this procedure for zebra finch fMRI (e.g., Boumans et al. 2007; Poirier et al. 2009, 2010). Prior work in mammals has found that isoflurane reduces the magnitude of hemodynamic responses, but their shape remains similar to that of awake animals (Fukuda et al., 2005; Shtoyerman, Arieli, Slovin, Vanzetta, & Grinvald, 2000; Zhao, Jin, Wang, & Kim, 2007). A number of studies in humans (Boveroux et al., 2010;

Greicius et al., 2003; Martuzzi et al., 2010) and macaques (Vincent et al., 2007) have also found that prominent resting-state networks, including the default-mode network, are preserved under a variety of anesthetics, although often with somewhat reduced correlations. Notably, a recent study directly compared BOLD responses to auditory stimuli in awake versus isoflurane anesthetized zebra finches (Van Ruijssevelt et al., 2017a). This study found no difference in the magnitude of auditory-evoked BOLD responses, nor differences in neural selectivity for natural versus synthetic sounds, between awake versus isoflurane anesthetized birds; in contrast, the spatial extent of activation was slightly larger under isoflurane (Van Ruijssevelt et al., 2017a). This study raises the possibility of confirming the presence of homotopic FC in awake zebra finches in future studies. As noted previously, recent evidence from rodents indicates that an increase in isoflurane dose from 1% to 2% is associated with a concomitant decrease in homotopic FC (Bukhari et al., 2018; Hutchison et al., 2014), and here we also found that higher isoflurane doses predicted selectively lower homotopic FC in zebra finches. If this trend also holds for lower doses of isoflurane, this predicts that awake zebra finches should exhibit greater homotopic FC than anesthetized zebra finches, an interesting possibility to be explored in future studies.

Although the present study is unique as a longitudinal whole-brain rs-fMRI investigation in zebra finches, it was the beneficiary of a growing body of literature focused on the neuroimaging of songbirds (e.g., Boumans et al. 2007; Poirier et al. 2009, 2010; Poirier and Van der Linden 2011; Ruijssevelt et al. 2017). For instance, we utilized a spin-echo fMRI sequence, as opposed to GE, to avoid susceptibility artefacts previously shown to be more prevalent in songbirds (Poirier & Van der Linden, 2011). In addition to these precautions, we applied a bandpass filter to remove high frequency components of cardiac and respiratory contributions to

the signal (> 0.10 Hz Biswal et al. 1996; Murphy et al. 2013), regressed out principal components of CSF signals to further remove physiological noise (Behzadi et al., 2007), and assured the quality of our resting-state signals using *tSNR* and power spectral analyses. We also measured and controlled for effects of Euclidean distance between ROIs, ROI volume, and body temperature. Even with these rigorous statistical controls, we still observed robust homotopic FC across much of the zebra finch brain, supporting a biological, rather than technical or artefactual, origin for these findings.

Conclusion

In sum, our results indicate that a homotopic functional brain architecture likely arose in animals prior to the evolution of the CC, suggesting that this marker of interhemispheric coordination may be a neural feature observed more broadly across phylogeny, beyond the Eutherian mammals. Accordingly, rather than serving as a necessary prerequisite for homotopic FC, the CC may have evolved to provide finer dynamic control over, or flexible switching between, bilateral coordination and hemispheric specialization (Aboitiz & Montiel, 2003; van der Knaap & van der Ham, 2011). Such insights, in conjunction with the present results, increase the plausibility of the notion that ancestral pathways such as the AC (Paterson & Bottjer, 2017) or symmetric ascending bilateral inputs (Ashmore et al., 2008) are sufficient to provide the balance of interhemispheric coordination and specialization required for complex multimodal cognition in non-Eutherian vertebrates. Future studies are merited to investigate links between homotopic FC in non-mammalian vertebrates and complex brain functions requiring hemispheric specialization and coordination, such as song learning.

CHAPTER 3 – LONGITUDINAL FUNCTIONAL CONNECTIVITY SIGNATURES OF TUTOR EXPERIENCE IN THE JUVENILE ZEBRA FINCH BRAIN

Introduction

What neural mechanisms support the learning of complex behaviors during development? The zebra finch (*Taeniopygia guttata*) songbird is a tractable model organism in which to study this fundamental question (Fee & Scharff, 2010; London, 2017). Much as humans acquire speech in early childhood, male zebra finches (females cannot sing) learn to sing from an adult "tutor" within the first three months of life (London, 2017; Tchernichovski et al., 2001). The foundation of learned song is the formation of a tutor song memory that serves as a "template" to guide subsequent motor patterning. Tutor song memorization occurs during a single restricted developmental phase, or critical period (CP), during which tutor experience has profound and persistent effects on the brain and behavior (Knudsen, 2004; London, 2017). The onset of the CP for tutor song memorization, occurring on around P30 (Eales, 1985, 1987; Roper & Zann, 2006), likely depends on neural maturation events that enable learning to commence (London, 2017). In contrast, the CP "close," after which a zebra finch can no longer memorize additional songs, is believed to result from tutor experience-dependent neural plasticity remodeling the underlying neural circuitry sufficiently to shift the balance from plasticity to stability (London, 2017). Accordingly, if a juvenile zebra finch is isolated from tutor experience during the CP ("Isolates"), learning potential remains high (Eales, 1985, 1987; Jones et al., 1996, 1992; Morrison & Nottebohm, 1993) well after the typical close of the CP at P65 (Böhner, 1990; Braaten, 2010; Clayton, 1987; Eales, 1985, 1987; Morrison & Nottebohm, 1993; Roper & Zann, 2006; Slater, Richards, & Mann, 1991). This insight presents the unique opportunity to disambiguate the neural effects of experience-dependent plasticity from the programmed outcomes associated with maturational age (Fee & Scharff, 2010; London, 2017). Moreover, the

ability to control tutor experience, and thereby manipulate the closing of the CP, may permit the discovery of neural mechanisms that more broadly promote or limit the ability to learn.

The association regions of the zebra finch auditory forebrain, NCM and CM, are known to be critical for the first stage of song learning, tutor song memorization. For example, pharmacological disruption of molecular signaling pathways within the juvenile zebra finch auditory forebrain during tutor song exposures results in diminished tutor song copying upon maturation (Ahmadiantehrani & London, 2017; London & Clayton, 2008). Specifically, London and Clayton (2008) demonstrated this via inhibition of the extracellular signal-regulated kinase (ERK) signaling pathway, which regulates immediate early gene (IEG) *ZENK* expression within the auditory forebrain (Cheng & Clayton, 2004) and is part of a signaling cascade important for long-term potentiation (Bozon et al., 2003). Similarly, Ahmadiantehrani and London (2017) found that either inhibition or constitutive activation of the mechanistic target of rapamycin (mTOR) signaling cascade, also known to contribute to learned behavior (Garza-Lombó & Gonsebatt, 2016; Giovannini & Lana, 2016; Hoeffer & Klann, 2010), decreased the fidelity of tutor song copying. Moreover, several immunocytochemistry studies have found that the density of IEG induction within NCM in response to tutor song playback positively correlates with the strength of song copying in both awake (Bolhuis, Hetebrij, Boer-Visser, Groot, & Zijlstra, 2001; Bolhuis, Zijlstra, Boer-Visser, & Zee, 2000; Terpstra, Bolhuis, & Boer-Visser, 2004) and sleeping (Gobes, Zandbergen, & Bolhuis, 2010) zebra finches. Finally, electrophysiological evidence indicates that neurons within the auditory forebrain are selectively tuned to tutor song in both juveniles (Yanagihara & Yazaki-Sugiyama, 2016) and adults (Phan et al., 2006). Given this converging evidence, the auditory association regions NCM and CMM may present

opportune targets in which to examine the neural mechanisms that underlie the CP for tutor song memorization (London, 2017).

Although *local* molecular signaling within the auditory forebrain is known to be critical for tutor song memorization (Ahmadiantehrani & London, 2017; London & Clayton, 2008), much less is known regarding the functional network correlates of tutor experience. That is, how does tutor experience shape functional interactions between the auditory forebrain and the rest of the zebra finch brain, potentially including components of the traditional zebra finch song network (Akutagawa & Konishi, 2010; Bauer et al., 2008; Fortune & Margoliash, 1995; Shaevitz & Theunissen, 2007; Vates et al., 1996)? Here, we sought to inform this question by leveraging the advantages of longitudinal rs-fMRI FC analyses. This methodological paradigm allows for non-invasive, whole-brain, longitudinal data collection, which may be particularly suitable for characterizing a developmental process such as song learning. Moreover, we have previously demonstrated the validity and efficacy of this paradigm in zebra finches (Layden, Schertz, London, & Berman, 2019).

Here, we quantified resting-state FC as the temporal correlations embedded within intrinsic infra-slow (< 0.1 Hz) brain activity, conveniently recorded as BOLD signals (Biswal et al., 2010, 1995; Mitra et al., 2018). We then analyzed the voxel-wise developmental trajectory of the ICC (Martuzzi et al., 2011), a measure that summarizes the centrality or importance of a given voxel or brain region within large-scale FC networks. We scanned eighteen male zebra finches at four ages: before (P25), during (P45), and at the end of the CP (P65) for tutor song memorization, as well as at the young adult stage (P90). Prior to the onset of the CP, birds were assigned to one of three rearing conditions: *Normal* (access to multiple potential tutors), *Tutored* (access to a single tutor), and *Isolate* (no access to tutors). Given the auditory forebrain's

important role in tutor song memorization, we hypothesized that Isolates would also show an altered pattern of ICC ontogeny within these regions across the CP. However, to conduct a more stringent test of this hypothesis, we conducted data-driven whole-brain analyses that would also allow for the detection of any rearing condition-related developmental differences in ICC outside of the hypothesized regions, including regions not currently known to be involved in song learning.

Method

Animals

All animal procedures were approved by the Institutional Animal Care and Use Committee of the University of Chicago in accordance with the NIH Guide for the Care and Use of Laboratory Animals. All birds were maintained under a 14/10 hour light/dark photoperiod throughout the experiment, with food and water provided *ad libidum*. We collected rs-fMRI scans for male zebra finches at four ages, capturing FC at various stages of the song learning process: prior to the CP for tutor song memorization (P25), in the approximate middle of the CP (P45), at the end of the CP (P65), and toward the end of the sensorimotor rehearsal period, when tutor song copying is complete and song stereotypy is high (P90). Zebra finches were assigned to one of three rearing conditions, sorted to separate brothers and to temporally batch birds into all of the rearing conditions following their P25 rs-fMRI scanning session, and before the onset of the CP at around P30 (Roper & Zann, 2006): *Normal* (aviary housed with access to multiple potential adult male tutors; N=5), *Tutored* (housed with one adult male tutor and one adult female; N=7), and *Isolate* (housed with two adult females, meaning no access to song tutors but having experience with conspecific vocalizations (females produce innate calls), and with the same complexity of social interactions as the Tutored group; N=6). Importantly, housing Isolate

birds with two adult females allowed us to measure effects specific to isolation from song, as opposed to social isolation more generally.

One Normal male died of unknown cause in the group aviary between P65 and P90 (unrelated to scanning). Additionally, a P25 scan was not successfully obtained for two Tutored birds and one Isolate bird, due to a scanner coil hardware failure. This yielded a total of 68 out of 72 possible successful scanning sessions across 18 male zebra finches. While the original head coil was sent out for repairs, a substitute head coil was used to scan seven P25 birds (2 Normal, 2 Tutored, and 3 Isolate), whereas the repaired original was used to scan all other target ages. To statistically control for any potential effects resulting from the use of different head coils, we included a categorical covariate denoting which head coil was used for scanning in all of the following analyses which utilized P25 scans. Importantly, this issue only impacted our P25 baseline data and not our target ages of primary interest (ages P45-P90).

Finally, due to weekday-only scanner availability and scheduling conflicts, not all birds could be scanned on exact target days, but the age range was kept as close as possible to the targets: P25 (range: P24-P26), P45 (range: P44-P46), P65 (range: P63-P67), and P90 (range: P88-P91). Importantly, age at scan time did not significantly vary by condition at any target age, nor across target ages (ANOVA, all p's > 0.17). Additionally, precise ages were recorded for each bird, and age was implemented as a continuous variable in all analyses described below.

Scanning Procedure and Preprocessing

MRI data collection was conducted at the MRIS Facility of the University of Chicago. Upon arrival, zebra finches were anesthetized using an admixture of oxygen and isoflurane gas (1.5-2.25%). Subsequently, a light maintenance dosage of isoflurane was maintained throughout

the experiment (0.5-2%). The use of isoflurane is well-established in task-based fMRI studies of zebra finches (Boumans et al., 2007; Poirier et al., 2009), and isoflurane was also used successfully in our previous resting-state fMRI zebra finch study (Layden et al., 2019). Importantly, although hemodynamic response magnitude is reduced by isoflurane anesthesia, hemodynamic response shape remains largely unchanged (Zhao et al., 2007). Following anesthesia administration, birds were fitted with a temperature probe and respiration monitoring pad, allowing for body temperature, respiratory rate, and isoflurane percentage to be monitored throughout the scanning period. The zebra finches were wrapped in a felt cloth to help maintain body temperature. Upon insertion into the scanner, a warm air feedback system was used to further maintain body temperature within a normal physiological range (40.0 ± 0.2 °C).

Imaging Data Acquisition. Neuroimaging data were acquired using a 30 cm bore 9.4 T Bruker small animal MRI scanner. A TurboRARE-T2 Multislice anatomical scan was acquired first during each scanning session (TR = 3.5 s, TE = 20 ms, Matrix Size: 256 x 256, in-plane resolution = 70.3 μm x 70.3 μm, slice-thickness = 200 μm, 59 slices, 9 averages). Resting-state RARE spin-echo T2-weighted MR images were then acquired (TR = 3.2 s, $TE_{effective}$ = 27 ms, 3 echoes per volume, Matrix Size: 128 x 36, in-plane resolution = 141 μm x 500 μm, slice-thickness = 750 μm, 15 slices). Slices were acquired in an interleaved, ascending order. 180 volumes were acquired consecutively with an effective sampling rate of 3.2 seconds per volume, yielding a total resting-state scan time of 9 minutes and 36 seconds. A spin-echo pulse sequence was utilized due to observations that gradient-echo imaging may be particularly vulnerable to susceptibility artifacts in zebra finch whole-brain fMRI (Poirier & Van der Linden, 2011). To avoid T1-equilibration effects, the first five volumes of each functional series were discarded.

Preprocessing. Image preprocessing was completed using a combination of ANTs (Avants et al., 2011, 2009), AFNI (Cox, 1996), and custom Matlab scripts. First, magnetic field intensity inhomogeneity was corrected for both functional and anatomical images using the "N4" bias field correction algorithm (Tustison et al., 2010). Second, an average of the bias-corrected anatomical scans was used to initialize SyGN (Avants et al., 2010) in ANTs. ANTs registration accuracy compares favorably among commonly used nonlinear deformation algorithms (Avants et al., 2011; Klein et al., 2009). Third, functional scans were corrected for slice timing differences using ANTs ImageMath SliceTimingCorrection. Slice timing correction may be particularly essential in the case of longer duration TRs (Sladky et al., 2011), and it is recommended that this step be performed prior to realignment for interleaved slice acquisitions (Johnstone et al., 2006). Fourth, motion correction was performed using the antsMotionCorr function in ANTs, and the six rigid-body motion parameters were retained for later nuisance regression. Fifth, average motion-corrected functionals were affine coregistered to their corresponding bias-corrected anatomical volumes using the antsRegistrationSyN function. Sixth, to minimize interpolations, we applied all transformations obtained from (1) motion correction, (2) coregistration, and (3) structural normalization to the slice-timing corrected functionals in a single step using the ANTs function antsApplyTransforms. Finally, we used the AFNI function 3dBlurInMask to smooth the functional data within our custom brain mask using a 0.8438 mm FWHM Gaussian kernel (corresponding to 6.00 x 1.69 x 1.12 voxels in the *x*, *y*, and *z* dimensions, respectively). This function avoids contaminating signals at the edge of the brain with signal from other surrounding tissues (or zeros). All subsequent analyses were carried out using normalized data at the functional image resolution (0.141 x 0.500 x 0.750 mm, 8,720 in-mask voxels), and results were interpolated to template resolution for display purposes.

Data Extraction and Denoising

We implemented denoising procedures using MRIqual and custom Matlab scripts. Physiological variables (body temperature and isoflurane dose), recorded at one-minute intervals, were interpolated using a clamped cubic spline function to the temporal resolution of our functional series. Then, a nuisance regression was performed in which the six rigid body motion parameters (Bright & Murphy, 2015), body temperature, isoflurane dose, and linear and quadratic trends (Tanabe et al., 2002) were removed from the voxel-wise time series. Following nuisance regression (Hallquist et al., 2013), the residual ROI time series were bandpass filtered (range: 0.008 to 0.1 Hz).

Intrinsic Connectivity Contrast (ICC) Analyses

We used a data-driven approach to investigate associations between rearing condition and brain-wide FC strength, measured using the ICC, which does not require arbitrary thresholding of functional connections (Martuzzi et al., 2011). ICC is computed at each brain voxel by averaging the squared Pearson correlations between a given voxel time series and every other voxel time series in the brain (Martuzzi et al., 2011); the voxel-wise distribution of ICC is then standardized (i.e., *Z*-scored) within each functional scan (Layden et al., 2017). ICC has previously proven effective for identifying functional hubs within the human brain associated with a variety of affective, social, and cognitive phenomena (e.g., Layden et al., 2017; Moreno-López, Sahakian, Manktelow, Menon, & Stamatakis, 2016; Vatansever, Manktelow, Sahakian, Menon, & Stamatakis, 2017).

Using an LME random intercept model, we regressed voxel-wise ICC onto age, rearing condition, an age by rearing condition interaction, isoflurane dose, body temperature, head coil,

and a random intercept for bird. For each voxel, we retained the *t*-statistic summarizing the age by rearing condition interaction effect. Significant clusters of voxels wherein the developmental trajectory of ICC differed by rearing condition were detected using the random field theory-based cluster-extent thresholding method, as implemented in the DPABI toolbox (cluster-defining threshold (CDT): *p-uncorrected* < 0.001, FWE-corrected cluster-extent threshold: *pFWE* < 0.05; Yan et al. 2016).

Normal versus Tutored contrast. Although our primary interest was in whether Isolate birds would exhibit a pattern of FC development distinguishable from both Normal and Tutored birds, we first examined whether Normal and Tutored birds were distinguishable via FC. Any such effects could potentially be related to social group size or the number of available tutors, rather than tutor experience or lack thereof.

Tutored versus non-tutored contrast. Given that the Normal vs. Tutored contrast did not yield significant results (see Results below), we combined these rearing conditions into a single "Tutored" condition to yield increased statistical power for our contrast of primary interest. We then examined whether the developmental trajectory of ICC differed in any brain regions between tutored (i.e., Normal and Tutored) and non-tutored birds (i.e., Isolates).

Seed-to-Voxel (S2V) Functional Connectivity Analyses

ICC enables the detection of clusters based on global FC strength but does not reveal the specific functional connections that may underlie any global FC differences observed. We therefore conducted a "seed-to-voxel" (S2V) analysis, in which we extracted the average BOLD signal from the voxels of the significant cluster detected in ICC analyses (see Results). We then computed S2V FC as the Fisher *Z*-transformed Pearson correlation between the cluster/seed

signal and the signal of every other brain voxel. At each voxel, we then regressed S2V FC onto age, rearing condition, an age by rearing condition interaction, isoflurane dose, body temperature, head coil, and a random intercept for bird. Finally, clusters of S2V FC showing developmental trajectories that differed by rearing condition were identified using the same cluster-extent thresholding method as for ICC analyses (CDT: *p-uncorrected* < 0.001, cluster-extent threshold: *pFWE* < 0.05).

Song Stereotypy

Song bouts were recorded in a sound isolation chamber for a period of approximately 24 hours prior to rs-fMRI scans at P65 (N = 12) and P90 (N = 16). Some birds did not sing during the recording period, thus resulting in the different sample sizes for each age.

Song stereotypy quantification. We quantified song stereotypy (i.e., self-similarity or consistency across song bouts) using Sound Analysis Pro 2011 (Tchernichovski, Nottebohm, Ho, Pesaran, & Mitra, 2000). Three standard measures of stereotypy were calculated: %-Similarity (a coarse-grained comparison of song segments using 50-70 ms time windows), Accuracy (a fine-grained comparison of song segments within 5-10 ms time windows), and %-Sequential (quantifying the extent to which matching sound segments occur with the same ordering in different song bouts). Additional details regarding the calculation of these metrics are available from the Sound Analysis Pro reference manual (Tchernichovski & Mitra, 2004).

We found that these three measures were highly correlated across birds (%-Similarity and Accuracy: $r(26) = 0.89$, %-Similarity and %-Sequential: $r(26) = 0.71$, Accuracy and %-Sequential: $r(26) = 0.78$). Moreover, the first principal component (PC) from principal component analysis explained 88.2% of total variance among the three stereotypy measures, and

this PC loaded highly on each individual measure (loadings: %-Similarity (r = 0.94), Accuracy (r = 0.96), %-Sequential (r = 0.89)). To avoid issues with both multicollinearity and multiple comparisons, we utilized the first PC of the three stereotypy measures as our variable of interest for subsequent analyses, and for simplicity, we will henceforth refer to this first PC as "stereotypy."

Condition-related differences in stereotypy. Tutor song memorization provides the foundation for song learning, but a partially overlapping sensorimotor learning phase (P35-P90) is important for the refinement of songs and depends upon successful tutor song memorization. Song bouts become increasingly stereotyped across the song crystallization phase of sensorimotor learning (Arnold, 1975); however, learning potential remains higher and stereotypy lower during this period for Isolates (Eales, 1987; Jones et al., 1996), although Isolate songs may become somewhat stereotyped as well by P100-120 (Morrison & Nottebohm, 1993). We therefore predicted that non-tutored birds would exhibit less stereotyped songs than Tutored birds at P65, during the plastic song phase, and potentially at P90 as well, toward the end of the song crystallization phase. Additionally, there are indications that the number of song bouts (i.e., the amount of practice) during the plastic song phase strongly predicts stereotypy at P112, whereas the number of song bouts during the song crystallization phase does not predict stereotypy at P112 (Johnson, Soderstrom, & Whitney, 2002). Therefore, we hypothesized that the four birds (2 Normal, 2 Tutored) who sang at P90 but not at P65 would exhibit lower stereotypy at P90.

To test these hypotheses, we implemented an LME model in which stereotypy served as the criterion variable, and the following were included as fixed-effects predictors: rearing condition (tutored vs. non-tutored), age, and a nominal factor denoting whether or not each bird

sang at P65; a random intercept was included for bird. With only two ages (P65 and P90) per bird, we found that the Hessian matrix was not positive definite for this LME model (i.e., the random intercept was not supported), so we dropped the random intercept and implemented the model using ordinary least squares (OLS) regression.

Predicting song stereotypy using FC features. We next investigated whether the cluster(s) identified based on ICC or S2V FC analyses predicted song stereotypy. To do so, we selected an optimal model for predicting stereotypy from among the FC features using the 'step' function from the "lmerTest" package (Kuznetsova, Brockhoff, & Christensen, 2017) in R. We performed stepwise model reduction based on reductions in AIC, requiring significant differences between nested models based on likelihood-ratio tests. The initial model included the following predictors: age, condition, average ICC of the significant cluster identified, ICC at the previous age (i.e., P45 ICC predicting P65 stereotypy), ICC change from the previous age (i.e., P65 ICC minus P45 ICC predicting P65 stereotypy), average S2V FC of the significant cluster identified, S2V FC at the previous age, S2V FC change from the previous age. We included ICC at the previous age and ICC change because we reasoned that more complex developmental trends might be involved than a simple one-to-one mapping between ICC and stereotypy.

FC mediation of stereotypy differences between rearing conditions. If merited by the previous analysis, we planned to empirically test whether ICC or S2V FC features statistically mediated stereotypy differences between rearing conditions (i.e. tutored vs. non-tutored). We used the "mediation" package in R (Tingley, Yamamoto, Hirose, Keele, & Imai, 2014) to estimate the average causal mediation effect (*ACME*), which corresponds to the proportion of the rearing condition effect mediated by a given FC feature. We also estimated the average direct effect (*ADE*), which corresponds to the proportion of the rearing condition effect not mediated

by the FC feature. Lastly, we estimated the total effect, which is a combination of the *ACME* and *ADE*. All effects were estimated using the non-parametric bias-corrected and accelerated bootstrap method with 10,000 iterations.

Results

Intrinsic Connectivity Contrast (ICC) Analyses

Normal versus Tutored comparison. No significant clusters were identified (CDT: *p-uncorrected* < 0.001, cluster-extent threshold: *pFWE* < 0.05).

Tutored versus Isolate comparison. Voxel-wise LME models identified a significant cluster of 19 functional space voxels (CDT: *p-uncorrected* < 0.001, cluster-extent threshold: *pFWE* < 0.05) centered within the left auditory forebrain (Figure 3.1). Specifically, 13 voxels (68.4% of the cluster) overlapped a ventral posterior portion of the left auditory forebrain, likely corresponding to NCM, and 6 voxels (31.6% of the cluster) overlapped an unlabeled region directly adjacent to the medial posterior portion of the left auditory forebrain.

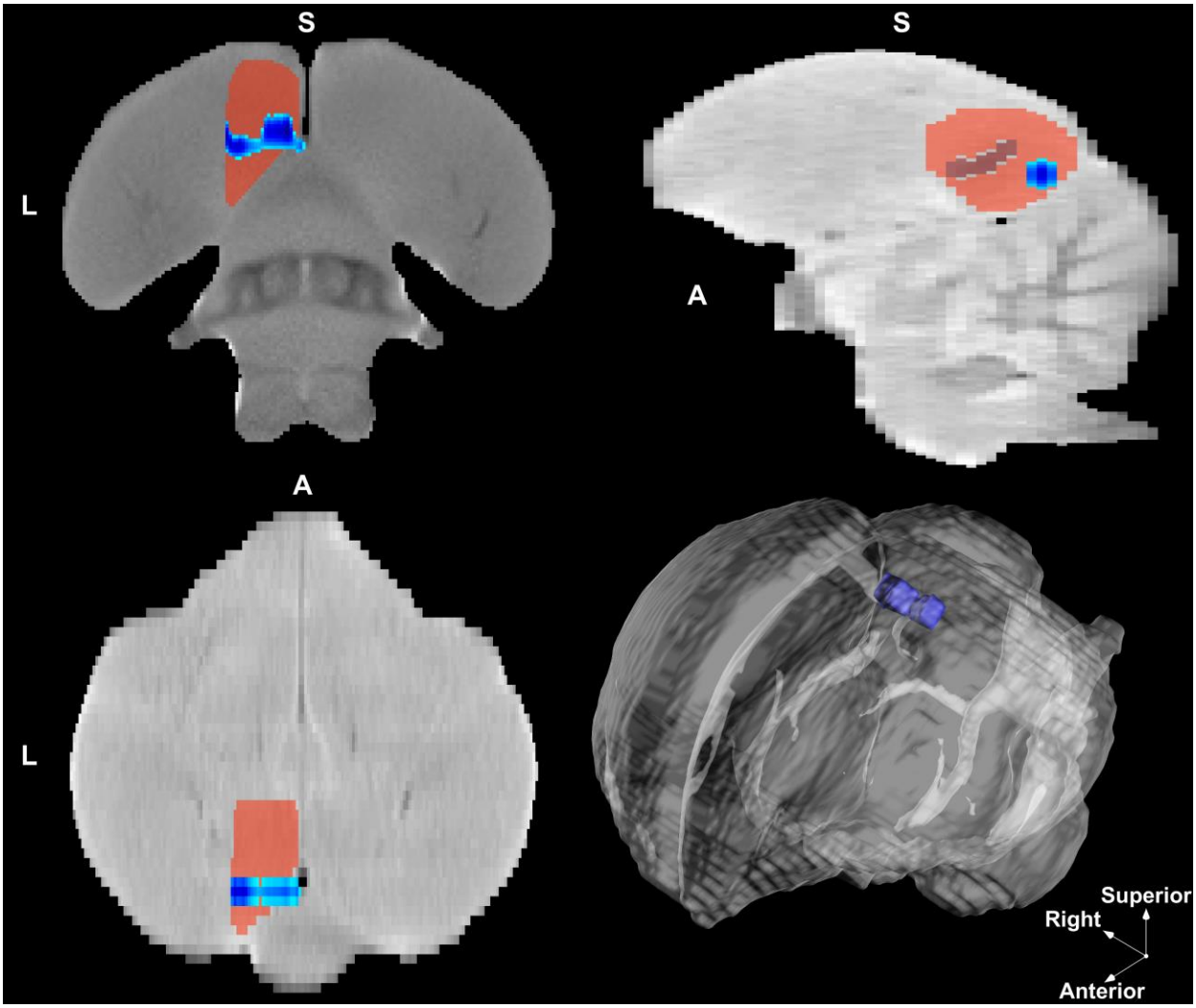

Figure 3.1. Intrinsic connectivity contrast cluster. Non-tutored male zebra finches showed decreasing ICC with age within this cluster, whereas tutored zebra finches showed increasing or stable ICC. From top-left to bottom-right: coronal view (slice 16), sagittal view (slice 148), axial view (slice 169), 3D rendering. All voxels depicted exhibited *t*-statistics ≤ -3.23 ($p < 0.001$) for the rearing condition by age interaction effect.

The average ICC level within this cluster significantly decreased with age in non-tutored relative to tutored birds ($\beta = -1.05$, $t(61) = -4.77$, $p < 0.001$). A follow-up analysis revealed that the ICC within this cluster marginally *increased* with age for Normal birds ($\beta = 0.44$, $t(14) = 1.93$, $p = 0.074$), non-significantly *increased* with age for tutored birds ($\beta = 0.21$, $t(21) = 1.31$, $p = 0.204$), and significantly *decreased* with age for Isolate birds ($\beta = -0.65$, $t(18) = -3.06$, $p = 0.007$). The

developmental trends in ICC are displayed for each individual bird in Figure 3.2. Finally, to assure that any potential baseline differences at P25 did not drive this effect, we repeated this analysis using data from only ages P45 to P90. We found that the average ICC level of the cluster still significantly decreased with age in non-tutored relative to tutored birds (β = -0.84, $t(47)$ = -2.86, p = 0.006).

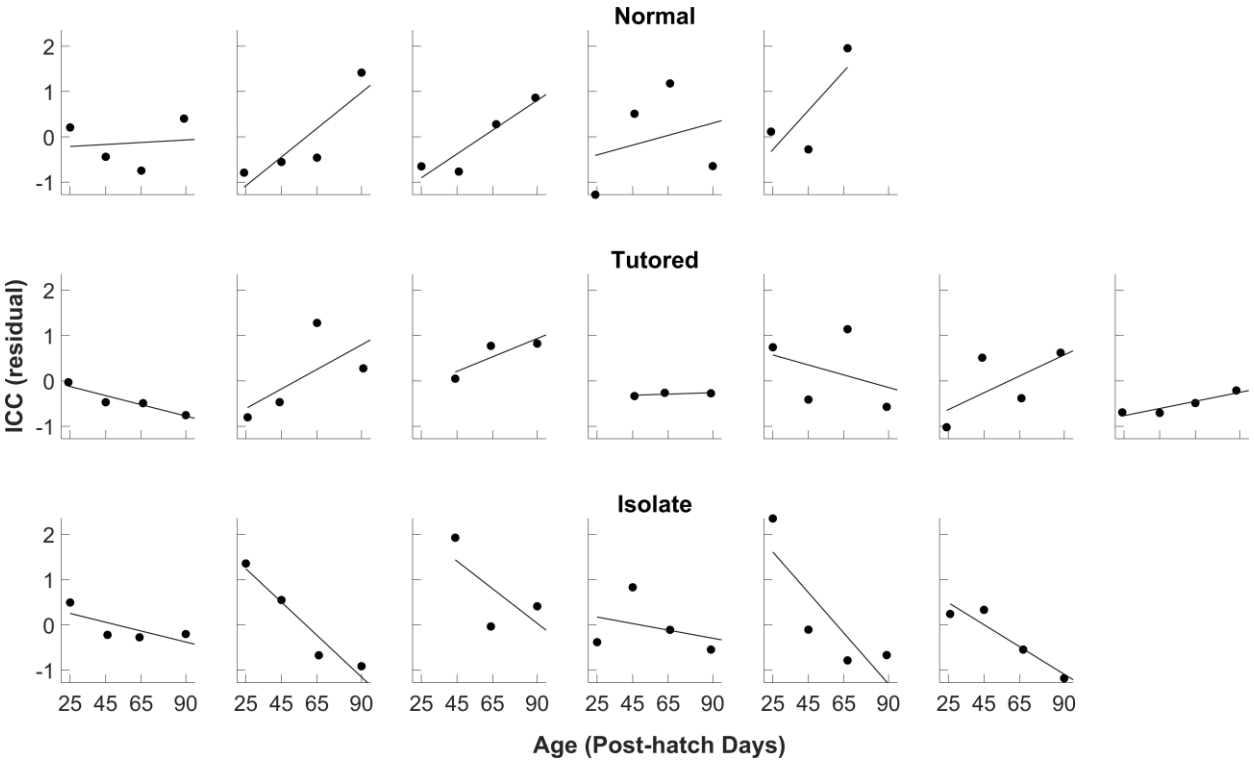

Figure 3.2. Developmental trends for the intrinsic connectivity contrast cluster. Separate scatter plots show the developmental trajectory of average cluster ICC across ages P25 to P90 (*x*-axis) for each individual bird. A within-subjects least-squares trend line is displayed for reference. ICC scores (*y*-axis) are residuals from a regression controlling ICC across birds for the effects of body temperature, isoflurane dose, and head coil.

Testing for lateralization. Given that the left NCM cluster appeared to be located exclusively within the left hemisphere, we conducted a follow-up analysis to test whether a similar effect could also be observed in a mirror-symmetric (i.e., homotopic) cluster within the right hemisphere, or if, alternatively, the effect was truly left lateralized. We found that the

average ICC level within a homotopic right-hemispheric cluster also significantly decreased with age in non-tutored relative to tutored birds (β = -0.89, $t(61)$ = -3.92, p = 0.002). This developmental difference was numerically smaller than that observed in the left hemisphere (β = -1.05). However, the effect sizes in each hemisphere were not significantly different, as revealed by an LME model in which we tested the three-way interaction between age, rearing condition, and hemisphere as a binary categorical variable (β = 0.35, $t(125)$ = 1.22, p = 0.224).

Seed-to-Voxel (S2V) Analyses

ICC measures the global FC strength of a given voxel or cluster; however, ICC alone does not reveal what specific functional connections underlie the level of global FC observed. To investigate whether region-specific FC also showed a differential developmental trajectory between tutored and non-tutored birds, we used the previously identified left NCM cluster as an FC "seed" region for S2V analyses. We identified one significant cluster of 21 voxels (Figure 3.3) that showed a rearing condition-related developmental difference in FC to the left NCM cluster seed (CDT: *p-uncorrected* = 0.001, cluster-extent threshold: *pFWE* < 0.05). Two voxels (9.5% of cluster volume) overlapped the left posterior auditory forebrain (i.e., NCM), whereas much of the rest of the cluster appeared to overlap the right dorsal cerebellum.

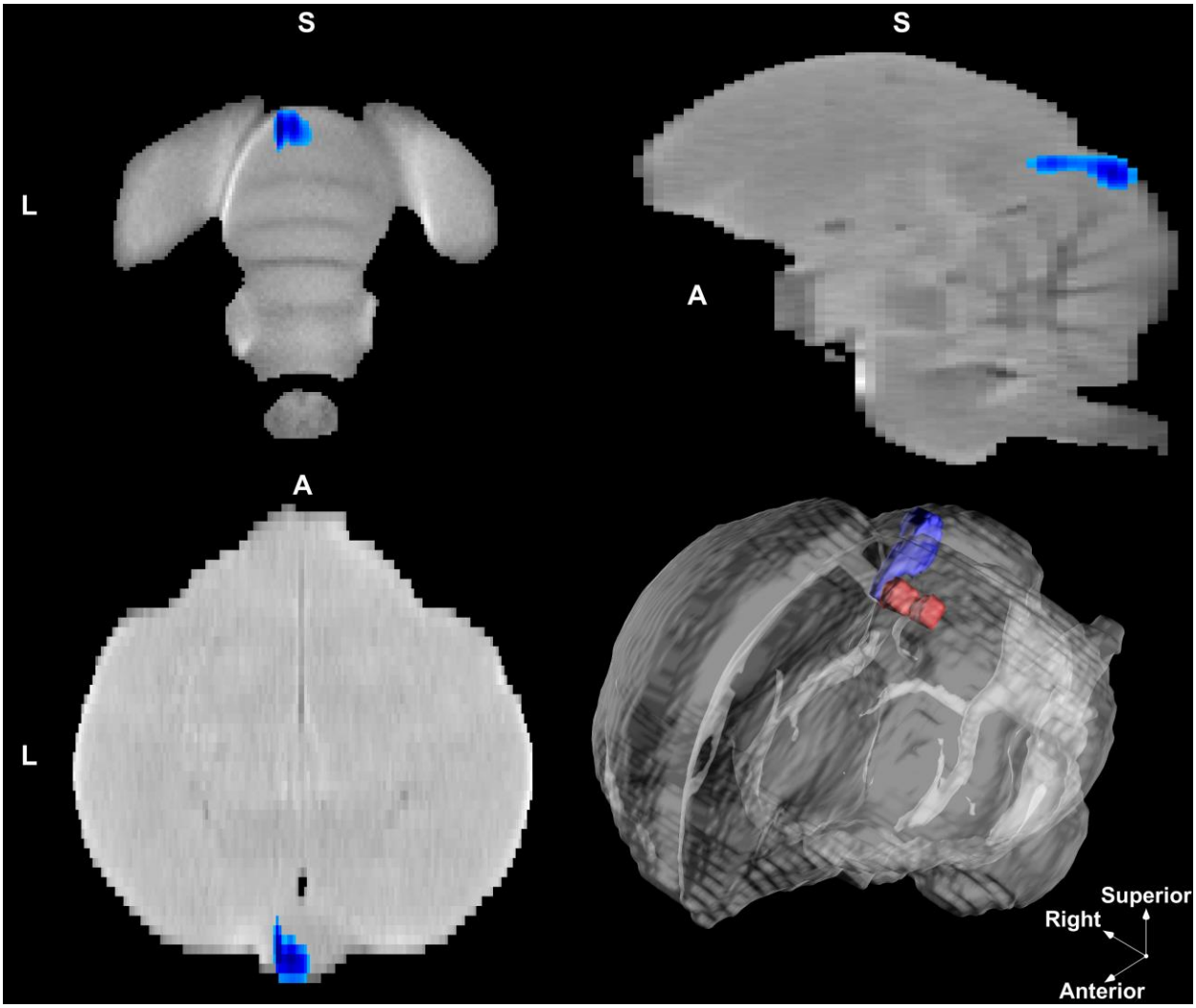

Figure 3.3. Seed-to-voxel functional connectivity cluster. The significant cluster of voxels wherein non-tutored male zebra finches, compared to tutored zebra finches, showed developmentally decreasing FC to the previously identified left NCM cluster. From top-left to bottom-right: coronal view (slice 10), sagittal view (slice 145), axial view (slice 172), 3D rendering. All voxels depicted exhibited *t*-statistics ≤ -3.23 ($p < 0.001$) for the rearing condition by age interaction. The red cluster depicted in the 3D rendering (bottom right) is the left NCM cluster from ICC analyses, used here as an FC seed region.

The developmental trajectory of FC for this connection markedly differed between non-tutored and tutored birds (non-tutored: $\beta = -1.14$, $t(61) = -5.65$, $p < 0.001$). Next, we conducted a follow-up analysis in which the age and S2V FC association was measured separately within each rearing condition. In both Normal and Tutored birds, S2V FC non-significantly *increased*

with age (Normal: $\beta = 0.28$, $t(14) = 1.11$, $p = 0.284$; Tutored: $\beta = 0.18$, $t(21) = 0.93$, $p = 0.362$). In contrast, the S2V FC strongly *decreased* with age in Isolate birds ($\beta = -0.94$, $t(18) = -7.15$, $p < 0.001$). The developmental trends of S2V FC are shown for each individual bird in Figure 3.4. Finally, to assure that any potential baseline differences at P25 did not drive this effect, we repeated this analysis using P45 to P90 data only. We found that S2V FC still significantly decreased with age in non-tutored relative to tutored birds ($\beta = -0.72$, $t(47) = -2.55$, $p = 0.014$).

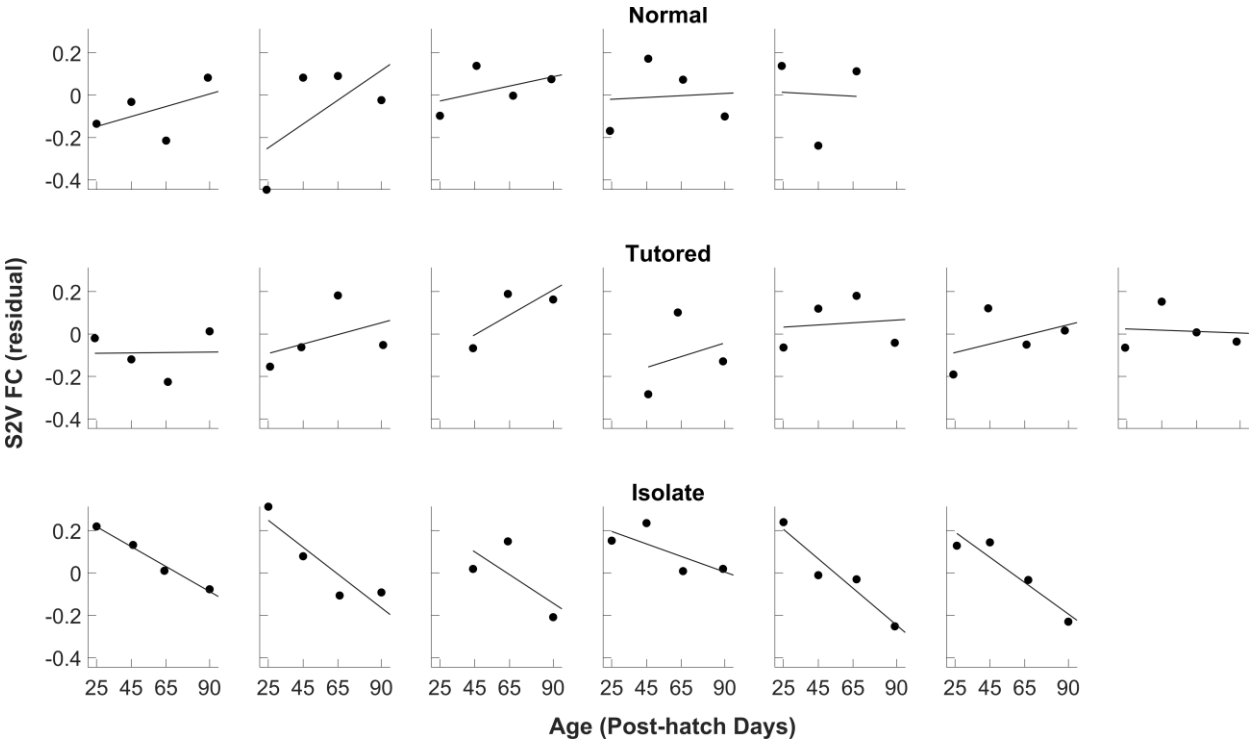

Figure 3.4. Developmental trends for the seed-to-voxel functional connectivity cluster. Separate scatter plots show the developmental trajectory of S2V FC across ages P25 to P90 (*x*-axis) for each individual bird. A within-subjects least-squares trend line is displayed for reference. S2V FC values (*y*-axis) are residuals from a regression controlling S2V FC across birds for the effects of body temperature, isoflurane dose, and head coil.

Song Stereotypy Analyses

In an OLS regression model predicting stereotypy via rearing condition (tutored vs. non-tutored), age, and a factor denoting whether each bird sang at P65, we found the following: non-

tutored birds' songs were significantly less stereotyped than tutored birds' across ages P65 and P90 (β = -0.97, $t(24)$ = -2.69, p = 0.013); the two Normal and two tutored birds who sang at P90 but not P65 exhibited markedly less stereotyped songs at P90 than those who sang at P65 (β = -1.27, $t(24)$ = -2.41, p = 0.024); and increasing age from P65 to P90 predicted marginally increased stereotypy (β = 0.33, $t(24)$ = 1.84, p = 0.078). Overall, this model explained 32.6% of the total stereotypy variance (*Adjusted* R^2 = 0.242). The developmental trends in song stereotypy are displayed in Figure 3.5.

A follow-up analysis did not support the inclusion of an age by condition interaction term in this model ($F(1, 23)$ = 0.04, $p > 0.80$; age by non-tutored: β = 0.08, $t(23)$ = 0.21, $p > 0.80$). However, separate two-sample *t*-tests at each age revealed that tutored birds were significantly more stereotyped than non-tutored at P65 ($t(10)$ = 2.65, p = 0.024) but not at P90 ($t(14)$ = 0.76, p = 0.46). The P90 condition difference remained non-significant, even after excluding the birds who did not sing at P65 ($t(10)$ = 1.71, p = 0.118). While this null result at P90 should be interpreted with caution based on the small sample size available for this contrast, it may possibly reflect the fact that these ages, P65 and P90, occur within different phases within the song learning process, i.e., the plastic song phase and song crystallization phase, respectively (Johnson et al., 2002).

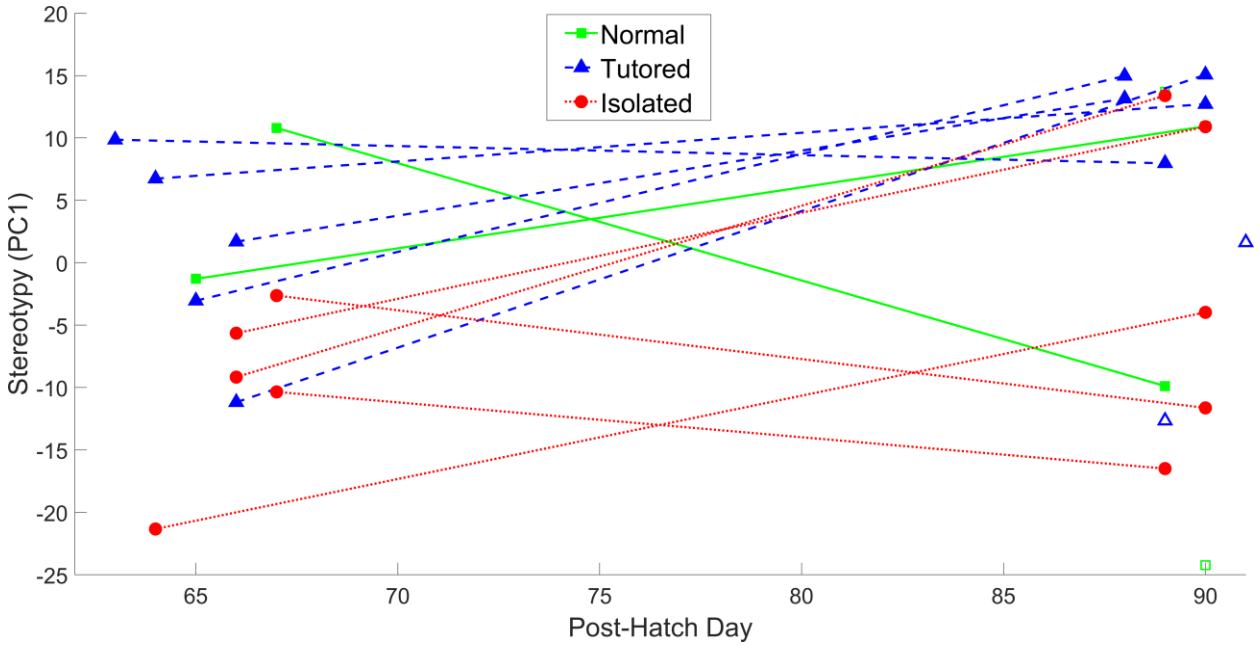

Figure 3.5. Stereotypy scores by age and condition. Each Normal condition bird is depicted with a solid green line connecting corresponding stereotypy scores at each age (square markers). Tutored birds are depicted with a dashed blue line connecting stereotypy scores (triangle markers). Isolate birds are depicted with red dotted lines connecting stereotypy scores (circle markers). Hollow markers are used to denote the four birds (2 Normal, 2 tutored) who sang at P90 but not P65. Ages (*x*-axis) correspond to age at rs-fMRI scan date.

Predicting song stereotypy using FC features. To examine whether the FC features identified in previous analyses predicted song stereotypy, we implemented backwards step-wise model selection, beginning with the following predictors: condition, age, average ICC of the significant cluster, ICC at the previous age, ICC change from the previous age, average S2V FC of the significant cluster, S2V FC at the previous age, and S2V FC change from the previous age. Step-wise model selection proceeded to eliminate (1) S2V FC at the previous age (ΔAIC = 2.00), (2) ICC at the previous age (ΔAIC = 2.00), (3) condition (ΔAIC = 1.79) and (4) S2V FC change (ΔAIC = 1.67). Further model reduction resulted in larger AIC values, and the final model is displayed in Table 3.1. This model explained 56.9% of total stereotypy variance (*Adjusted* R^2 = 0.49).

Table 3.1. Prediction of stereotypy

Predictor	Estimate	*SE*	*B*	*t*	*p*
Intercept	-20.60	11.86	0.00	-1.74	0.096
ICC	-7.50	3.87	-0.40	-1.94	0.065
ICC Change	9.47	2.25	0.75	4.21	0.000
S2V	53.41	17.71	0.52	3.02	0.006
Age	0.29	0.15	0.29	1.92	0.067

Note. *DFE* = 23, R^2 = 0.569, *Adjusted* R^2 = 0.494

We found that a larger change in ICC relative to the previous age was a strong positive predictor of song stereotypy at the current age, across both P65 and P90 (β = 0.75, $t(23) = 4.21$, $p < 0.001$). Similarly, the average S2V FC between the ICC cluster and the S2V cluster positively predicted stereotypy (β = 0.52, $t(23) = 3.02$, $p = 0.006$). Age marginally positively predicted stereotypy (β = 0.29, $t(23) = 1.92$, $p = 0.067$). Finally, the effect of average ICC was non-significant and negative (β = -0.40, $t(23) = -1.94$, $p = 0.065$). Notably, this non-significant *negative* effect likely resulted from a statistical suppression effect (Tu, Gunnell, & Gilthorpe, 2008) and should not be interpreted as a true negative association. Specifically, the bivariate association between average ICC and stereotypy was positive (β = 0.35, $t(26) = 1.90$, $p = 0.069$), becoming negative only after conditioning on two moderately correlated covariates, ICC change ($r(26) = 0.61$, $p < 0.001$) and S2V FC ($r(26) = 0.47$, $p = 0.011$). The association of ICC and ICC change with stereotypy is visually depicted in Figure 3.6 below.

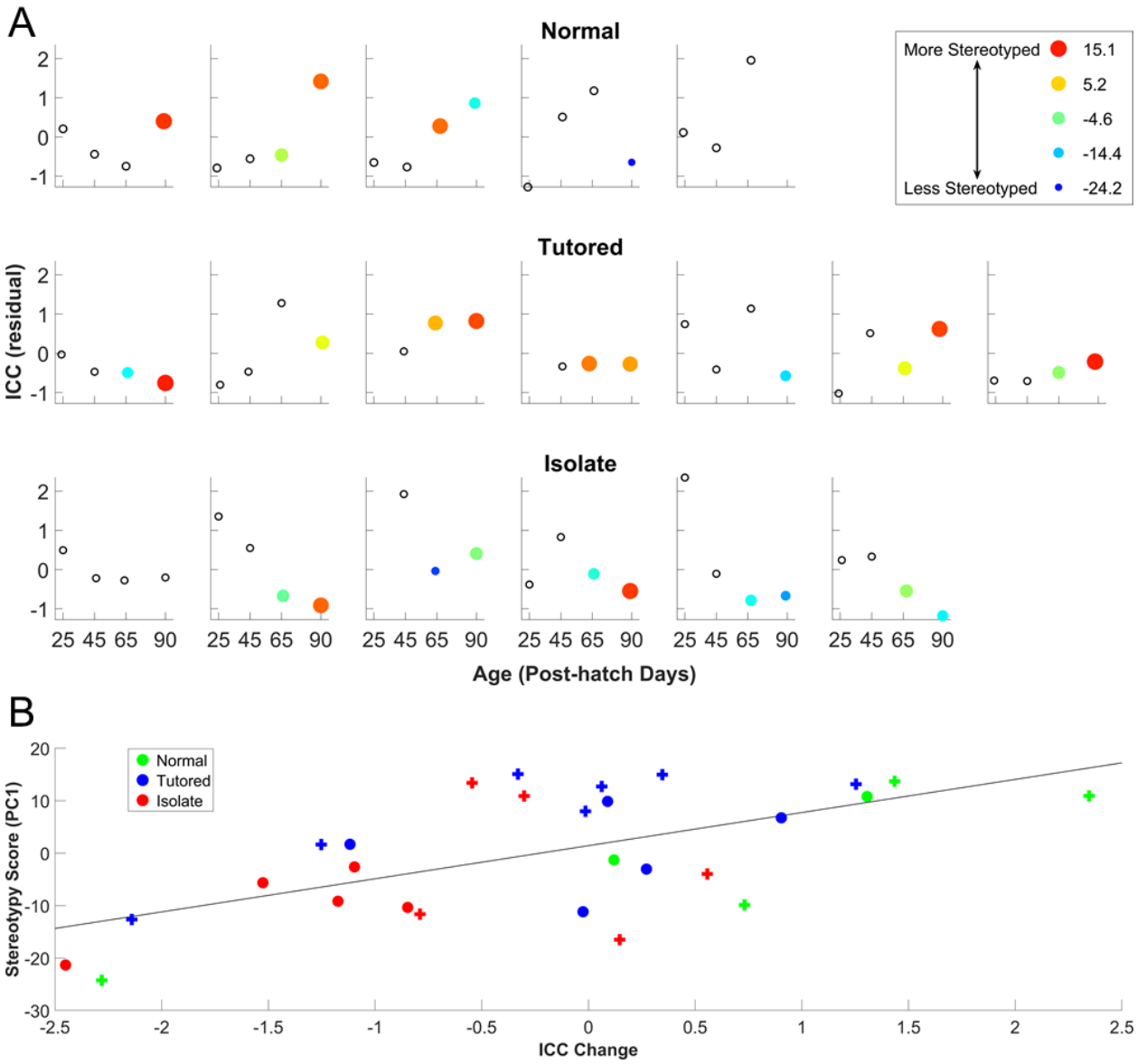

Figure 3.6. Intrinsic connectivity contrast developmental trends and stereotypy. **A:** Scatter plots for each individual bird showing the developmental trajectory of cluster ICC from P25 to P90. Hollow data points denote a lack of stereotypy data for a given age (*x*-axis), whereas both the color and size of filled data points denote the level of stereotypy in units of the first principal component scores. ICC scores (*y*-axis) are residuals from a regression controlling for the effects of body temperature, isoflurane dose, and head coil. **B:** A scatter plot showing the association between change in ICC from the previous age and stereotypy across all birds. An OLS regression line is displayed (R^2 = 0.37). Ages P65 (o) and P90 (+) are denoted with distinct markers.

FC mediates stereotypy differences between rearing conditions. Given that ICC change from the previous age was the strongest predictor of stereotypy, and rearing condition

was no longer a significant predictor when controlling for this factor, we conducted a mediation analysis to determine whether ICC change statistically mediated rearing condition-related differences in stereotypy. We found that ICC change significantly mediated the rearing condition effect (*ACME* = 0.43, *CI*: [0.08, 0.98], $p = 0.022$). The portion of the rearing condition effect *not* mediated by ICC change was non-significant (*ADE* = 0.31, *CI*: [-0.43, 1.06], $p = 0.388$), whereas the total effect (i.e., a combination of the *ACME* and *ADE*) was significant (*TE* = 0.75, *CI*: [-0.01, 1.41], $p = 0.046$). ICC change mediated approximately 58.1% of the total effect (*CI*: [11.3%, 544%], $p = 0.061$). A mediation path diagram and the bootstrap distribution of the *ACME* are displayed in Figure 3.7.

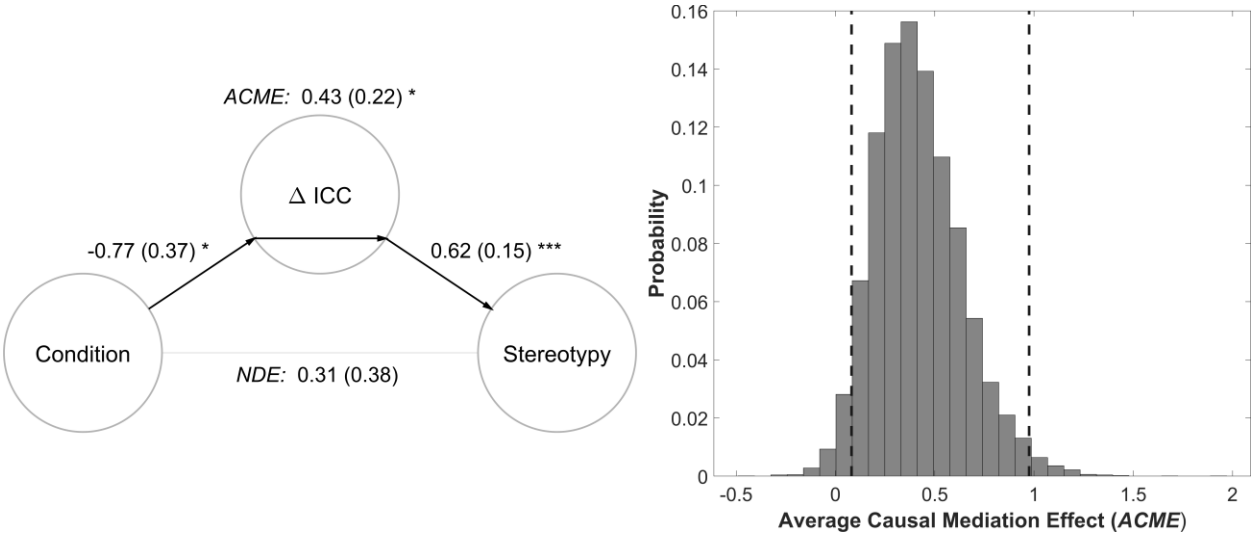

Figure 3.7. Mediation of rearing condition-related differences in stereotypy. **Left:** Path model for the mediation of rearing condition-related differences in stereotypy by change in left NCM ICC from the previous age. Coefficient estimates are reported with standard errors in parentheses. *$p < 0.01$, **$p < 0.005$, ***$p < 0.001$. **Right:** A probability scale histogram of the bootstrap distribution for the indirect effect, also known as the average causal mediation effect (*ACME*). Dashed lines demarcate the 95% confidence interval of the mediation effect.

Discussion

The current study identified FC signatures of tutor experience across the CP for song learning in zebra finches. Data-driven whole-brain analyses identified a cluster centered within left NCM in which ICC decreased across the CP for Isolates but increased or was stable for Normal and Tutored birds. S2V analyses revealed that the FC between the left NCM cluster and a cluster centered within the left dorsal cerebellum exhibited parallel developmental trends. Surprisingly, both the change in left NCM ICC and the magnitude of FC between the left NCM and dorsal cerebellum clusters strongly predicted the juvenile zebra finches' emerging song stereotypy at P65 and P90, in the middle and towards the end of the sensorimotor learning period. Additionally, changes in left NCM ICC from the previous age statistically mediated Isolates' lower levels of stereotypy. Together, these findings suggest that the development of left NCM FC may be highly dependent upon tutor experience during the CP, consistent with previous reports that NCM undergoes experience-dependent neural plasticity in support of tutor song memorization (for reviews, see Bolhuis & Moorman, 2015; London, 2017). Additionally, the association between left NCM ICC and the subsequent emergence of song stereotypy during sensorimotor learning suggests that the functional connections of the auditory forebrain may play an important role in successful sensorimotor learning (Akutagawa & Konishi, 2010; Bauer et al., 2008; Fortune & Margoliash, 1995; Shaevitz & Theunissen, 2007; Vates et al., 1996; Yanagihara & Yazaki-Sugiyama, 2016).

The observation that left NCM ICC depends upon tutor experience during the CP is consistent with a large and growing body of evidence indicating that NCM undergoes tutor experience-dependent plasticity in support of tutor song memorization (for reviews, see Bolhuis & Moorman, 2015; London, 2017). The current results extend these findings to the systems level

using rs-fMRI. Moreover, they indicate that, not only does *local* tutor experience-dependent plasticity occur within NCM itself, but tutor experience also appears to support the development of NCM's centrality or importance within broader functional networks. Specifically, the developmental decline in ICC observed within the left NCM of Isolates suggests that tutor experience during the CP may be critical for preserving or strengthening functional connections between NCM and other regions. If tutor experience does not occur, then NCM FC may weaken with relative disuse.

Interestingly, some evidence suggests that NCM may be functionally left lateralized for tutor song sensory learning (for review, see Moorman & Nicol, 2015; cf. Phan & Vicario, 2010; Voss et al., 2007). For instance, Moorman et al. (2012) found that NCM IEG *ZENK* expression was left lateralized specifically in response to tutor song playback during the sensory learning period, but not for the playback of novel song or silence (Moorman et al., 2012). Moreover, the degree of NCM left lateralization was strongly correlated with the extent of tutor song copying (Moorman et al., 2012). A similar result was reported for spontaneous NCM *ZENK* expression in juveniles during sleep: good learners (i.e., superior tutor song copying) showed significantly more left lateralization for NCM activity, whereas poor learners tended to be right lateralized (Moorman et al., 2015). In the current study, we identified a cluster confined within the left hemisphere, wherein ICC was developmentally dependent on tutor experience. However, a follow-up analysis revealed that a homotopic right NCM cluster also showed a parallel rearing condition-related developmental difference in ICC. The effect size in the right NCM cluster was numerically smaller than that observed in left NCM, but these were effects not significantly different ($p = 0.224$). It is possible that the current study was simply insufficiently powered to detect a small lateralization effect ($\beta = 0.35$). However, this result also seems to indicate that the

rearing condition-related developmental difference observed in NCM was, at least to some extent, bilateral in nature. The cluster detected did not extend into the right hemisphere possibly due to the use of a stringent CDT, which is unfortunately necessary for valid statistical inference with the cluster-extent threshold method (Woo, Krishnan, & Wager, 2014). Notably, the lack of a lateralization effect also seems consistent with our previous finding that the auditory forebrain shows strong homotopic FC (Layden et al., 2019).

In addition to left NCM, the present results also highlighted the potential involvement of a novel cluster encompassing part of the left dorsal cerebellum. Although the cerebellum has a widely recognized, if incompletely understood, role in fine motor control (for review, see Manto et al., 2012), its potential contribution to song learning and/or production has received relatively little attention. In contrast, a large and growing body of evidence suggests that the cerebellum plays important roles in various aspects of human language (for reviews, see Hertrich, Mathiak, & Ackermann, 2016; Pleger & Timmann, 2018; Ziegler & Ackermann, 2017), including linguistic prediction (D'Mello, Turkeltaub, & Stoodley, 2017; Lesage, Hansen, & Miall, 2017; Lesage, Morgan, Olson, Meyer, & Miall, 2012; Moberget, Gullesen, Andersson, Ivry, & Endestad, 2014), verbal working memory (Chen & Desmond, 2005; Kirschen, Chen, Schraedley-Desmond, & Desmond, 2005; Ravizza et al., 2006), and word generation (Arasanz, Staines, Roy, & Schweizer, 2012). Recently, a link was found between the songbird AFP (Perkel, 2004) and the cerebellum. Previously, it was known that Area X (basal ganglia) of the AFP projects to the dorsolateral nucleus of the anterior thalamus (DLM). However, it was only recently discovered that Area X also receives a projection from DLM, as well as from an adjacent region that provides cerebellar input (Hamaide et al., 2018; Nicholson, Roberts, & Sober, 2018). Although this connection does not provide a direct structural connectivity pathway between NCM and the

cerebellum, it does at least establish a structural link between the cerebellum and the song network. Given the parallels between human speech acquisition and zebra finch song learning, this link, and potentially other yet undiscovered links, between the cerebellum and song network may merit further investigation for potential roles in song learning or production.

Limitations

Although our results suggest that left NCM ICC is linked to the emergence of song stereotypy, we were unable to determine whether left NCM ICC was also related to the extent of tutor song copying. Tutor song similarity data was obviously not available for Isolates, given that they were not tutored, but it was also not known which adult males served as tutors for the aviary-reared Normal condition birds. Future studies might utilize a larger sample of Tutored condition birds to examine whether left NCM FC is also associated with the extent of tutor song copying, in addition to song stereotypy.

Conclusion

Overall, our results suggest that tutor experience during the CP for tutor song memorization strongly modulates the development and maintenance of left NCM FC, consistent with prior indications that NCM is critical for tutor song memorization. Moreover, left NCM ICC strongly predicted the emergence of song stereotypy during the sensorimotor learning period. Future investigations are merited to determine whether left NCM FC similarly predicts the extent of tutor song copying, and we hope that the current study lays the groundwork for such investigations. In conclusion, we hope that the current study has underlined the utility of the rs-fMRI FC paradigm for conducting comparative studies to investigate the neural mechanisms that support the developmental learning of complex behaviors.

GENERAL DISCUSSION

This dissertation has described the novel use of rs-fMRI FC analyses to study interhemispheric coordination in the zebra finch brain and to investigate FC signatures of tutor experience during the CP for song learning. Chapter 1 discussed the selection of scanning parameters (pulse sequence, TR, and TE), the construction of a custom zebra finch brain template using ANTs, and the creation of two custom Matlab toolboxes (NeuroViz and MRIqual). NeuroViz allowed us to extract our custom zebra finch brain template from surrounding tissues and to delineate a set of twenty ROIs important for sensory, sensorimotor, and premotor processing of zebra finch song. With MRIqual, we conducted *tSNR* validation analyses and power spectral analyses, which helped to assure the quality of our rs-fMRI data.

Chapter 2 focused on a pattern of bilaterally symmetric intrinsic brain activity (i.e., homotopic FC) in the zebra finch brain across development. Homotopic FC was not only identified among a set of structurally connected homotopic ROIs, but also throughout the zebra finch song network, which lacks direct homotopic SC. Additionally, we conducted VMHC analyses, which indicated that homotopic FC was a global feature of the zebra finch brain network, not restricted to our *a priori* ROIs. The presence of homotopic FC in a non-Eutherian vertebrate suggests that ancestral pathways, potentially including indirect connectivity via the AC, are sufficient to maintain a homotopic functional architecture without the CC in normal ontogeny, an insight with potentially broad implications for understanding interhemispheric coordination across phylogeny.

Chapter 2 raises a number of interesting questions for future research to explore. First, given that homotopic FC has been observed in humans (Shen et al., 2015; Stark et al., 2008; Zhang et al., 2014; Zuo et al., 2010), macaques (Shen et al., 2015), rodents (Matsui et al., 2016;

Pan et al., 2011), and now in an avian species (Layden et al., 2019), this begs the question of whether homotopic FC is also present within other classes of encephalized vertebrates. For example, might homotopic FC also be identified within the brains of reptiles, amphibians, or fish? If so, this may suggest that, just as bilaterians are characterized by having a bilaterally symmetric body morphology, perhaps encephalized vertebrates are also characterized by bilaterally symmetric intrinsic brain activity. That is, perhaps homotopic FC is a fundamental property of the two-sided brain, enabling interhemispheric coordination between the two hemispheres, which are then able to individually specialize in different aspects of processing without a resultant loss of function within the global brain network (Gazzaniga, 2000).

A second fundamental question is whether homotopic FC is a signature of underlying information exchange between homotopic regions, or if it instead represents some form of interhemispheric coordination that does not result from direct communication between hemispheres. The extant literature, while certainly offering some hints, does not yet appear to offer a conclusive answer to this question. We therefore remained agnostic in Chapter 2 by adopting the term "coordination," rather than "communication." If homotopic FC is *primarily* mediated by the CC in mammals, as substantial evidence indeed suggests (Hermesdorf et al., 2016; Jarbo et al., 2012; Johnston et al., 2008; Roland et al., 2017; Shen et al., 2015), then this would potentially support a role for homotopic FC in interhemispheric communication (at least in Eutherian mammals), as it is well established that the CC transfers critical information between hemispheres (for review, see van der Knaap & van der Ham, 2011). In the zebra finch brain, it is also possible that homotopic FC could be a signature of interhemispheric communication, but this would need to be mediated instead by multisynaptic pathways, traversing the more evolutionarily ancient AC (Letzner et al., 2016), thalamus, or hindbrain

(Ashmore et al., 2008; Schmidt et al., 2006). Additionally, while shy of definitively demonstrating a role in interhemispheric communication, some studies have linked homotopic FC to correlations in the band limited power fluctuations of LFPs (Nir et al., 2008; Pan et al., 2011), thus directly establishing that homotopic FC is at least of neural origin. However, additional research is needed to definitively determine whether homotopic FC plays a role in interhemispheric communication or merely coordination. Future studies may benefit from (1) analyzing homotopic FC on faster time scales than rs-fMRI (e.g., using magnetoencephalography or LFPs), (2) using measures of effective connectivity or predictive causality rather than correlation-based FC (e.g., Granger causality; for review, see Friston, 2011; Friston, Moran, & Seth, 2013), and (3) investigating dynamic rather than static measures of connectivity (for review, see Hutchison et al., 2013).

The results presented in Chapter 2 elicit a third important question, concerning the role of SC: if interhemispheric coordination remains intact without the CC in normal ontogeny, what then is the precise function of the CC in mammals? Surprisingly, this question is still stringently debated (for reviews, see Bloom & Hynd, 2005; van der Knaap & van der Ham, 2011). The CC does not merely mediate interhemispheric coordination. Rather, it is also believed to enforce hemispheric lateralization in some cases (Chiarello & Maxfield, 1996; Cook, 1984a, 1984b; McGilchrist, 2010; Meyer, Röricht, von Einsiedel, Kruggel, & Weindl, 1995), potentially including for human language (Josse, Seghier, Kherif, & Price, 2008; but see Hines, Chiu, McAdams, Bentler, & Lipcamon, 1992; Lassonde, Bryden, & Demers, 1990). Although most CC fibers are excitatory in nature (i.e., glutamergic), some crossing fibers synapse onto inhibitory interneurons within the contralateral hemisphere, meaning that callosal transmission can result in initial excitation followed by prolonged inhibition (Conti & Manzoni, 1994; Kawaguchi, 1992;

McGilchrist, 2010). Such observations have given rise to competing inhibitory (lateralization) and excitatory (coordination) models of CC function, both of which appear to be well-evidenced (Bloom & Hynd, 2005; van der Knaap & van der Ham, 2011). Indeed, a broad synthesis of the evidence suggests that the CC may play either excitatory or inhibitory roles in different contexts (van der Knaap & van der Ham, 2011). Further, it has been suggested that the CC may in fact specialize in the regulation of an adaptive balance between interhemispheric coordination and hemispheric specialization, capable of dynamically shifting this balance to accommodate varying task demands (Bloom & Hynd, 2005; Schulte & Müller-Oehring, 2010; Welcome & Chiarello, 2008). Interestingly, in the broader context of functional brain networks, this dynamic interplay between functional segregation and integration has been captured by the construct of neural complexity (Sporns, Tononi, & Edelman, 2000; Tononi, Edelman, & Sporns, 1998; Tononi, Sporns, & Edelman, 1994). It may be informative to examine whether this balance between coordination and lateralization also dynamically shifts within the zebra finch brain during the resting-state versus during singing, despite lacking the CC.

As mentioned, Chapter 2 extensively discussed the balance between interhemispheric coordination and hemispheric specialization for complex multimodal processes, including vocal learning. These topics provide some important links between Chapters 2 and 3. First, a number of studies have identified (albeit sometimes conflicting) evidence of lateralization for different aspects of neural processing that support learned vocalizations in zebra finches (for reviews, see Moorman & Nicol, 2015; Rogers, Koboroff, & Kaplan, 2018). For example, using auditory fMRI, Van Ruijssevelt, Washington, et al., (2017) found that left NCM was more sensitive to the temporal structure of conspecific songs, whereas right NCM was more sensitive to spectral features, providing a parallel to the hemispheric specialization observed in human auditory

cortex (Zatorre, Belin, & Penhune, 2002). Additionally, some studies have found that IEG expression within NCM exhibits a left-lateralized response specific to tutor song playback (Moorman et al., 2015, 2012), with indications that the degree of lateralization may be linked to successful song learning (Moorman et al., 2015). Interestingly, a subsequent study found that asymmetric responses within NCM may be related to the recentness of auditory memories, with left NCM preferentially responding to the reactivation of recent auditory memories and right NCM preferentially responding to the reactivation of distant auditory memories (Olson, Maeda, & Gobes, 2016). Although hemispheric specialization may be important for the auditory processing of song, it is also known that zebra finches must tightly synchronize premotor activity to successfully produce song (Ashmore et al., 2008; Schmidt et al., 2006). Together, these findings suggest that, similar to the neural processing that supports human speech, zebra finches also balance hemispheric specialization and interhemispheric coordination to support complex learned behavior. The widespread homotopic FC identified in Study 2 suggests the possibility that there may be additional uses for interhemispheric coordination in the zebra finch brain yet to be discovered. Future studies are therefore merited to investigate the broader relevance of homotopic FC within the zebra finch brain for behavior, including for learned vocalizations.

In Chapter 3, we identified brain regions that exhibited developmental differences in FC across the CP for tutor song memorization, based on tutor experience or lack thereof. Specifically, we found that a cluster encompassing parts of left NCM showed decreasing ICC from P25 to P90 in Isolates, whereas ICC was constant or increased across development for Normal and Tutored birds. Second, we identified a parallel developmental difference in the FC between the left NCM cluster and a previously uncharacterized cluster residing primarily within the left dorsal cerebellum. Surprisingly, we found that FC features strongly predicted the

developmental emergence of song stereotypy at P65 and P90, even when controlling for tutor experience. In fact, changes in ICC within the left NCM cluster statistically mediated Isolates' lower levels of stereotypy. This result is perhaps particularly notable, given that previous investigations of vocal variability and song stereotypy have largely focused on components of the AFP (Kao & Brainard, 2006; Kao, Doupe, & Brainard, 2005; Thompson, Basista, Wu, Bertram, & Johnson, 2011; Woolley & Kao, 2015), rather than auditory pathways. In sum, our results further highlight the likely importance of links between the auditory forebrain and the traditional song network (i.e., PMP and AFP) for sensorimotor learning (Akutagawa & Konishi, 2010; Bauer et al., 2008; Fortune & Margoliash, 1995; Shaevitz & Theunissen, 2007; Vates et al., 1996), and they also highlight a potential functional link between the auditory forebrain and the cerebellum to be explored in future research.

Interestingly, Isolates exhibited a developmental trend of decreasing ICC within the left NCM cluster across the CP, consistent with diminishing NCM participation in large-scale functional networks. This suggests the possibility that the use or disuse of NCM for the memorization of tutor song may be a critical factor, not only for molecular signaling within NCM itself (Ahmadiantehrani & London, 2017; Chew, Mello, Nottebohm, Jarvis, & Vicario, 1995; Chew et al., 1996; London & Clayton, 2008; Mello, Velho, & Pinaud, 2004), but also for the centrality or importance of NCM within broader brain networks.

An interesting parallel to this usage-dependent interpretation of developmental FC strength involves neurogenesis in the zebra finch brain, which occurs extensively within NCM in both juveniles (DeWulf & Bottjer, 2005; Nordeen & Nordeen, 1988) and adults (Barnea, Mishal, & Nottebohm, 2006; Lipkind, Nottebohm, Rado, & Barnea, 2002; Nottebohm, 2002; Pytte, Parent, Wildstein, Varghese, & Oberlander, 2010). It has been suggested that the survival of

newly generated neurons within NCM is linked to auditory exposure to conspecific songs (Adar, Lotem, & Barnea, 2008), and a recent study found that zebra finches deafened in adulthood (>P90) showed significantly decreased neuronal incorporation within NCM (Pytte et al., 2010). Interestingly, newly generated neurons are known to facilitate synaptic plasticity (Nissant, Bardy, Katagiri, Murray, & Lledo, 2009; Schmidt-Hieber, Jonas, & Bischofberger, 2004). Additionally, several forms of learning, potentially including tutor song memorization (Nottebohm, 2002), are promoted by neurogenesis (Gould, Beylin, Tanapat, Reeves, & Shors, 1999; Praag, Christie, Sejnowski, & Gage, 1999; Shors et al., 2001). This usage-dependent model of neurogenesis in NCM supports the plausibility of the hypothesis that the incorporation of NCM into large-scale functional networks might similarly depend upon use or disuse. In this case, however, use would be specific to tutor experience during the CP, and perhaps to tutor song memorization, as opposed to auditory or social experience more broadly.

Additional research is merited to better integrate the developmental FC findings presented in Chapter 3 with prior findings based on molecular signaling, electrophysiological, and lesion-based methods. A number of prior studies have indicated that NCM undergoes local tutor experience-dependent neural plasticity critical for tutor song memorization (e.g., Ahmadiantehrani & London, 2017; Bolhuis et al., 2001, 2000; London & Clayton, 2008; Terpstra et al., 2004). Our findings in Chapter 3 suggest that NCM may also undergo changes in the level of participation in large-scale brain networks in response to tutor experience. To what extent, then, does tutor experience-dependent plasticity involve strengthening or refinement of local connections within NCM versus modification of longer-range connections emanating from or projecting to external regions? Interestingly, evidence suggests that local inhibitory interneurons within NCM may be critical for tutor song selective electrophysiological responses

(Yanagihara & Yazaki-Sugiyama, 2016). However, it is plausible that connections with other external brain regions might be particularly important for other functions, such as comparing the bird's own song to the tutor song template. This is an interesting question that could be explored in future research. Additionally, although we identified a novel functional connection between the left NCM and the dorsal cerebellum, future research could further examine which specific functional connections underlie the ICC effects we observed here, potentially focusing on links between the auditory forebrain and motor pathways.

In conclusion, these chapters have described the development of methods for the preprocessing and analysis of rs-fMRI data in small animals, identified a pattern of bilaterally symmetric intrinsic brain activity in the zebra finch, and identified a developmental FC signature of tutor experience during the sensory learning CP. It is my hope that these efforts have helped to lay the groundwork for future studies to continue exploring the interplay between hemispheric specialization and interhemispheric coordination, as well as the neural mechanisms that support the learning of complex behaviors, in comparative rs-fMRI studies across phylogeny.

REFERENCES

Aboitiz, F., & Montiel, J. (2003). One hundred million years of interhemispheric communication: the history of the corpus callosum. *Brazilian Journal of Medical and Biological Research*, *36*(4), 409–420.

Adar, E., Lotem, A., & Barnea, A. (2008). The effect of social environment on singing behavior in the zebra finch (Taeniopygia guttata) and its implication for neuronal recruitment. *Behavioural Brain Research*, *187*(1), 178–184. https://doi.org/10.1016/j.bbr.2007.09.011

Ahmadiantehrani, S., & London, S. E. (2017). Bidirectional manipulation of mTOR signaling disrupts socially mediated vocal learning in juvenile songbirds. *Proceedings of the National Academy of Sciences*, *114*(35), 9463–9468.

Akutagawa, E., & Konishi, M. (2010). New brain pathways found in the vocal control system of a songbird. *Journal of Comparative Neurology*, *518*(15), 3086–3100. https://doi.org/10.1002/cne.22383

Arasanz, C. P., Staines, W. R., Roy, E. A., & Schweizer, T. A. (2012). The cerebellum and its role in word generation: A cTBS study. *Cortex*, *48*(6), 718–724. https://doi.org/10.1016/j.cortex.2011.02.021

Arnold, A. P. (1975). The effects of castration on song development in zebra finches (Poephila guttata). *Journal of Experimental Zoology*, *191*(2), 261–277. https://doi.org/10.1002/jez.1401910212

Aronov, D., Andalman, A. S., & Fee, M. S. (2008). A specialized forebrain circuit for vocal babbling in the juvenile songbird. *Science*, *320*(5876), 630–634.

Ashburner, J., & Friston, K. J. (2005). Unified segmentation. *NeuroImage*, *26*(3), 839–851. https://doi.org/10.1016/j.neuroimage.2005.02.018

Ashmore, R. C., Bourjaily, M., & Schmidt, M. F. (2008). Hemispheric coordination is necessary for song production in adult birds: implications for a dual role for forebrain nuclei in vocal motor control. *Journal of Neurophysiology*, *99*(1), 373–385.

Avants, B. B., Epstein, C. L., Grossman, M., & Gee, J. C. (2008). Symmetric diffeomorphic image registration with cross-correlation: Evaluating automated labeling of elderly and neurodegenerative brain. *Medical Image Analysis*, *12*(1), 26–41. https://doi.org/10.1016/j.media.2007.06.004

Avants, B. B., Tustison, N. J., Song, G., Cook, P. A., Klein, A., & Gee, J. C. (2011). A reproducible evaluation of ANTs similarity metric performance in brain image registration. *Neuroimage*, *54*(3), 2033–2044.

Avants, B. B., Tustison, N., & Song, G. (2009). Advanced normalization tools (ANTS). *Insight j*, *2*, 1–35.

Avants, B. B., Yushkevich, P., Pluta, J., Minkoff, D., Korczykowski, M., Detre, J., & Gee, J. C. (2010). The optimal template effect in hippocampus studies of diseased populations. *Neuroimage*, *49*(3), 2457–2466.

Avey, M. T., Phillmore, L. S., & MacDougall-Shackleton, S. A. (2005). Immediate early gene expression following exposure to acoustic and visual components of courtship in zebra finches. *Behavioural Brain Research*, *165*(2), 247–253. https://doi.org/10.1016/j.bbr.2005.07.002

Babadi, B., & Brown, E. N. (2014). A Review of Multitaper Spectral Analysis. *IEEE Transactions on Biomedical Engineering*, *61*(5), 1555–1564. https://doi.org/10.1109/TBME.2014.2311996

Barnea, A., Mishal, A., & Nottebohm, F. (2006). Social and spatial changes induce multiple survival regimes for new neurons in two regions of the adult brain: An anatomical representation of time? *Behavioural Brain Research*, *167*(1), 63–74. https://doi.org/10.1016/j.bbr.2005.08.018

Barth, M., & Norris, D. G. (2007). Very high-resolution three-dimensional functional MRI of the human visual cortex with elimination of large venous vessels. *NMR in Biomedicine*, *20*(5), 477–484. https://doi.org/10.1002/nbm.1158

Bassett, D. S., Wymbs, N. F., Porter, M. A., Mucha, P. J., Carlson, J. M., & Grafton, S. T. (2011). Dynamic reconfiguration of human brain networks during learning. *Proceedings of the National Academy of Sciences*, *108*(18), 7641–7646. https://doi.org/10.1073/pnas.1018985108

Bauer, E. E., Coleman, M. J., Roberts, T. F., Roy, A., Prather, J. F., & Mooney, R. (2008). A Synaptic Basis for Auditory–Vocal Integration in the Songbird. *Journal of Neuroscience*, *28*(6), 1509–1522. https://doi.org/10.1523/JNEUROSCI.3838-07.2008

Beaty, R. E., Kenett, Y. N., Christensen, A. P., Rosenberg, M. D., Benedek, M., Chen, Q., … Silvia, P. J. (2018). Robust prediction of individual creative ability from brain functional connectivity. *Proceedings of the National Academy of Sciences*, *115*(5), 1087–1092. https://doi.org/10.1073/pnas.1713532115

Behzadi, Y., Restom, K., Liau, J., & Liu, T. T. (2007). A component based noise correction method (CompCor) for BOLD and perfusion based fMRI. *NeuroImage*, *37*(1), 90–101. https://doi.org/10.1016/j.neuroimage.2007.04.042

Bernstein, M. A., King, K. F., & Zhou, X. J. (2004). *Handbook of MRI Pulse Sequences*. Elsevier.

Biswal, B. B., Mennes, M., Zuo, X.-N., Gohel, S., Kelly, C., Smith, S. M., … Milham, M. P. (2010). Toward discovery science of human brain function. *Proceedings of the National Academy of Sciences*, *107*(10), 4734–4739. https://doi.org/10.1073/pnas.0911855107

Biswal, B., Deyoe, E. A., & Hyde, J. S. (1996). Reduction of physiological fluctuations in fMRI using digital filters. *Magnetic Resonance in Medicine*, *35*(1), 107–113. https://doi.org/10.1002/mrm.1910350114

Biswal, B., Yetkin, F. Z., Haughton, V. M., & Hyde, J. S. (1995). Functional connectivity in the motor cortex of resting human brain using echo-planar mri. *Magnetic Resonance in Medicine*, *34*(4), 537–541. https://doi.org/10.1002/mrm.1910340409

Bloom, J. S., & Hynd, G. W. (2005). The Role of the Corpus Callosum in Interhemispheric Transfer of Information: Excitation or Inhibition? *Neuropsychology Review*, *15*(2), 59–71. https://doi.org/10.1007/s11065-005-6252-y

Böhner, J. (1990). Early acquisition of song in the zebra finch, Taeniopygia guttata. *Animal Behaviour*, *39*(2), 369–374. https://doi.org/10.1016/S0003-3472(05)80883-8

Bolhuis, J. J., & Gahr, M. (2006). Neural mechanisms of birdsong memory. *Nature Reviews Neuroscience*, *7*(5), 347–357. https://doi.org/10.1038/nrn1904

Bolhuis, J. J., Hetebrij, E., Boer-Visser, A. M. D., Groot, J. H. D., & Zijlstra, G. G. O. (2001). Localized immediate early gene expression related to the strength of song learning in socially reared zebra finches. *European Journal of Neuroscience*, *13*(11), 2165–2170. https://doi.org/10.1046/j.0953-816x.2001.01588.x

Bolhuis, J. J., & Moorman, S. (2015). Birdsong memory and the brain: In search of the template. *Neuroscience & Biobehavioral Reviews*, *50*, 41–55. https://doi.org/10.1016/j.neubiorev.2014.11.019

Bolhuis, J. J., Okanoya, K., & Scharff, C. (2010). Twitter evolution: converging mechanisms in birdsong and human speech. *Nature Reviews Neuroscience*, *11*(11), 747–759. https://doi.org/10.1038/nrn2931

Bolhuis, J. J., Zijlstra, G. G. O., Boer-Visser, A. M. den, & Zee, E. A. V. der. (2000). Localized neuronal activation in the zebra finch brain is related to the strength of song learning. *Proceedings of the National Academy of Sciences*, *97*(5), 2282–2285. https://doi.org/10.1073/pnas.030539097

Bottjer, S. W., Miesner, E. A., & Arnold, A. P. (1984). Forebrain lesions disrupt development but not maintenance of song in passerine birds. *Science*, *224*(4651), 901–903. https://doi.org/10.1126/science.6719123

Boumans, T., Gobes, S. M. H., Poirier, C., Theunissen, F. E., Vandersmissen, L., Pintjens, W., … Linden, A. V. der. (2008a). Functional MRI of Auditory Responses in the Zebra Finch Forebrain Reveals a Hierarchical Organisation Based on Signal Strength but Not Selectivity. *PLOS ONE*, *3*(9), e3184. https://doi.org/10.1371/journal.pone.0003184

Boumans, T., Theunissen, F. E., Poirier, C., & Van Der Linden, A. (2007). Neural representation of spectral and temporal features of song in the auditory forebrain of zebra finches as revealed by functional MRI. *European Journal of Neuroscience*, *26*(9), 2613–2626.

Boumans, T., Vignal, C., Smolders, A., Sijbers, J., Verhoye, M., Van Audekerke, J., … Van der Linden, A. (2008b). Functional Magnetic Resonance Imaging in Zebra Finch Discerns the Neural Substrate Involved in Segregation of Conspecific Song From Background Noise. *Journal of Neurophysiology*, *99*(2), 931–938. https://doi.org/10.1152/jn.00483.2007

Boveroux, P., Vanhaudenhuyse, A., Bruno, M.-A., Noirhomme, Q., Lauwick, S., Luxen, A., … Boly, M. (2010). Breakdown of within- and between-network Resting State Functional Magnetic Resonance Imaging Connectivity during Propofol-induced Loss of Consciousness. *Anesthesiology: The Journal of the American Society of Anesthesiologists*, *113*(5), 1038–1053. https://doi.org/10.1097/ALN.0b013e3181f697f5

Bozon, B., Kelly, Á., Josselyn, S. A., Silva, A. J., Davis, S., & Laroche, S. (2003). MAPK, CREB and zif268 are all required for the consolidation of recognition memory. *Philosophical Transactions of the Royal Society of London. Series B: Biological Sciences*, *358*(1432), 805–814. https://doi.org/10.1098/rstb.2002.1224

Braaten, R. F. (2010). Song recognition in zebra finches: Are there sensitive periods for song memorization? *Learning and Motivation*, *41*(3), 202–212. https://doi.org/10.1016/j.lmot.2010.04.005

Bright, M. G., & Murphy, K. (2015). Is fMRI "noise" really noise? Resting state nuisance regressors remove variance with network structure. *NeuroImage*, *114*, 158–169.

Budde, J., Shajan, G., Zaitsev, M., Scheffler, K., & Pohmann, R. (2014). Functional MRI in human subjects with gradient-echo and spin-echo EPI at 9.4 T. *Magnetic Resonance in Medicine*, *71*(1), 209–218. https://doi.org/10.1002/mrm.24656

Bukhari, Q., Schroeter, A., & Rudin, M. (2018). Increasing isoflurane dose reduces homotopic correlation and functional segregation of brain networks in mice as revealed by resting-state fMRI. *Scientific Reports*, *8*(1), 10591. https://doi.org/10.1038/s41598-018-28766-3

Bullmore, E., & Sporns, O. (2009). Complex brain networks: graph theoretical analysis of structural and functional systems. *Nature Reviews Neuroscience*, *10*(3), 186–198. https://doi.org/10.1038/nrn2575

Burnham, K. P., & Anderson, D. R. (2004). Multimodel Inference: Understanding AIC and BIC in Model Selection. *Sociological Methods & Research*, *33*(2), 261–304. https://doi.org/10.1177/0049124104268644

Casimo, K., Grassia, F., Poliachik, S. L., Novotny, E., Poliakov, A., & Ojemann, J. G. (2018). Preservation of electrophysiological functional connectivity after partial corpus callosotomy: case report. *Journal of Neurosurgery: Pediatrics*, *22*(2), 214–219. https://doi.org/10.3171/2018.2.PEDS17549

Chang, W.-T., Puspitasari, F., Garcia-Miralles, M., Yeow, L. Y., Tay, H.-C., Koh, K. B., … Chuang, K.-H. (2018). Connectomic imaging reveals Huntington-related pathological and

pharmaceutical effects in a mouse model. *NMR in Biomedicine*, *31*(12), e4007. https://doi.org/10.1002/nbm.4007

Charlesworth, J. D., Warren, T. L., & Brainard, M. S. (2012). Covert skill learning in a cortical-basal ganglia circuit. *Nature*, *486*(7402), 251–255. https://doi.org/10.1038/nature11078

Chen, S. H. A., & Desmond, J. E. (2005). Cerebrocerebellar networks during articulatory rehearsal and verbal working memory tasks. *NeuroImage*, *24*(2), 332–338. https://doi.org/10.1016/j.neuroimage.2004.08.032

Cheng, H.-Y., & Clayton, D. F. (2004). Activation and Habituation of Extracellular Signal-Regulated Kinase Phosphorylation in Zebra Finch Auditory Forebrain during Song Presentation. *Journal of Neuroscience*, *24*(34), 7503–7513. https://doi.org/10.1523/JNEUROSCI.1405-04.2004

Chew, S. J., Mello, C., Nottebohm, F., Jarvis, E., & Vicario, D. S. (1995). Decrements in auditory responses to a repeated conspecific song are long-lasting and require two periods of protein synthesis in the songbird forebrain. *Proceedings of the National Academy of Sciences*, *92*(8), 3406–3410. https://doi.org/10.1073/pnas.92.8.3406

Chew, S. J., Vicario, D. S., & Nottebohm, F. (1996). A large-capacity memory system that recognizes the calls and songs of individual birds. *Proceedings of the National Academy of Sciences*, *93*(5), 1950–1955. https://doi.org/10.1073/pnas.93.5.1950

Chiarello, C., & Maxfield, L. (1996). Varieties of Interhemispheric Inhibition, or How to Keep a Good Hemisphere Down. *Brain and Cognition*, *30*(1), 81–108. https://doi.org/10.1006/brcg.1996.0006

Clayton, N. S. (1987). Song Learning in Cross-Fostered Zebra Finches: a Re-Examination of the Sensitive Phase. *Behaviour*, *102*(1–2), 67–81. https://doi.org/10.1163/156853986X00054

Conti, F., & Manzoni, T. (1994). The neurotransmitters and postsynaptic actions of callosally projecting neurons. *Behavioural Brain Research*, *64*(1), 37–53. https://doi.org/10.1016/0166-4328(94)90117-1

Cook, N. D. (1984a). Callosal inhibition: The key to the brain code. *Behavioral Science*, *29*(2), 98–110. https://doi.org/10.1002/bs.3830290203

Cook, N. D. (1984b). Homotopic callosal inhibition. *Brain and Language*, *23*(1), 116–125. https://doi.org/10.1016/0093-934X(84)90010-5

Cordes, D., Haughton, V. M., Arfanakis, K., Carew, J. D., Turski, P. A., Moritz, C. H., … Meyerand, M. E. (2001). Frequencies contributing to functional connectivity in the cerebral cortex in "resting-state" data. *American Journal of Neuroradiology*, *22*(7), 1326–1333.

Cox, R. W. (1996). AFNI: Software for Analysis and Visualization of Functional Magnetic Resonance Neuroimages. *Computers and Biomedical Research*, *29*(3), 162–173. https://doi.org/10.1006/cbmr.1996.0014

Cynx, J., Williams, H., & Nottebohm, F. (1992). Hemispheric differences in avian song discrimination. *Proceedings of the National Academy of Sciences*, *89*(4), 1372–1375. https://doi.org/10.1073/pnas.89.4.1372

De Groof, G., Jonckers, E., Güntürkün, O., Denolf, P., Van Auderkerke, J., & Van der Linden, A. (2013). Functional MRI and functional connectivity of the visual system of awake pigeons. *Behavioural Brain Research*, *239*, 43–50. https://doi.org/10.1016/j.bbr.2012.10.044

De Groof, G., Verhoye, M., Van Meir, V., Tindemans, I., Leemans, A., & Van der Linden, A. (2006). In vivo diffusion tensor imaging (DTI) of brain subdivisions and vocal pathways in songbirds. *Neuroimage*, *29*(3), 754–763.

De Luca, M., Beckmann, C. F., De Stefano, N., Matthews, P. M., & Smith, S. M. (2006). fMRI resting state networks define distinct modes of long-distance interactions in the human brain. *NeuroImage*, *29*(4), 1359–1367. https://doi.org/10.1016/j.neuroimage.2005.08.035

de Zwart, J. A., van Gelderen, P., Fukunaga, M., & Duyn, J. H. (2008). Reducing Correlated Noise in fMRI Data. *Magnetic Resonance in Medicine*, *59*(4), 939–945. https://doi.org/10.1002/mrm.21507

Desai, M., Kahn, I., Knoblich, U., Bernstein, J., Atallah, H., Yang, A., … Boyden, E. S. (2010). Mapping brain networks in awake mice using combined optical neural control and fMRI. *Journal of Neurophysiology*, *105*(3), 1393–1405. https://doi.org/10.1152/jn.00828.2010

Deshpande, G., Kerssens, C., Sebel, P. S., & Hu, X. (2010). Altered local coherence in the default mode network due to sevoflurane anesthesia. *Brain Research*, *1318*, 110–121. https://doi.org/10.1016/j.brainres.2009.12.075

DeWulf, V., & Bottjer, S. W. (2005). Neurogenesis within the juvenile zebra finch telencephalic ventricular zone: A map of proliferative activity. *Journal of Comparative Neurology*, *481*(1), 70–83. https://doi.org/10.1002/cne.20352

Dietrich, O., Raya, J. G., Reeder, S. B., Reiser, M. F., & Schoenberg, S. O. (2007). Measurement of signal-to-noise ratios in MR images: Influence of multichannel coils, parallel imaging, and reconstruction filters. *Journal of Magnetic Resonance Imaging*, *26*(2), 375–385. https://doi.org/10.1002/jmri.20969

D'Mello, A. M., Turkeltaub, P. E., & Stoodley, C. J. (2017). Cerebellar tDCS Modulates Neural Circuits during Semantic Prediction: A Combined tDCS-fMRI Study. *Journal of Neuroscience*, *37*(6), 1604–1613. https://doi.org/10.1523/JNEUROSCI.2818-16.2017

Doupe, A. J., & Kuhl, P. K. (1999). Birdsong and human speech: common themes and mechanisms. *Annual Review of Neuroscience*, *22*(1), 567–631.

Doupe, A. J., Perkel, D. J., Reiner, A., & Stern, E. A. (2005). Birdbrains could teach basal ganglia research a new song. *Trends in Neurosciences*, *28*(7), 353–363. https://doi.org/10.1016/j.tins.2005.05.005

Duff, E. P., Johnston, L. A., Xiong, J., Fox, P. T., Mareels, I., & Egan, G. F. (2008). The power of spectral density analysis for mapping endogenous BOLD signal fluctuations. *Human Brain Mapping*, *29*(7), 778–790.

Duong, T. Q., Yacoub, E., Adriany, G., Hu, X., Uğurbil, K., & Kim, S.-G. (2003). Microvascular BOLD contribution at 4 and 7 T in the human brain: Gradient-echo and spin-echo fMRI with suppression of blood effects. *Magnetic Resonance in Medicine*, *49*(6), 1019–1027. https://doi.org/10.1002/mrm.10472

Eales, L. A. (1985). Song learning in zebra finches: some effects of song model availability on what is learnt and when. *Animal Behaviour*, *33*(4), 1293–1300. https://doi.org/10.1016/S0003-3472(85)80189-5

Eales, L. A. (1987). Song learning in female-raised zebra finches: another look at the sensitive phase. *Animal Behaviour*, *35*(5), 1356–1365. https://doi.org/10.1016/S0003-3472(87)80008-8

Eklund, A., Nichols, T. E., & Knutsson, H. (2016). Cluster failure: Why fMRI inferences for spatial extent have inflated false-positive rates. *Proceedings of the National Academy of Sciences*, 201602413. https://doi.org/10.1073/pnas.1602413113

Everitt, B. J., & Robbins, and T. W. (1997). Central Cholinergic Systems and Cognition. *Annual Review of Psychology*, *48*(1), 649–684. https://doi.org/10.1146/annurev.psych.48.1.649

Fee, M. S., & Scharff, C. (2010). The Songbird as a Model for the Generation and Learning of Complex Sequential Behaviors. *ILAR Journal*, *51*(4), 362–377. https://doi.org/10.1093/ilar.51.4.362

Fortune, E. S., & Margoliash, D. (1995). Parallel pathways and convergence onto HVc and adjacent neostriatum of adult zebra finches (Taeniopygia guttata). *Journal of Comparative Neurology*, *360*(3), 413–441. https://doi.org/10.1002/cne.903600305

Fox, M. D., Snyder, A. Z., Vincent, J. L., Corbetta, M., Essen, D. C. V., & Raichle, M. E. (2005). The human brain is intrinsically organized into dynamic, anticorrelated functional networks. *Proceedings of the National Academy of Sciences*, *102*(27), 9673–9678. https://doi.org/10.1073/pnas.0504136102

Friedman, L., Glover, G. H., & The FBIRN Consortium. (2006). Reducing interscanner variability of activation in a multicenter fMRI study: Controlling for signal-to-fluctuation-noise-ratio (SFNR) differences. *NeuroImage*, *33*(2), 471–481. https://doi.org/10.1016/j.neuroimage.2006.07.012

Friston, K. J. (2011). Functional and Effective Connectivity: A Review. *Brain Connectivity*, *1*(1), 13–36. https://doi.org/10.1089/brain.2011.0008

Friston, K. J., Ashburner, J., Frith, C. D., Poline, J.-B., Heather, J. D., & Frackowiak, R. S. J. (1995). Spatial registration and normalization of images. *Human Brain Mapping*, *3*(3), 165–189. https://doi.org/10.1002/hbm.460030303

Friston, K., Moran, R., & Seth, A. K. (2013). Analysing connectivity with Granger causality and dynamic causal modelling. *Current Opinion in Neurobiology*, *23*(2), 172–178. https://doi.org/10.1016/j.conb.2012.11.010

Fukuda, M., Rajagopalan, U. M., Homma, R., Matsumoto, M., Nishizaki, M., & Tanifuji, M. (2005). Localization of Activity-dependent Changes in Blood Volume to Submillimeter-scale Functional Domains in Cat Visual Cortex. *Cerebral Cortex*, *15*(6), 823–833. https://doi.org/10.1093/cercor/bhh183

Galvis, D., Wu, W., Hyson, R. L., Johnson, F., & Bertram, R. (2018). Interhemispheric dominance switching in a neural network model for birdsong. *Journal of Neurophysiology*, *120*(3), 1186–1197. https://doi.org/10.1152/jn.00153.2018

Garza-Lombó, C., & Gonsebatt, M. E. (2016). Mammalian Target of Rapamycin: Its Role in Early Neural Development and in Adult and Aged Brain Function. *Frontiers in Cellular Neuroscience*, *10*. https://doi.org/10.3389/fncel.2016.00157

Gazzaniga, M. S. (2000). Cerebral specialization and interhemispheric communication: Does the corpus callosum enable the human condition? *Brain*, *123*(7), 1293–1326.

Geschwind, N. (1970). The organization of language and the brain. *Science*, *170*(3961), 940–944.

Giovannini, M. G., & Lana, D. (2016). Chapter 10 - mTOR Involvement in the Mechanisms of Memory: An Overview of Animal Studies. In K. Maiese (Ed.), *Molecules to Medicine with mTOR* (pp. 169–184). https://doi.org/10.1016/B978-0-12-802733-2.00018-9

Glickstein, M. (2009). Paradoxical inter-hemispheric transfer after section of the cerebral commissures. *Experimental Brain Research*, *192*(3), 425. https://doi.org/10.1007/s00221-008-1524-4

Glickstein, M., Buchbinder, S., & Iii, J. L. M. (1998). Visual control of the arm, the wrist and the fingers: pathways through the brain. *Neuropsychologia*, *36*(10), 981–1001. https://doi.org/10.1016/S0028-3932(98)00053-0

Glickstein, M., & Sperry, R. W. (1960). Intermanual somesthetic transfer in split-brain rhesus monkeys. *Journal of Comparative and Physiological Psychology*, *53*(4), 322–327. https://doi.org/10.1037/h0046386

Gobes, S. M. H., Zandbergen, M. A., & Bolhuis, J. J. (2010). Memory in the making: localized brain activation related to song learning in young songbirds. *Proceedings of the Royal Society of London B: Biological Sciences*, *277*(1698), 3343–3351. https://doi.org/10.1098/rspb.2010.0870

Gould, E., Beylin, A., Tanapat, P., Reeves, A., & Shors, T. J. (1999). Learning enhances adult neurogenesis in the hippocampal formation. *Nature Neuroscience*, *2*(3), 260. https://doi.org/10.1038/6365

Grandjean, J., Schroeter, A., Batata, I., & Rudin, M. (2014). Optimization of anesthesia protocol for resting-state fMRI in mice based on differential effects of anesthetics on functional connectivity patterns. *Neuroimage*, *102*, 838–847.

Graybiel, A. M. (2005). The basal ganglia: learning new tricks and loving it. *Current Opinion in Neurobiology*, *15*(6), 638–644. https://doi.org/10.1016/j.conb.2005.10.006

Greicius, M. D., Flores, B. H., Menon, V., Glover, G. H., Solvason, H. B., Kenna, H., … Schatzberg, A. F. (2007). Resting-State Functional Connectivity in Major Depression: Abnormally Increased Contributions from Subgenual Cingulate Cortex and Thalamus. *Biological Psychiatry*, *62*(5), 429–437. https://doi.org/10.1016/j.biopsych.2006.09.020

Greicius, M. D., Kiviniemi, V., Tervonen, O., Vainionpää, V., Alahuhta, S., Reiss, A. L., & Menon, V. (2008). Persistent default-mode network connectivity during light sedation. *Human Brain Mapping*, *29*(7), 839–847. https://doi.org/10.1002/hbm.20537

Greicius, M. D., Krasnow, B., Reiss, A. L., & Menon, V. (2003). Functional connectivity in the resting brain: a network analysis of the default mode hypothesis. *Proceedings of the National Academy of Sciences*, *100*(1), 253–258.

Gudbjartsson, H., & Patz, S. (1995). The rician distribution of noisy mri data. *Magnetic Resonance in Medicine*, *34*(6), 910–914. https://doi.org/10.1002/mrm.1910340618

Guilfoyle, D. N., Dyakin, V. V., O'Shea, J., Pell, G. S., & Helpern, J. A. (2003). Quantitative measurements of proton spin-lattice (T1) and spin–spin (T2) relaxation times in the mouse brain at 7.0 T. *Magnetic Resonance in Medicine*, *49*(3), 576–580. https://doi.org/10.1002/mrm.10371

Hacker, C. D., Snyder, A. Z., Pahwa, M., Corbetta, M., & Leuthardt, E. C. (2017). Frequency-specific electrophysiologic correlates of resting state fMRI networks. *NeuroImage*, *149*, 446–457. https://doi.org/10.1016/j.neuroimage.2017.01.054

Hallquist, M. N., Hwang, K., & Luna, B. (2013). The nuisance of nuisance regression: spectral misspecification in a common approach to resting-state fMRI preprocessing reintroduces noise and obscures functional connectivity. *Neuroimage*, *82*, 208–225.

Hamaguchi, K., Tanaka, M., & Mooney, R. (2016). A Distributed Recurrent Network Contributes to Temporally Precise Vocalizations. *Neuron*, *91*(3), 680–693. https://doi.org/10.1016/j.neuron.2016.06.019

Hamaide, J., De Groof, G., Van Steenkiste, G., Jeurissen, B., Van Audekerke, J., Naeyaert, M., … Verhoye, M. (2017). Exploring sex differences in the adult zebra finch brain: in vivo diffusion tensor imaging and ex vivo super-resolution track density imaging. *NeuroImage*, *146*, 789–803.

Hamaide, J., Lukacova, K., Van Audekerke, J., Verhoye, M., Kubikova, L., & Van der Linden, A. (2018). Neuroplasticity in the cerebello-thalamo-basal ganglia pathway: A longitudinal in vivo MRI study in male songbirds. *NeuroImage*, *181*, 190–202. https://doi.org/10.1016/j.neuroimage.2018.07.010

Harmer, J., Sanchez-Panchuelo, R. M., Bowtell, R., & Francis, S. T. (2012). Spatial location and strength of BOLD activation in high-spatial-resolution fMRI of the motor cortex: a comparison of spin echo and gradient echo fMRI at 7 T. *NMR in Biomedicine*, *25*(5), 717–725. https://doi.org/10.1002/nbm.1783

He, B. J., Snyder, A. Z., Zempel, J. M., Smyth, M. D., & Raichle, M. E. (2008). Electrophysiological correlates of the brain's intrinsic large-scale functional architecture. *Proceedings of the National Academy of Sciences*, *105*(41), 16039–16044. https://doi.org/10.1073/pnas.0807010105

Heath, C. J., & Jones, E. G. (1971). Interhemispheric pathways in the absence of a corpus callosum. An experimental study of commissural connexions in the marsupial phalanger. *Journal of Anatomy*, *109*(Pt 2), 253–270.

Hermesdorf, M., Sundermann, B., Feder, S., Schwindt, W., Minnerup, J., Arolt, V., … Wersching, H. (2016). Major depressive disorder: Findings of reduced homotopic connectivity and investigation of underlying structural mechanisms. *Human Brain Mapping*, *37*(3), 1209–1217. https://doi.org/10.1002/hbm.23097

Hertrich, I., Mathiak, K., & Ackermann, H. (2016). Chapter 2 - The Role of the Cerebellum in Speech Perception and Language Comprehension. In P. Mariën & M. Manto (Eds.), *The Linguistic Cerebellum* (pp. 33–50). https://doi.org/10.1016/B978-0-12-801608-4.00002-5

Heston, J. B., & White, S. A. (2015). Behavior-Linked FoxP2 Regulation Enables Zebra Finch Vocal Learning. *Journal of Neuroscience*, *35*(7), 2885–2894. https://doi.org/10.1523/JNEUROSCI.3715-14.2015

Hines, M., Chiu, L., McAdams, L. A., Bentler, P. M., & Lipcamon, J. (1992). Cognition and the corpus callosum: Verbal fluency, visuospatial ability, and language lateralization related to midsagittal surface areas of callosal subregions. *Behavioral Neuroscience*, *106*(1), 3–14. https://doi.org/10.1037/0735-7044.106.1.3

Hoeffer, C. A., & Klann, E. (2010). mTOR signaling: At the crossroads of plasticity, memory and disease. *Trends in Neurosciences*, *33*(2), 67–75. https://doi.org/10.1016/j.tins.2009.11.003

Honey, C. J., Sporns, O., Cammoun, L., Gigandet, X., Thiran, J.-P., Meuli, R., & Hagmann, P. (2009). Predicting human resting-state functional connectivity from structural connectivity. *Proceedings of the National Academy of Sciences*, *106*(6), 2035–2040.

Horovitz, S. G., Braun, A. R., Carr, W. S., Picchioni, D., Balkin, T. J., Fukunaga, M., & Duyn, J. H. (2009). Decoupling of the brain's default mode network during deep sleep.

Proceedings of the National Academy of Sciences, *106*(27), 11376–11381. https://doi.org/10.1073/pnas.0901435106

Horovitz, S. G., Fukunaga, M., Zwart, J. A. de, Gelderen, P. van, Fulton, S. C., Balkin, T. J., & Duyn, J. H. (2008). Low frequency BOLD fluctuations during resting wakefulness and light sleep: A simultaneous EEG-fMRI study. *Human Brain Mapping*, *29*(6), 671–682. https://doi.org/10.1002/hbm.20428

Hu, Y., & Glover, G. H. (2007). Three-dimensional spiral technique for high-resolution functional MRI. *Magnetic Resonance in Medicine*, *58*(5), 947–951. https://doi.org/10.1002/mrm.21328

Huber, L., Tse, D. H. Y., Wiggins, C. J., Uludağ, K., Kashyap, S., Jangraw, D. C., … Ivanov, D. (2018). Ultra-high resolution blood volume fMRI and BOLD fMRI in humans at 9.4 T: Capabilities and challenges. *NeuroImage*, *178*, 769–779. https://doi.org/10.1016/j.neuroimage.2018.06.025

Hutchison, R. M., Hutchison, M., Manning, K. Y., Menon, R. S., & Everling, S. (2014). Isoflurane induces dose-dependent alterations in the cortical connectivity profiles and dynamic properties of the brain's functional architecture. *Human Brain Mapping*, *35*(12), 5754–5775.

Hutchison, R. M., Mirsattari, S. M., Jones, C. K., Gati, J. S., & Leung, L. S. (2010). Functional Networks in the Anesthetized Rat Brain Revealed by Independent Component Analysis of Resting-State fMRI. *Journal of Neurophysiology*, *103*(6), 3398–3406. https://doi.org/10.1152/jn.00141.2010

Hutchison, R. M., Womelsdorf, T., Allen, E. A., Bandettini, P. A., Calhoun, V. D., Corbetta, M., … Chang, C. (2013). Dynamic functional connectivity: Promise, issues, and interpretations. *NeuroImage*, *80*, 360–378. https://doi.org/10.1016/j.neuroimage.2013.05.079

Hutton, C., Josephs, O., Stadler, J., Featherstone, E., Reid, A., Speck, O., … Weiskopf, N. (2011). The impact of physiological noise correction on fMRI at 7T. *NeuroImage*, *57*(1), 101–112. https://doi.org/10.1016/j.neuroimage.2011.04.018

Immelmann, K. (1969). Song development in the zebra finch and other estrildid finches. *Bird Vocalizations*, 61–77.

Jarbo, K., Verstynen, T., & Schneider, W. (2012). In vivo quantification of global connectivity in the human corpus callosum. *NeuroImage*, *59*(3), 1988–1996. https://doi.org/10.1016/j.neuroimage.2011.09.056

Jarvis, E. D. (2004). Learned Birdsong and the Neurobiology of Human Language. *Annals of the New York Academy of Sciences*, *1016*(1), 749–777. https://doi.org/10.1196/annals.1298.038

Jin, T., Wang, P., Tasker, M., Zhao, F., & Kim, S.-G. (2006). Source of nonlinearity in echo-time-dependent BOLD fMRI. *Magnetic Resonance in Medicine*, *55*(6), 1281–1290. https://doi.org/10.1002/mrm.20918

Johnson, F., Soderstrom, K., & Whitney, O. (2002). Quantifying song bout production during zebra finch sensory-motor learning suggests a sensitive period for vocal practice. *Behavioural Brain Research*, *131*(1), 57–65. https://doi.org/10.1016/S0166-4328(01)00374-6

Johnston, J. M., Vaishnavi, S. N., Smyth, M. D., Zhang, D., He, B. J., Zempel, J. M., … Raichle, M. E. (2008). Loss of resting interhemispheric functional connectivity after complete section of the corpus callosum. *Journal of Neuroscience*, *28*(25), 6453–6458.

Johnstone, T., Ores Walsh, K. S., Greischar, L. L., Alexander, A. L., Fox, A. S., Davidson, R. J., & Oakes, T. R. (2006). Motion correction and the use of motion covariates in multiple-subject fMRI analysis. *Human Brain Mapping*, *27*(10), 779–788.

Jonckers, E., Audekerke, J. V., Visscher, G. D., Linden, A. V. der, & Verhoye, M. (2011). Functional Connectivity fMRI of the Rodent Brain: Comparison of Functional Connectivity Networks in Rat and Mouse. *PLOS ONE*, *6*(4), e18876. https://doi.org/10.1371/journal.pone.0018876

Jones, A. E., ten Cate, C., & Slater, P. J. B. (1996). Early experience and plasticity of song in adult male zebra finches (Taeniopygia guttata). *Journal of Comparative Psychology*, *110*(4), 354–369. https://doi.org/10.1037/0735-7036.110.4.354

Jones, A., ten Cate, C., & Slater, P. J. B. (1992). Can Lack of Experience Delay the End of the Sensitive Phase for Song Learning? *Netherlands Journal of Zoology*, *43*(1–2), 80–90. https://doi.org/10.1163/156854293X00223

Josse, G., Seghier, M. L., Kherif, F., & Price, C. J. (2008). Explaining Function with Anatomy: Language Lateralization and Corpus Callosum Size. *Journal of Neuroscience*, *28*(52), 14132–14139. https://doi.org/10.1523/JNEUROSCI.4383-08.2008

Kalthoff, D., Seehafer, J. U., Po, C., Wiedermann, D., & Hoehn, M. (2011). Functional connectivity in the rat at 11.7 T: Impact of physiological noise in resting state fMRI. *Neuroimage*, *54*(4), 2828–2839.

Kannurpatti, S. S., Biswal, B. B., Kim, Y. R., & Rosen, B. R. (2008). Spatio-temporal characteristics of low-frequency BOLD signal fluctuations in isoflurane-anesthetized rat brain. *Neuroimage*, *40*(4), 1738–1747.

Kao, M. H., & Brainard, M. S. (2006). Lesions of an Avian Basal Ganglia Circuit Prevent Context-Dependent Changes to Song Variability. *Journal of Neurophysiology*, *96*(3), 1441–1455. https://doi.org/10.1152/jn.01138.2005

Kao, M. H., Doupe, A. J., & Brainard, M. S. (2005). Contributions of an avian basal ganglia–forebrain circuit to real-time modulation of song. *Nature*, *433*(7026), 638–643. https://doi.org/10.1038/nature03127

Kawaguchi, Y. (1992). Receptor subtypes involved in callosally-induced postsynaptic potentials in rat frontal agranular cortex in vitro. *Experimental Brain Research*, *88*(1), 33–40. https://doi.org/10.1007/BF02259126

Kelly, C., Zuo, X.-N., Gotimer, K., Cox, C. L., Lynch, L., Brock, D., … Castellanos, F. X. (2011). Reduced interhemispheric resting state functional connectivity in cocaine addiction. *Biological Psychiatry*, *69*(7), 684–692.

Kemper, V. G., De Martino, F., Vu, A. T., Poser, B. A., Feinberg, D. A., Goebel, R., & Yacoub, E. (2015). Sub-millimeter T2 weighted fMRI at 7 T: comparison of 3D-GRASE and 2D SE-EPI. *Frontiers in Neuroscience*, *9*. https://doi.org/10.3389/fnins.2015.00163

Khanna, P. C., Poliakov, A. V., Ishak, G. E., Poliachik, S. L., Friedman, S. D., Saneto, R. P., … Shaw, D. W. W. (2012). Preserved interhemispheric functional connectivity in a case of corpus callosum agenesis. *Neuroradiology*, *54*(2), 177–179. https://doi.org/10.1007/s00234-011-0883-x

Kim, J., Van Dijk, K. R., Libby, A., & Napadow, V. (2014). Frequency-dependent relationship between resting-state functional magnetic resonance imaging signal power and head motion is localized within distributed association networks. *Brain Connectivity*, *4*(1), 30–39.

Kirschen, M. P., Chen, S. H. A., Schraedley-Desmond, P., & Desmond, J. E. (2005). Load- and practice-dependent increases in cerebro-cerebellar activation in verbal working memory: an fMRI study. *NeuroImage*, *24*(2), 462–472. https://doi.org/10.1016/j.neuroimage.2004.08.036

Klein, A., Andersson, J., Ardekani, B. A., Ashburner, J., Avants, B., Chiang, M.-C., … Parsey, R. V. (2009). Evaluation of 14 nonlinear deformation algorithms applied to human brain MRI registration. *NeuroImage*, *46*(3), 786–802. https://doi.org/10.1016/j.neuroimage.2008.12.037

Knudsen, E. I. (2004). Sensitive Periods in the Development of the Brain and Behavior. *Journal of Cognitive Neuroscience*, *16*(8), 1412–1425. https://doi.org/10.1162/0898929042304796

Ko, A. L., Darvas, F., Poliakov, A., Ojemann, J., & Sorensen, L. B. (2011). Quasi-periodic Fluctuations in Default Mode Network Electrophysiology. *Journal of Neuroscience*, *31*(32), 11728–11732. https://doi.org/10.1523/JNEUROSCI.5730-10.2011

Kuznetsova, A., Brockhoff, P. B., & Christensen, R. H. B. (2017). lmerTest Package: Tests in Linear Mixed Effects Models. *Journal of Statistical Software*, *82*(13). https://doi.org/10.18637/jss.v082.i13

Lai, S., & Glover, G. H. (1998). Three-dimensional spiral fMRI technique: A comparison with 2D spiral acquisition. *Magnetic Resonance in Medicine*, *39*(1), 68–78. https://doi.org/10.1002/mrm.1910390112

Larson-Prior, L. J., Zempel, J. M., Nolan, T. S., Prior, F. W., Snyder, A. Z., & Raichle, M. E. (2009). Cortical network functional connectivity in the descent to sleep. *Proceedings of the National Academy of Sciences*, *106*(11), 4489–4494. https://doi.org/10.1073/pnas.0900924106

Lassonde, M., Bryden, M. P., & Demers, P. (1990). The corpus callosum and cerebral speech lateralization. *Brain and Language*, *38*(2), 195–206. https://doi.org/10.1016/0093-934X(90)90110-3

Layden, E. A., Cacioppo, J. T., Cacioppo, S., Cappa, S. F., Dodich, A., Falini, A., & Canessa, N. (2017). Perceived social isolation is associated with altered functional connectivity in neural networks associated with tonic alertness and executive control. *NeuroImage*, *145*, 58–73. https://doi.org/10.1016/j.neuroimage.2016.09.050

Layden, E. A., Schertz, K. E., London, S. E., & Berman, M. G. (2019). Interhemispheric functional connectivity in the zebra finch brain, absent the corpus callosum in normal ontogeny. *NeuroImage*, *195*, 113–127. https://doi.org/10.1016/j.neuroimage.2019.03.064

Lee, S.-P., Silva, A. C., Ugurbil, K., & Kim, S.-G. (1999). Diffusion-weighted spin-echo fMRI at 9.4 T: Microvascular/tissue contribution to BOLD signal changes. *Magnetic Resonance in Medicine*, *42*(5), 919–928. https://doi.org/10.1002/(SICI)1522-2594(199911)42:5<919::AID-MRM12>3.0.CO;2-8

Lesage, E., Hansen, P. C., & Miall, R. C. (2017). Right Lateral Cerebellum Represents Linguistic Predictability. *Journal of Neuroscience*, *37*(26), 6231–6241. https://doi.org/10.1523/JNEUROSCI.3203-16.2017

Lesage, E., Morgan, B. E., Olson, A. C., Meyer, A. S., & Miall, R. C. (2012). Cerebellar rTMS disrupts predictive language processing. *Current Biology*, *22*(18), R794–R795. https://doi.org/10.1016/j.cub.2012.07.006

Letzner, S., Simon, A., & Güntürkün, O. (2016). Connectivity and neurochemistry of the commissura anterior of the pigeon (Columba livia). *Journal of Comparative Neurology*, *524*(2), 343–361. https://doi.org/10.1002/cne.23858

Li, T., & Mirowitz, S. A. (2003). Fast T2-weighted MR imaging: impact of variation in pulse sequence parameters on image quality and artifacts. *Magnetic Resonance Imaging*, *21*(7), 745–753. https://doi.org/10.1016/S0730-725X(03)00173-5

Lipkind, D., Nottebohm, F., Rado, R., & Barnea, A. (2002). Social change affects the survival of new neurons in the forebrain of adult songbirds. *Behavioural Brain Research*, *133*(1), 31–43. https://doi.org/10.1016/S0166-4328(01)00416-8

Liska, A., Galbusera, A., Schwarz, A. J., & Gozzi, A. (2015). Functional connectivity hubs of the mouse brain. *Neuroimage*, *115*, 281–291.

London, S. E. (2017). Developmental song learning as a model to understand neural mechanisms that limit and promote the ability to learn. *Behavioural Processes*. https://doi.org/10.1016/j.beproc.2017.11.008

London, S. E., & Clayton, D. F. (2008). Functional identification of sensory mechanisms required for developmental song learning. *Nature Neuroscience*, *11*(5), 579–586. https://doi.org/10.1038/nn.2103

Lu, J., Liu, H., Zhang, M., Wang, D., Cao, Y., Ma, Q., … Li, K. (2011). Focal Pontine Lesions Provide Evidence That Intrinsic Functional Connectivity Reflects Polysynaptic Anatomical Pathways. *Journal of Neuroscience*, *31*(42), 15065–15071. https://doi.org/10.1523/JNEUROSCI.2364-11.2011

Luo, Z.-X., Yuan, C.-X., Meng, Q.-J., & Ji, Q. (2011). A Jurassic eutherian mammal and divergence of marsupials and placentals. *Nature*, *476*(7361), 442–445.

Mantini, D., Perrucci, M. G., Gratta, C. D., Romani, G. L., & Corbetta, M. (2007). Electrophysiological signatures of resting state networks in the human brain. *Proceedings of the National Academy of Sciences*, *104*(32), 13170–13175. https://doi.org/10.1073/pnas.0700668104

Manto, M., Bower, J. M., Conforto, A. B., Delgado-García, J. M., da Guarda, S. N. F., Gerwig, M., … Timmann, D. (2012). Consensus Paper: Roles of the Cerebellum in Motor Control—The Diversity of Ideas on Cerebellar Involvement in Movement. *The Cerebellum*, *11*(2), 457–487. https://doi.org/10.1007/s12311-011-0331-9

Marcus, D. S., Harms, M. P., Snyder, A. Z., Jenkinson, M., Wilson, J. A., Glasser, M. F., … Van Essen, D. C. (2013). Human Connectome Project informatics: Quality control, database services, and data visualization. *NeuroImage*, *80*, 202–219. https://doi.org/10.1016/j.neuroimage.2013.05.077

Martuzzi, R., Ramani, R., Qiu, M., Rajeevan, N., & Constable, R. T. (2010). Functional connectivity and alterations in baseline brain state in humans. *NeuroImage*, *49*(1), 823–834. https://doi.org/10.1016/j.neuroimage.2009.07.028

Martuzzi, R., Ramani, R., Qiu, M., Shen, X., Papademetris, X., & Constable, R. T. (2011). A whole-brain voxel based measure of intrinsic connectivity contrast reveals local changes in tissue connectivity with anesthetic without a priori assumptions on thresholds or regions of interest. *NeuroImage*, *58*(4), 1044–1050. https://doi.org/10.1016/j.neuroimage.2011.06.075

Matsui, T., Murakami, T., & Ohki, K. (2016). Transient neuronal coactivations embedded in globally propagating waves underlie resting-state functional connectivity. *Proceedings of the National Academy of Sciences*, *113*(23), 6556–6561.

McGilchrist, I. (2010). Reciprocal organization of the cerebral hemispheres. *Dialogues in Clinical Neuroscience*, *12*(4), 503–515.

Mechling, A. E., Hübner, N. S., Lee, H.-L., Hennig, J., von Elverfeldt, D., & Harsan, L.-A. (2014). Fine-grained mapping of mouse brain functional connectivity with resting-state fMRI. *NeuroImage*, *96*, 203–215. https://doi.org/10.1016/j.neuroimage.2014.03.078

Mello, C. V., Velho, T. A. F., & Pinaud, R. (2004). Song-Induced Gene Expression: A Window on Song Auditory Processing and Perception. *Annals of the New York Academy of Sciences*, *1016*(1), 263–281. https://doi.org/10.1196/annals.1298.021

Meltzer, J. A., Postman-Caucheteux, W. A., McArdle, J. J., & Braun, A. R. (2009). Strategies for longitudinal neuroimaging studies of overt language production. *NeuroImage*, *47*(2), 745–755. https://doi.org/10.1016/j.neuroimage.2009.04.089

Meyer, B.-U., Röricht, S., von Einsiedel, H. G., Kruggel, F., & Weindl, A. (1995). Inhibitory and excitatory interhemispheric transfers between motor cortical areas in normal humans and patients with abnormalities of the corpus callosum. *Brain*, *118*(2), 429–440. https://doi.org/10.1093/brain/118.2.429

Mikl, M., Mareček, R., Hluštík, P., Pavlicová, M., Drastich, A., Chlebus, P., … Krupa, P. (2008). Effects of spatial smoothing on fMRI group inferences. *Magnetic Resonance Imaging*, *26*(4), 490–503. https://doi.org/10.1016/j.mri.2007.08.006

Mišić, B., Fatima, Z., Askren, M. K., Buschkuehl, M., Churchill, N., Cimprich, B., … Korostil, M. (2014). The functional connectivity landscape of the human brain. *PloS One*, *9*(10), e111007.

Mitra, A., Kraft, A., Wright, P., Acland, B., Snyder, A. Z., Rosenthal, Z., … Raichle, M. E. (2018). Spontaneous Infra-slow Brain Activity Has Unique Spatiotemporal Dynamics and Laminar Structure. *Neuron*, *98*(2), 297-305.e6. https://doi.org/10.1016/j.neuron.2018.03.015

Moberget, T., Gullesen, E. H., Andersson, S., Ivry, R. B., & Endestad, T. (2014). Generalized Role for the Cerebellum in Encoding Internal Models: Evidence from Semantic Processing. *Journal of Neuroscience*, *34*(8), 2871–2878. https://doi.org/10.1523/JNEUROSCI.2264-13.2014

Molloy, E. K., Meyerand, M. E., & Birn, R. M. (2014). The influence of spatial resolution and smoothing on the detectability of resting-state and task fMRI. *NeuroImage*, *86*, 221–230. https://doi.org/10.1016/j.neuroimage.2013.09.001

Mooney, R. (2000). Different Subthreshold Mechanisms Underlie Song Selectivity in Identified HVc Neurons of the Zebra Finch. *Journal of Neuroscience*, *20*(14), 5420–5436. https://doi.org/10.1523/JNEUROSCI.20-14-05420.2000

Mooney, R. (2009). Neural mechanisms for learned birdsong. *Learning & Memory*, *16*(11), 655–669. https://doi.org/10.1101/lm.1065209

Mooney, R., & Rao, M. (1994). Waiting periods versus early innervation: the development of axonal connections in the zebra finch song system. *Journal of Neuroscience*, *14*(11), 6532–6543.

Moorman, S., Gobes, S. M. H., van de Kamp, F. C., Zandbergen, M. A., & Bolhuis, J. J. (2015). Learning-related brain hemispheric dominance in sleeping songbirds. *Scientific Reports*, *5*, 9041. https://doi.org/10.1038/srep09041

Moorman, S., Gobes, S. M., Kuijpers, M., Kerkhofs, A., Zandbergen, M. A., & Bolhuis, J. J. (2012). Human-like brain hemispheric dominance in birdsong learning. *Proceedings of the National Academy of Sciences*, *109*(31), 12782–12787.

Moorman, S., & Nicol, A. U. (2015). Memory-related brain lateralisation in birds and humans. *Neuroscience & Biobehavioral Reviews*, *50*, 86–102. https://doi.org/10.1016/j.neubiorev.2014.07.006

Moreno-López, L., Sahakian, B. J., Manktelow, A., Menon, D. K., & Stamatakis, E. A. (2016). Depression following traumatic brain injury: A functional connectivity perspective. *Brain Injury*, *30*(11), 1319–1328. https://doi.org/10.1080/02699052.2016.1186839

Morrison, R. G., & Nottebohm, F. (1993). Role of a telencephalic nucleus in the delayed song learning of socially isolated zebra finches. *Journal of Neurobiology*, *24*(8), 1045–1064. https://doi.org/10.1002/neu.480240805

Mueller, S., Wang, D., Fox, M. D., Pan, R., Lu, J., Li, K., … Liu, H. (2015). Reliability Correction for Functional Connectivity: Theory and Implementation. *Human Brain Mapping*, *36*(11), 4664–4680. https://doi.org/10.1002/hbm.22947

Murphy, K., Birn, R. M., & Bandettini, P. A. (2013). Resting-state fMRI confounds and cleanup. *NeuroImage*, *80*, 349–359. https://doi.org/10.1016/j.neuroimage.2013.04.001

Murphy, K., Bodurka, J., & Bandettini, P. A. (2007). How long to scan? The relationship between fMRI temporal signal to noise ratio and necessary scan duration. *Neuroimage*, *34*(2), 565–574.

Nicholson, D. A., Roberts, T. F., & Sober, S. J. (2018). Thalamostriatal and cerebellothalamic pathways in a songbird, the Bengalese finch. *Journal of Comparative Neurology*, *526*(9), 1550–1570. https://doi.org/10.1002/cne.24428

Nir, Y., Mukamel, R., Dinstein, I., Privman, E., Harel, M., Fisch, L., … Malach, R. (2008). Interhemispheric correlations of slow spontaneous neuronal fluctuations revealed in human sensory cortex. *Nature Neuroscience*, *11*(9), 1100–1108. https://doi.org/10.1038/nn.2177

Nissant, A., Bardy, C., Katagiri, H., Murray, K., & Lledo, P.-M. (2009). Adult neurogenesis promotes synaptic plasticity in the olfactory bulb. *Nature Neuroscience*, *12*(6), 728–730. https://doi.org/10.1038/nn.2298

Nordeen, K. W., & Nordeen, E. J. (1988). Projection neurons within a vocal motor pathway are born during song learning in zebra finches. *Nature*, *334*(6178), 149. https://doi.org/10.1038/334149a0

Nottebohm, F. (1969). The "Critical Period" for Song Learning. *Ibis*, *111*(3), 386–387. https://doi.org/10.1111/j.1474-919X.1969.tb02551.x

Nottebohm, F. (2002). Neuronal replacement in adult brain. *Brain Research Bulletin*, *57*(6), 737–749. https://doi.org/10.1016/S0361-9230(02)00750-5

Nottebohm, F., Stokes, T., & Leonard, C. (1976). Central control of song in the canary, Serinus canarius. *Journal of Comparative Neurology*, *165*(4), 457–486.

Olson, E. M., Maeda, R. K., & Gobes, S. M. H. (2016). Mirrored patterns of lateralized neuronal activation reflect old and new memories in the avian auditory cortex. *Neuroscience*, *330*, 395–402. https://doi.org/10.1016/j.neuroscience.2016.06.009

Ölveczky, B. P., Andalman, A. S., & Fee, M. S. (2005). Vocal Experimentation in the Juvenile Songbird Requires a Basal Ganglia Circuit. *PLOS Biology*, *3*(5), e153. https://doi.org/10.1371/journal.pbio.0030153

O'Reilly, J. X., Croxson, P. L., Jbabdi, S., Sallet, J., Noonan, M. P., Mars, R. B., … Baxter, M. G. (2013). Causal effect of disconnection lesions on interhemispheric functional connectivity in rhesus monkeys. *Proceedings of the National Academy of Sciences*, *110*(34), 13982–13987. https://doi.org/10.1073/pnas.1305062110

Pan, W.-J., Thompson, G., Magnuson, M., Majeed, W., Jaeger, D., & Keilholz, S. (2011). Broadband local field potentials correlate with spontaneous fluctuations in functional magnetic resonance imaging signals in the rat somatosensory cortex under isoflurane anesthesia. *Brain Connectivity*, *1*(2), 119–131.

Paterson, A. K., & Bottjer, S. W. (2017). Cortical inter-hemispheric circuits for multimodal vocal learning in songbirds. *Journal of Comparative Neurology*.

Paul, L. K., Brown, W. S., Adolphs, R., Tyszka, J. M., Richards, L. J., Mukherjee, P., & Sherr, E. H. (2007). Agenesis of the corpus callosum: genetic, developmental and functional aspects of connectivity. *Nature Reviews Neuroscience*, *8*(4), 287. https://doi.org/10.1038/nrn2107

Pawela, C. P., Biswal, B. B., Cho, Y. R., Kao, D. S., Li, R., Jones, S. R., … Hyde, J. S. (2008). Resting-state functional connectivity of the rat brain. *Magnetic Resonance in Medicine*, *59*(5), 1021–1029. https://doi.org/10.1002/mrm.21524

Penny, W. D., Friston, K. J., Ashburner, J. T., Kiebel, S. J., & Nichols, T. E. (2011). *Statistical parametric mapping: the analysis of functional brain images*. Academic press.

Perkel, D. J. (2004). Origin of the Anterior Forebrain Pathway. *Annals of the New York Academy of Sciences*, *1016*(1), 736–748. https://doi.org/10.1196/annals.1298.039

Phan, M. L., Pytte, C. L., & Vicario, D. S. (2006). Early auditory experience generates long-lasting memories that may subserve vocal learning in songbirds. *Proceedings of the National Academy of Sciences, 103*(4), 1088–1093. https://doi.org/10.1073/pnas.0510136103

Phan, M. L., & Vicario, D. S. (2010). Hemispheric differences in processing of vocalizations depend on early experience. *Proceedings of the National Academy of Sciences*, *107*(5), 2301–2306. https://doi.org/10.1073/pnas.0900091107

Pieper, S., Halle, M., & Kikinis, R. (2004). 3D Slicer. *2004 2nd IEEE International Symposium on Biomedical Imaging: Nano to Macro (IEEE Cat No. 04EX821)*, 632-635 Vol. 1. https://doi.org/10.1109/ISBI.2004.1398617

Pleger, B., & Timmann, D. (2018). The role of the human cerebellum in linguistic prediction, word generation and verbal working memory: evidence from brain imaging, non-invasive cerebellar stimulation and lesion studies. *Neuropsychologia*, *115*, 204–210. https://doi.org/10.1016/j.neuropsychologia.2018.03.012

Plewes, D. B., & Kucharczyk, W. (2012). Physics of MRI: A primer. *Journal of Magnetic Resonance Imaging*, *35*(5), 1038–1054. https://doi.org/10.1002/jmri.23642

Poirier, C., Boumans, T., Verhoye, M., Balthazart, J., & Van der Linden, A. (2009). Own-song recognition in the songbird auditory pathway: selectivity and lateralization. *Journal of Neuroscience*, *29*(7), 2252–2258.

Poirier, C., & Van der Linden, A.-M. (2011). Spin echo BOLD fMRI on songbirds. *In Vivo NMR Imaging: Methods and Protocols*, 569–576.

Poirier, C., Vellema, M., Verhoye, M., Van Meir, V., Wild, J. M., Balthazart, J., & Van Der Linden, A. (2008). A three-dimensional MRI atlas of the zebra finch brain in stereotaxic coordinates. *NeuroImage*, *41*(1), 1–6. https://doi.org/10.1016/j.neuroimage.2008.01.069

Poirier, C., Verhoye, M., Boumans, T., & Linden, A. V. der. (2010). Implementation of spin-echo blood oxygen level-dependent (BOLD) functional MRI in birds. *NMR in Biomedicine*, *23*(9), 1027–1032. https://doi.org/10.1002/nbm.1525

Poser, B. A., & Norris, D. G. (2007). Fast spin echo sequences for BOLD functional MRI. *Magnetic Resonance Materials in Physics, Biology and Medicine*, *20*(1), 11. https://doi.org/10.1007/s10334-006-0063-x

Power, J. D., Cohen, A. L., Nelson, S. M., Wig, G. S., Barnes, K. A., Church, J. A., … Petersen, S. E. (2011). Functional Network Organization of the Human Brain. *Neuron*, *72*(4), 665–678. https://doi.org/10.1016/j.neuron.2011.09.006

Praag, H. van, Christie, B. R., Sejnowski, T. J., & Gage, F. H. (1999). Running enhances neurogenesis, learning, and long-term potentiation in mice. *Proceedings of the National Academy of Sciences*, *96*(23), 13427–13431. https://doi.org/10.1073/pnas.96.23.13427

Preibisch, C., Pilatus, U., Bunke, J., Hoogenraad, F., Zanella, F., & Lanfermann, H. (2003). Functional MRI using sensitivity-encoded echo planar imaging (SENSE-EPI). *NeuroImage*, *19*(2), 412–421. https://doi.org/10.1016/S1053-8119(03)00080-6

Pytte, C. L., Parent, C., Wildstein, S., Varghese, C., & Oberlander, S. (2010). Deafening decreases neuronal incorporation in the zebra finch caudomedial nidopallium (NCM). *Behavioural Brain Research*, *211*(2), 141–147. https://doi.org/10.1016/j.bbr.2010.03.029

Quigley, M., Cordes, D., Turski, P., Moritz, C., Haughton, V., Seth, R., & Meyerand, M. E. (2003). Role of the Corpus Callosum in Functional Connectivity. *American Journal of Neuroradiology*, *24*(2), 208–212.

Ravizza, S. M., McCormick, C. A., Schlerf, J. E., Justus, T., Ivry, R. B., & Fiez, J. A. (2006). Cerebellar damage produces selective deficits in verbal working memory. *Brain*, *129*(2), 306–320. https://doi.org/10.1093/brain/awh685

Rogers, L. J., Koboroff, A., & Kaplan, G. (2018). Lateral Asymmetry of Brain and Behaviour in the Zebra Finch, Taeniopygia guttata. *Symmetry*, *10*(12), 679. https://doi.org/10.3390/sym10120679

Roland, J. L., Snyder, A. Z., Hacker, C. D., Mitra, A., Shimony, J. S., Limbrick, D. D., … Leuthardt, E. C. (2017). On the role of the corpus callosum in interhemispheric functional connectivity in humans. *Proceedings of the National Academy of Sciences*, *114*(50), 13278–13283. https://doi.org/10.1073/pnas.1707050114

Roper, A., & Zann, R. (2006). The Onset of Song Learning and Song Tutor Selection in Fledgling Zebra Finches. *Ethology*, *112*(5), 458–470. https://doi.org/10.1111/j.1439-0310.2005.01169.x

Rorden, C. (2012). *MRIcroGL*. Retrieved from http://www.cabiatl.com/mricrogl/

Rosenberg, M. D., Finn, E. S., Scheinost, D., Papademetris, X., Shen, X., Constable, R. T., & Chun, M. M. (2016). A neuromarker of sustained attention from whole-brain functional connectivity. *Nature Neuroscience*, *19*(1), 165–171. https://doi.org/10.1038/nn.4179

Rua, C., Costagli, M., Symms, M. R., Biagi, L., Donatelli, G., Cosottini, M., … Tosetti, M. (2017). Characterization of high-resolution Gradient Echo and Spin Echo EPI for fMRI in the human visual cortex at 7T. *Magnetic Resonance Imaging*, *40*, 98–108. https://doi.org/10.1016/j.mri.2017.04.008

Ryan, S. M., & Arnold, A. P. (1981). Evidence for cholinergic participation in the control of bird song: Acetylcholinesterase distribution and muscarinic receptor autoradiography in the zebra finch brain. *Journal of Comparative Neurology*, *202*(2), 211–219. https://doi.org/10.1002/cne.902020207

Sadaghiani, S., Scheeringa, R., Lehongre, K., Morillon, B., Giraud, A.-L., & Kleinschmidt, A. (2010). Intrinsic Connectivity Networks, Alpha Oscillations, and Tonic Alertness: A Simultaneous Electroencephalography/Functional Magnetic Resonance Imaging Study.

Journal of Neuroscience, *30*(30), 10243–10250. https://doi.org/10.1523/JNEUROSCI.1004-10.2010

Sakaguchi, H., & Saito, N. (1989). The acetylcholine and catecholamine contents in song control nuclei of zebra finch during song ontogeny. *Developmental Brain Research*, *47*(2), 313–317. https://doi.org/10.1016/0165-3806(89)90189-2

Salvador, R., Martinez, A., Pomarol-Clotet, E., Gomar, J., Vila, F., Sarró, S., … Bullmore, E. (2008). A simple view of the brain through a frequency-specific functional connectivity measure. *Neuroimage*, *39*(1), 279–289.

Salvador, R., Suckling, J., Schwarzbauer, C., & Bullmore, E. (2005). Undirected graphs of frequency-dependent functional connectivity in whole brain networks. *Philosophical Transactions of the Royal Society of London B: Biological Sciences*, *360*(1457), 937–946.

Scharff, C., & Nottebohm, F. (1991). A comparative study of the behavioral deficits following lesions of various parts of the zebra finch song system: implications for vocal learning. *Journal of Neuroscience*, *11*(9), 2896–2913. https://doi.org/10.1523/JNEUROSCI.11-09-02896.1991

Schmidt, M. F., Ashmore, R. C., & Vu, E. T. (2006). Bilateral Control and Interhemispheric Coordination in the Avian Song Motor System. *Annals of the New York Academy of Sciences*, *1016*(1), 171–186. https://doi.org/10.1196/annals.1298.014

Schmidt-Hieber, C., Jonas, P., & Bischofberger, J. (2004). Enhanced synaptic plasticity in newly generated granule cells of the adult hippocampus. *Nature*, *429*(6988), 184. https://doi.org/10.1038/nature02553

Schulte, T., & Müller-Oehring, E. M. (2010). Contribution of Callosal Connections to the Interhemispheric Integration of Visuomotor and Cognitive Processes. *Neuropsychology Review*, *20*(2), 174–190. https://doi.org/10.1007/s11065-010-9130-1

Sforazzini, F., Schwarz, A. J., Galbusera, A., Bifone, A., & Gozzi, A. (2014). Distributed BOLD and CBV-weighted resting-state networks in the mouse brain. *NeuroImage*, *87*, 403–415. https://doi.org/10.1016/j.neuroimage.2013.09.050

Shaevitz, S. S., & Theunissen, F. E. (2007). Functional Connectivity Between Auditory Areas Field L and CLM and Song System Nucleus HVC in Anesthetized Zebra Finches. *Journal of Neurophysiology*, *98*(5), 2747–2764. https://doi.org/10.1152/jn.00294.2007

Shen, J. (2014). *Tools for NIfTI and ANALYZE image*. Retrieved from https://www.mathworks.com/matlabcentral/fileexchange/8797-tools-for-nifti-and-analyze-image

Shen, K., Mišić, B., Cipollini, B. N., Bezgin, G., Buschkuehl, M., Hutchison, R. M., … Everling, S. (2015). Stable long-range interhemispheric coordination is supported by direct anatomical projections. *Proceedings of the National Academy of Sciences*, *112*(20), 6473–6478.

Shirer, W. R., Ryali, S., Rykhlevskaia, E., Menon, V., & Greicius, M. D. (2012). Decoding Subject-Driven Cognitive States with Whole-Brain Connectivity Patterns. *Cerebral Cortex*, *22*(1), 158–165. https://doi.org/10.1093/cercor/bhr099

Shors, T. J., Miesegaes, G., Beylin, A., Zhao, M., Rydel, T., & Gould, E. (2001). Neurogenesis in the adult is involved in the formation of trace memories. *Nature*, *410*(6826), 372. https://doi.org/10.1038/35066584

Shtoyerman, E., Arieli, A., Slovin, H., Vanzetta, I., & Grinvald, A. (2000). Long-Term Optical Imaging and Spectroscopy Reveal Mechanisms Underlying the Intrinsic Signal and Stability of Cortical Maps in V1 of Behaving Monkeys. *Journal of Neuroscience*, *20*(21), 8111–8121. https://doi.org/10.1523/JNEUROSCI.20-21-08111.2000

Simpson, H. B., & Vicario, D. S. (1990). Brain pathways for learned and unlearned vocalizations differ in zebra finches. *Journal of Neuroscience*, *10*(5), 1541–1556. https://doi.org/10.1523/JNEUROSCI.10-05-01541.1990

Sladky, R., Friston, K. J., Tröstl, J., Cunnington, R., Moser, E., & Windischberger, C. (2011). Slice-timing effects and their correction in functional MRI. *Neuroimage*, *58*(2), 588–594.

Slater, P. J. B., Richards, C., & Mann, N. I. (1991). Song Learning in Zebra Finches Exposed to a Series of Tutors during the Sensitive Phase. *Ethology*, *88*(2), 163–171. https://doi.org/10.1111/j.1439-0310.1991.tb00271.x

Smith, S. M. (2002). Fast robust automated brain extraction. *Human Brain Mapping*, *17*(3), 143–155. https://doi.org/10.1002/hbm.10062

Smith, S. M., Beckmann, C. F., Andersson, J., Auerbach, E. J., Bijsterbosch, J., Douaud, G., … Glasser, M. F. (2013). Resting-state fMRI in the Human Connectome Project. *NeuroImage*, *80*, 144–168. https://doi.org/10.1016/j.neuroimage.2013.05.039

Sohrabji, F., Nordeen, E. J., & Nordeen, K. W. (1990). Selective impairment of song learning following lesions of a forebrain nucleus in the juvenile zebra finch. *Behavioral and Neural Biology*, *53*(1), 51–63. https://doi.org/10.1016/0163-1047(90)90797-A

Sperry, R. W. (1968). Plasticity of neural maturation. *Developmental Biology*, *2*, 306–327.

Sporns, O., Tononi, G., & Edelman, G. M. (2000). Connectivity and complexity: the relationship between neuroanatomy and brain dynamics. *Neural Networks*, *13*(8), 909–922. https://doi.org/10.1016/S0893-6080(00)00053-8

Stark, D. E., Margulies, D. S., Shehzad, Z. E., Reiss, P., Kelly, A. C., Uddin, L. Q., … Castellanos, F. X. (2008). Regional variation in interhemispheric coordination of intrinsic hemodynamic fluctuations. *Journal of Neuroscience*, *28*(51), 13754–13764.

Striedter, G. F., & Vu, E. T. (1998). Bilateral feedback projections to the forebrain in the premotor network for singing in zebra finches. *Developmental Neurobiology*, *34*(1), 27–40.

Stripling, R., Kruse, A. A., & Clayton, D. F. (2001). Development of song responses in the zebra finch caudomedial neostriatum: Role of genomic and electrophysiological activities. *Journal of Neurobiology*, *48*(3), 163–180. https://doi.org/10.1002/neu.1049

Tadel, F., Baillet, S., Mosher, J. C., Pantazis, D., & Leahy, R. M. (2011). Brainstorm: A User-friendly Application for MEG/EEG Analysis. *Intell. Neuroscience*, *2011*, 8:1–8:13. https://doi.org/10.1155/2011/879716

Tanabe, J., Miller, D., Tregellas, J., Freedman, R., & Meyer, F. G. (2002). Comparison of detrending methods for optimal fMRI preprocessing. *NeuroImage*, *15*(4), 902–907.

Tchernichovski, O., & Mitra, P. P. (2004). *Sound analysis pro user manual.* CCNY, New York.

Tchernichovski, O., Mitra, P. P., Lints, T., & Nottebohm, F. (2001). Dynamics of the vocal imitation process: how a zebra finch learns its song. *Science*, *291*(5513), 2564–2569.

Tchernichovski, O., Nottebohm, F., Ho, C. E., Pesaran, B., & Mitra, P. P. (2000). A procedure for an automated measurement of song similarity. *Animal Behaviour*, *59*(6), 1167–1176. https://doi.org/10.1006/anbe.1999.1416

Teramitsu, I., Kudo, L. C., London, S. E., Geschwind, D. H., & White, S. A. (2004). Parallel FoxP1 and FoxP2 expression in songbird and human brain predicts functional interaction. *Journal of Neuroscience*, *24*(13), 3152–3163.

Terpstra, N. J., Bolhuis, J. J., & Boer-Visser, A. M. den. (2004). An Analysis of the Neural Representation of Birdsong Memory. *Journal of Neuroscience*, *24*(21), 4971–4977. https://doi.org/10.1523/JNEUROSCI.0570-04.2004

Thompson, J. A., Basista, M. J., Wu, W., Bertram, R., & Johnson, F. (2011). Dual Pre-Motor Contribution to Songbird Syllable Variation. *Journal of Neuroscience*, *31*(1), 322–330. https://doi.org/10.1523/JNEUROSCI.5967-09.2011

Thulborn, K. R., Chang, S. Y., Shen, G. X., & Voyvodic, J. T. (1997). High-resolution echo-planar fMRI of human visual cortex at 3.0 tesla. *NMR in Biomedicine*, *10*(4–5), 183–190. https://doi.org/10.1002/(SICI)1099-1492(199706/08)10:4/5<183::AID-NBM469>3.0.CO;2-W

Tingley, D., Yamamoto, T., Hirose, K., Keele, L., & Imai, K. (2014). *Mediation: R package for causal mediation analysis*.

Tononi, G., Edelman, G. M., & Sporns, O. (1998). Complexity and coherency: integrating information in the brain. *Trends in Cognitive Sciences*, *2*(12), 474–484. https://doi.org/10.1016/S1364-6613(98)01259-5

Tononi, G., Sporns, O., & Edelman, G. M. (1994). A measure for brain complexity: relating functional segregation and integration in the nervous system. *Proceedings of the National Academy of Sciences*, *91*(11), 5033–5037.

Toulmin, H., Beckmann, C. F., O'Muircheartaigh, J., Ball, G., Nongena, P., Makropoulos, A., … Edwards, A. D. (2015). Specialization and integration of functional thalamocortical connectivity in the human infant. *Proceedings of the National Academy of Sciences*, *112*(20), 6485–6490. https://doi.org/10.1073/pnas.1422638112

Tovar-Moll, F., Monteiro, M., Andrade, J., Bramati, I. E., Vianna-Barbosa, R., Marins, T., … de Oliveira-Souza, R. (2014). Structural and functional brain rewiring clarifies preserved interhemispheric transfer in humans born without the corpus callosum. *Proceedings of the National Academy of Sciences*, *111*(21), 7843–7848.

Triantafyllou, C., Hoge, R. D., Krueger, G., Wiggins, C. J., Potthast, A., Wiggins, G. C., & Wald, L. L. (2005). Comparison of physiological noise at 1.5 T, 3 T and 7 T and optimization of fMRI acquisition parameters. *NeuroImage*, *26*(1), 243–250. https://doi.org/10.1016/j.neuroimage.2005.01.007

Tsang, O., Gholipour, A., Kehtarnavaz, N., Gopinath, K., Briggs, R., & Panahi, I. (2008). Comparison of tissue segmentation algorithms in neuroimage analysis software tools. *2008 30th Annual International Conference of the IEEE Engineering in Medicine and Biology Society*, 3924–3928. https://doi.org/10.1109/IEMBS.2008.4650068

Tu, Y.-K., Gunnell, D., & Gilthorpe, M. S. (2008). Simpson's Paradox, Lord's Paradox, and Suppression Effects are the same phenomenon – the reversal paradox. *Emerging Themes in Epidemiology*, *5*, 2. https://doi.org/10.1186/1742-7622-5-2

Turchi, J., Chang, C., Ye, F. Q., Russ, B. E., Yu, D. K., Cortes, C. R., … Leopold, D. A. (2018). The Basal Forebrain Regulates Global Resting-State fMRI Fluctuations. *Neuron*, *97*(4), 940-952.e4. https://doi.org/10.1016/j.neuron.2018.01.032

Tustison, N. J., Avants, B. B., Cook, P. A., Zheng, Y., Egan, A., Yushkevich, P. A., & Gee, J. C. (2010). N4ITK: improved N3 bias correction. *IEEE Transactions on Medical Imaging*, *29*(6), 1310–1320.

Tyszka, J. M., Kennedy, D. P., Adolphs, R., & Paul, L. K. (2011). Intact bilateral resting-state networks in the absence of the corpus callosum. *Journal of Neuroscience*, *31*(42), 15154–15162.

Tzourio-Mazoyer, N., Joliot, M., Marie, D., & Mazoyer, B. (2016). Variation in homotopic areas' activity and inter-hemispheric intrinsic connectivity with type of language lateralization: an FMRI study of covert sentence generation in 297 healthy volunteers. *Brain Structure and Function*, *221*(5), 2735–2753. https://doi.org/10.1007/s00429-015-1068-x

Uddin, L. Q., Mooshagian, E., Zaidel, E., Scheres, A., Margulies, D. S., Kelly, A. M. C., … Milham, M. P. (2008). Residual functional connectivity in the split-brain revealed with resting-state fMRI. *Neuroreport*, *19*(7), 703–709. https://doi.org/10.1097/WNR.0b013e3282fb8203

Uludağ, K., Müller-Bierl, B., & Uğurbil, K. (2009). An integrative model for neuronal activity-induced signal changes for gradient and spin echo functional imaging. *NeuroImage*, *48*(1), 150–165. https://doi.org/10.1016/j.neuroimage.2009.05.051

van den Heuvel, M. P., & Hulshoff Pol, H. E. (2010). Exploring the brain network: A review on resting-state fMRI functional connectivity. *European Neuropsychopharmacology*, *20*(8), 519–534. https://doi.org/10.1016/j.euroneuro.2010.03.008

van der Knaap, L. J., & van der Ham, I. J. (2011). How does the corpus callosum mediate interhemispheric transfer? A review. *Behavioural Brain Research*, *223*(1), 211–221.

van der Zwaag, W., Francis, S., Head, K., Peters, A., Gowland, P., Morris, P., & Bowtell, R. (2009). fMRI at 1.5, 3 and 7 T: Characterising BOLD signal changes. *NeuroImage*, *47*(4), 1425–1434. https://doi.org/10.1016/j.neuroimage.2009.05.015

Van Dijk, K. R. A., Sabuncu, M. R., & Buckner, R. L. (2012). The influence of head motion on intrinsic functional connectivity MRI. *NeuroImage*, *59*(1), 431–438. https://doi.org/10.1016/j.neuroimage.2011.07.044

Van Essen, D. C. (2005). Corticocortical and thalamocortical information flow in the primate visual system. In *Cortical Function: A View from the Thalamus*: *Vol. 149*. *Progress in Brain Research* (pp. 173–185). https://doi.org/10.1016/S0079-6123(05)49013-5

Van Meir, V., Boumans, T., De Groof, G., Van Audekerke, J., Smolders, A., Scheunders, P., … Van der Linden, A. (2005). Spatiotemporal properties of the BOLD response in the songbirds' auditory circuit during a variety of listening tasks. *NeuroImage*, *25*(4), 1242–1255. https://doi.org/10.1016/j.neuroimage.2004.12.058

Van Ruijssevelt, L., De Groof, G., Van der Kant, A., Poirier, C., Van Audekerke, J., Verhoye, M., & Van der Linden, A. (2013). Functional Magnetic Resonance Imaging (fMRI) with Auditory Stimulation in Songbirds. *Journal of Visualized Experiments : JoVE*, (76). https://doi.org/10.3791/4369

Van Ruijssevelt, L., Hamaide, J., Gurp, M. T. V., Verhoye, M., & Linden, A. V. der. (2017a). Auditory evoked BOLD responses in awake compared to lightly anaesthetized zebra finches. *Scientific Reports*, *7*(1), 13563. https://doi.org/10.1038/s41598-017-13014-x

Van Ruijssevelt, L., Washington, S. D., Hamaide, J., Verhoye, M., Keliris, G. A., & Van der Linden, A. (2017b). Song Processing in the Zebra Finch Auditory Forebrain Reflects Asymmetric Sensitivity to Temporal and Spectral Structure. *Frontiers in Neuroscience*, *11*. https://doi.org/10.3389/fnins.2017.00549

Vatansever, D., Manktelow, A. E., Sahakian, B. J., Menon, D. K., & Stamatakis, E. A. (2017). Angular default mode network connectivity across working memory load: Angular Default Network in Working Memory. *Human Brain Mapping*, *38*(1), 41–52. https://doi.org/10.1002/hbm.23341

Vates, G. E., Broome, B. M., Mello, C. V., & Nottebohm, F. (1996). Auditory pathways of caudal telencephalon and their relation to the song system of adult male zebra finches (Taenopygia guttata). *Journal of Comparative Neurology*, *366*(4), 613–642. https://doi.org/10.1002/(SICI)1096-9861(19960318)366:4<613::AID-CNE5>3.0.CO;2-7

Vincent, J. L., Patel, G. H., Fox, M. D., Snyder, A. Z., Baker, J. T., Essen, D. C. V., … Raichle, M. E. (2007). Intrinsic functional architecture in the anaesthetized monkey brain. *Nature*, *447*(7140), 83–86. https://doi.org/10.1038/nature05758

Voss, H. U., Salgado-Commissariat, D., & Helekar, S. A. (2010). Altered Auditory BOLD Response to Conspecific Birdsong in Zebra Finches with Stuttered Syllables. *PLOS ONE*, *5*(12), e14415. https://doi.org/10.1371/journal.pone.0014415

Voss, H. U., Tabelow, K., Polzehl, J., Tchernichovski, O., Maul, K. K., Salgado-Commissariat, D., … Helekar, S. A. (2007). Functional MRI of the zebra finch brain during song stimulation suggests a lateralized response topography. *Proceedings of the National Academy of Sciences*, *104*(25), 10667–10672.

Waites, A. B., Stanislavsky, A., Abbott, D. F., & Jackson, G. D. (2005). Effect of prior cognitive state on resting state networks measured with functional connectivity. *Human Brain Mapping*, *24*(1), 59–68. https://doi.org/10.1002/hbm.20069

Wang, J., Wang, L., Zang, Y., Yang, H., Tang, H., Gong, Q., … He, Y. (2009). Parcellation-dependent small-world brain functional networks: a resting-state fMRI study. *Human Brain Mapping*, *30*(5), 1511–1523.

Welch, P. (1967). The use of fast Fourier transform for the estimation of power spectra: A method based on time averaging over short, modified periodograms. *IEEE Transactions on Audio and Electroacoustics*, *15*(2), 70–73. https://doi.org/10.1109/TAU.1967.1161901

Welcome, S. E., & Chiarello, C. (2008). How dynamic is interhemispheric interaction? Effects of task switching on the across-hemisphere advantage. *Brain and Cognition*, *67*(1), 69–75. https://doi.org/10.1016/j.bandc.2007.11.005

Welvaert, M., & Rosseel, Y. (2013). On the definition of signal-to-noise ratio and contrast-to-noise ratio for fMRI data. *PloS One*, *8*(11), e77089.

White, S. A., Fisher, S. E., Geschwind, D. H., Scharff, C., & Holy, T. E. (2006). Singing Mice, Songbirds, and More: Models for FOXP2 Function and Dysfunction in Human Speech and Language. *Journal of Neuroscience*, *26*(41), 10376–10379. https://doi.org/10.1523/JNEUROSCI.3379-06.2006

Whitfield-Gabrieli, S., & Nieto-Castanon, A. (2012). Conn: A Functional Connectivity Toolbox for Correlated and Anticorrelated Brain Networks. *Brain Connectivity*, *2*(3), 125–141. https://doi.org/10.1089/brain.2012.0073

Wild, J. M., Li, D., & Eagleton, C. (1997). Projections of the dorsomedial nucleus of the intercollicular complex (DM) in relation to respiratory-vocal nuclei in the brainstem of

pigeon (Columba livia) and zebra finch (Taeniopygia guttata). *Journal of Comparative Neurology*, *377*(3), 392–413.

Wild, J. M., Williams, M. N., & Suthers, R. A. (2000). Neural pathways for bilateral vocal control in songbirds. *Journal of Comparative Neurology*, *423*(3), 413–426.

Woo, C.-W., Krishnan, A., & Wager, T. D. (2014). Cluster-extent based thresholding in fMRI analyses: Pitfalls and recommendations. *NeuroImage*, *91*, 412–419. https://doi.org/10.1016/j.neuroimage.2013.12.058

Woolley, S. C., & Kao, M. H. (2015). Variability in action: Contributions of a songbird cortical-basal ganglia circuit to vocal motor learning and control. *Neuroscience*, *296*, 39–47. https://doi.org/10.1016/j.neuroscience.2014.10.010

Yacoub, E., Duong, T. Q., Moortele, P.-F. V. D., Lindquist, M., Adriany, G., Kim, S.-G., … Hu, X. (2003). Spin-echo fMRI in humans using high spatial resolutions and high magnetic fields. *Magnetic Resonance in Medicine*, *49*(4), 655–664. https://doi.org/10.1002/mrm.10433

Yan, C.-G., Wang, X.-D., Zuo, X.-N., & Zang, Y.-F. (2016). DPABI: data processing & analysis for (resting-state) brain imaging. *Neuroinformatics*, *14*(3), 339–351.

Yanagihara, S., & Yazaki-Sugiyama, Y. (2016). Auditory experience-dependent cortical circuit shaping for memory formation in bird song learning. *Nature Communications*, *7*, 11946. https://doi.org/10.1038/ncomms11946

Yoshida, K., Mimura, Y., Ishihara, R., Nishida, H., Komaki, Y., Minakuchi, T., … Takata, N. (2016). Physiological effects of a habituation procedure for functional MRI in awake mice using a cryogenic radiofrequency probe. *Journal of Neuroscience Methods*, *274*, 38–48. https://doi.org/10.1016/j.jneumeth.2016.09.013

Zatorre, R. J., Belin, P., & Penhune, V. B. (2002). Structure and function of auditory cortex: music and speech. *Trends in Cognitive Sciences*, *6*(1), 37–46. https://doi.org/10.1016/S1364-6613(00)01816-7

Zeng, L.-L., Shen, H., Liu, L., Wang, L., Li, B., Fang, P., … Hu, D. (2012). Identifying major depression using whole-brain functional connectivity: a multivariate pattern analysis. *Brain*, *135*(5), 1498–1507. https://doi.org/10.1093/brain/aws059

Zhang, J., Kendrick, K. M., Lu, G., & Feng, J. (2014). The fault lies on the other side: Altered brain functional connectivity in psychiatric disorders is mainly caused by counterpart regions in the opposite hemisphere. *Cerebral Cortex*, *25*(10), 3475–3486.

Zhao, F., Jin, T., Wang, P., & Kim, S.-G. (2007). Isoflurane anesthesia effect in functional imaging studies. *Neuroimage*, *38*(1), 3.

Zhao, F., Wang, P., & Kim, S.-G. (2004). Cortical depth-dependent gradient-echo and spin-echo BOLD fMRI at 9.4T. *Magnetic Resonance in Medicine*, *51*(3), 518–524. https://doi.org/10.1002/mrm.10720

Zhou, Y., Milham, M., Zuo, X.-N., Kelly, C., Jaggi, H., Herbert, J., … Ge, Y. (2013). Functional homotopic changes in multiple sclerosis with resting-state functional MR imaging. *American Journal of Neuroradiology*, *34*(6), 1180–1187.

Ziegler, W., & Ackermann, H. (2017). Subcortical Contributions to Motor Speech: Phylogenetic, Developmental, Clinical. *Trends in Neurosciences*, *40*(8), 458–468. https://doi.org/10.1016/j.tins.2017.06.005

Zuo, X.-N., Kelly, C., Di Martino, A., Mennes, M., Margulies, D. S., Bangaru, S., … Castellanos, F. X. (2010). Growing together and growing apart: regional and sex differences in the lifespan developmental trajectories of functional homotopy. *Journal of Neuroscience*, *30*(45), 15034–15043.

Zwaag, W. van der, Marques, J. P., Kober, T., Glover, G., Gruetter, R., & Krueger, G. (2012). Temporal SNR characteristics in segmented 3D-EPI at 7T. *Magnetic Resonance in Medicine*, *67*(2), 344–352. https://doi.org/10.1002/mrm.23007